Charles University in Prague

Faculty of Mathematics and Physics

DOCTORAL THESIS

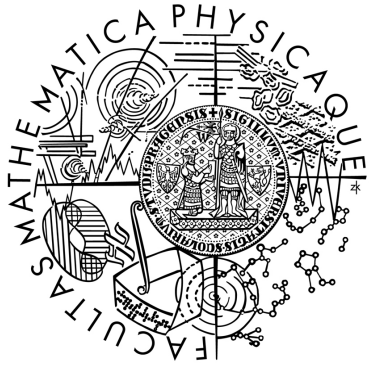

Ivan Gordeev

Thin films of plasma polymers as stable supports for biomedical applications

Charles University in Prague, Department of Macromolecular Physics

Supervisor of the doctoral thesis: Doc. Ing. Andrey Shukurov, Ph.D.

Study programme: Physics
Specialization: F4 – Biophysics, Chemical and Macromolecular physics

Prague 2012

Without the help of many colleagues and friends from the Charles University and Institute of Plasma Physics, this work could not come into being even as little perfect as it is in its current “final” stage. Therefore I would like to acknowledge the generous support of all these people.

First of all I am very indebted to my supervisor Doc. Ing. Andrey Shukurov Ph.D. for inestimable help in writing this thesis, in neat remarks and current discussions of results during the course of this work. And also I am very thankful to my consultants Prof. RNDr. Hynek Biederman DrSc, Mgr. Jan Hanuš Ph.D. and RNDr. Ondřej Kylián Ph.D. from the Charles University in Prague and RNDr. Milan Šimek Ph.D. from the Institute of Plasma Physics v.v.i. (IPP) for their continuous interest, advises and help in accomplishing the experiments and writing the thesis.

I am very obliged to fellow members of Prof. Biederman’s group: Doc. Danka Slavínská CSc, Anna Artemenko, Oleksandr Polonskyi, Jaroslav Kousal PhD, Jindřich Matoušek, Martin Drábik PhD, Pavel Solař, Dmitry Arzhakov, Anton Serov, Doc. RNDr. Ivan Krakovský CSc, Juraj Čechvala and Marcela Búryová (Ublanska) for a good and memorable time and for their help in implementation of different measurements and analysis of several results. I would like to thank Mgr. Marta Vandrovcova Ph.D. from the Institute of Physiology, Academy of Sciences of the Czech Republic, Prague, Jesica Ponti, Chiara Uboldi and Elisa Alloa from the Joint Research Centre, Institute for Health and Consumer Protection, European Commission, in Ispra, Italy, and Ing. Cesar Rodriguez-Emmenegger from the Institute of Macromolecular Chemistry, Academy of Sciences of the Czech Republic, v.v.i., Prague, Czech Republic for performing the biological tests.

I am very obliged to fellow members of the department of pulse plasma systems, IPP: Oleksandr Frolov PhD, RNDr. Karel Koláček CSc, Petr Lukeš PhD, Václav Prukner PhD and Antonín Baumruk for their help and various supports.

And at last but not at least, I am obliged very much to my family and friends (Irina Velichko, Dmitry Zemlin, Alexandr Fokin, Evgeniya Bokova, Marya Barinova, Ivan Zhukov and others) for the encouragements and untold support.

I declare that I carried out this doctoral thesis independently, and only with the cited sources, literature and other professional sources.

I understand that my work relates to the rights and obligations under the Act No. 121/2000 Coll., the Copyright Act, as amended, in particular the fact that the Charles University in Prague has the right to conclude a license agreement on the use of this work as a school work pursuant to Section 60 paragraph 1 of the Copyright Act.

In Prague date..... signature

Název práce: Příprava tenkých vrstev plazmovou polymerací jako stabilních podložek pro biolékařské aplikace

Autor: Ivan Gordeev

Katedra/Ústav: Katedra Makromolekulární fyziky/Univerzita Karlova v Praze

Vedoucí doktorské práce: Doc. Ing. Andrey Shukurov, Ph.D., Katedra Makromolekulární Fyziky

Abstrakt: Plazmové polymery jsou všeobecně považovány za vhodné pro použití jako biologicky aktivní vrstvy. V biomedicíně jsou obzvláště důležité povrchy, které odolávají vytváření biovrstev. Tato práce je zaměřena na vývoj nových metod využívajících plazma pro depozice bio-rezistentních ("non-fouling") plazmových polymerů. Pro tyto účely byl vybrán jako vhodný materiál poly(ethylen oxid) (PEO). R.f. magnetronové naprašování, tepelná depozice za asistence plazmatu a amplitudově-modulovaný AC povrchový dielektrický bariérový výboj za atmosférického tlaku jsou metody, které byly přizpůsobeny pro přípravu tenkých filmů s laditelným chemickým složením, hustotou sesíťování a laditelnou biologickou odezvou. Byly získány nové poznatky o procesech plazmové polymerace a jejich vlivu na složení a strukturu výsledných vrstev s řízenými biologickými vlastnostmi.

Klíčová slova: plazmová polymerizace, PEO, "non-fouling" vlastnosti, adsorpce proteinů, adheze buněk

Title: Thin films of plasma polymers as stable supports for biomedical applications

Author: Ivan Gordeev

Department/Institute: Department of Macromolecular Physics/Charles University in Prague

Supervisor of the doctoral thesis: Doc. Ing. Andrey Shukurov, Ph.D, Department of Macromolecular Physics.

Abstract: Plasma polymers have been widely considered for use as bio-active coatings. In biomedicine, the surfaces that withstand accumulation of biofilms are of particular importance. This thesis is focused on development of new plasma-based methods for deposition of bio-resistant (non-fouling) plasma polymers. Poly(ethylene oxide) was the subject material. R.f. magnetron sputtering, plasma-assisted thermal vapour deposition and amplitude modulated atmospheric pressure surface dielectric barrier discharge were the methods adapted to fabricate thin films with tunable chemical composition, cross-link density and biological response. A new insight was gained into the processes of plasma polymerization as well as into composition/structure relationship and its effect on biological properties of resultant films.

Keywords: plasma polymerization, PEO, 'non-fouling' properties, protein adsorption, cell adhesion

Contents

Aims

This study was focused on development of novel plasma-based methods for deposition of biologically non-fouling plasma polymers. The following aims were set:

- Application of low pressure magnetron sputtering, plasma-assisted thermal vapour deposition and atmospheric pressure amplitude modulated AC surface dielectric barrier discharge for deposition of poly(ethylene oxide)-like (PEO) plasma polymers.
- Detailed characterization of deposited films aimed to determine their structure, morphology and chemical composition.
- Analysis of swelling/dissolution behaviour of the PEO-like plasma polymers in an aqueous environment.
- Study of biological response of the PEO-like plasma polymers in terms of adsorption of various proteins and adhesion of cells.

Elucidation of the key factors governing the non-fouling behaviour of the PEO-like plasma polymers.

1. State of the Art

1.1. Basics of plasma polymerization

1.1.1. Plasma and plasma polymers

Plasma is a quasi-neutral state of matter characterized by a certain degree of ionization and by approximately equal concentrations of positive and negative charges. Low temperature plasma is only 1-10 % ionized with the rest of the gas remaining as neutral atoms or molecules. The electrons are not in thermal equilibrium with other species. Plasma can be maintained at different pressures that determine the ranges of low pressure (up to hundreds of Pa) and high pressure (up to atmospheric pressure) discharges. Different types of excitation can be used:

- Direct current (DC) discharge;
- Radio frequency (RF) discharge (frequency of the applied voltage 100 kHz – 30 MHz, typically 13.56 MHz is used);
- Microwave (MW) discharge (frequency of the applied voltage 100 MHz and more).

If an organic gas is introduced into the zone of plasma, the formation of a thin quazi-polymeric film on adjacent surfaces is possible. Such films, often called plasma polymers, are characterized by randomly branched structure with a high degree of cross-linking. In this sense, plasma polymers (Figure 1.1) are substantially different as compared to conventional polymers that consist of long macromolecular chains with regularly repeating monomeric units (Figure 1.2). Disorder in plasma polymers is given by the diversity of species participating in plasma polymerization processes, their random interactions as well as by ion bombardment and UV radiation.

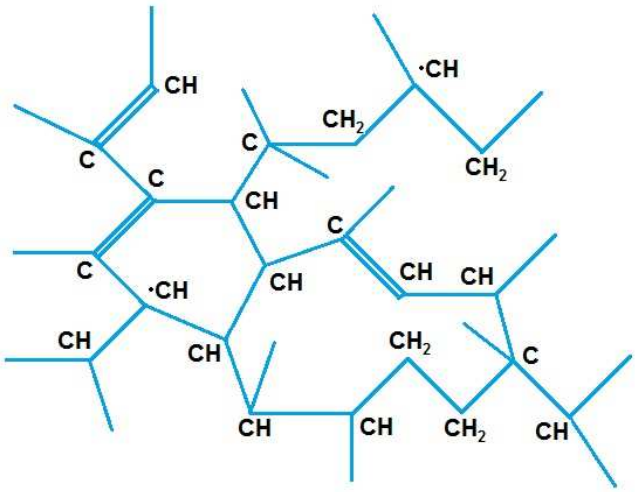

Figure 1.1. Hypothetical structure of a hydrocarbon plasma polymer (*adapted from [1]*).

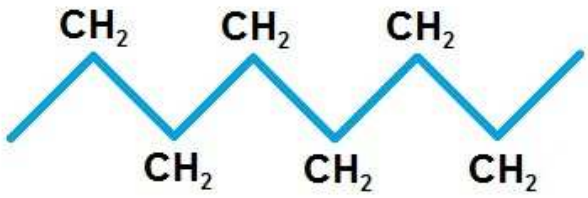

Figure 1.2. Schematic representation of poly(ethylene) chain (*adapted from [1]*).

1.1.2. Low pressure plasma polymerization of volatile precursors

In this process, the glow discharge is ignited at low pressure in an atmosphere of organic monomer vapours. The highly reactive environment is created due to interaction of 'hot' electrons with precursor molecules. The electrons in such plasmas gain average kinetic energy of 1-5 eV that may be sufficient to cleave the chemical bonds and to generate radicals, with or without fragmentation of the precursor. Ionization threshold of organic molecules (~9-13 eV) is much higher than the energy of their chemical bonds (~3-4 eV) and therefore the concentration of free radicals is generally much higher than that of the ions in low temperature organic plasmas. Highly reactive radicals tend to recombine in numerous chemical reactions which may lead to propagation and/or termination of the macromolecular chains. Because of the low pressure, the probability of the reactions in the plasma volume is negligible and growth of plasma polymers occurs predominantly on adjacent

surfaces. Such heterogeneous formation of plasma polymers was first modelled and experimentally proven by Lam et al [2]. They showed that plasma polymerization of styrene was initiated in a gas phase by electron impact and then it was followed by the steps of propagation and termination of polymeric chains on the surfaces.

Any isolated body immersed into plasma acquires a negative bias (floating potential) with respect to plasma potential due to higher mobility of electrons. Therefore, the film growing on substrates may be subject to positive ion bombardment. Depending on the conditions, the floating potential and intensity of ion bombardment may be significant to induce additional changes in plasma polymers (densification, re-arrangement, ablation etc). This effect was first addressed to by Yasuda in his Competitive Ablation and Polymerization model [3]. Yasuda considered plasma polymerization as a rapid step-growth process via free radicals with the following reactions: chain propagating reactions through the repeated addition of radicals to the inactivated species; termination through radical recombination; recombination of mono- and biradicals forming another monofunctional radical and other.

Since the deposition rate and the properties of plasma polymers depend strongly on variety of parameters, direct comparison of the films fabricated under different experimental conditions is complicated unless a certain generalization is performed. Yasuda [3] was also the first to suggest a parameter W/FM to compare the depositions performed at different power of discharge W (watt), monomer molar flow rate F ($mol \cdot s^{-1}$), and monomer molar mass M ($kg \cdot mol^{-1}$). In such notation, the Yasuda parameter represents the specific power, that is the power per mass flow rate of a precursor. Analogous plasma deposits can be obtained at different powers provided that the flow rate is correspondingly adjusted to keep the same level of the specific power.

Yasuda based his model on the experimental results obtained for various hydrocarbons. In recent years, interest has been renewed to expand the applicability of the macroscopic kinetic approach to analysis of other plasma polymerizations. Hegemann with co-workers examined plasma polymerization of different monomers and found an Arrhenius-type dependence of $\frac{R_m}{F} = G \exp\left(-\frac{E_a}{W/F}\right)$, where R_m is the mass deposition rate, G is a reactor-depending geometrical factor and E_a is the apparent activation energy corresponding to the monomer used. Findings of

Hegemann gave rise to a vigorous debate to this issue. Main criticism was addressed to significant deviations of the dependence from the Arrhenius type at low and high specific power inputs. Furthermore, obscure chemical meaning of E_a and failure to include pressure into the formula derivation were also criticized [4]. At present, plasma polymerization community is still far from reaching a consensus. Apparently, the macroscopic kinetic approach can not serve as a universal tool and for each case of the plasma polymerization process the range of linear dependence of the semilog plot of $\frac{R_m}{F}$ versus $(W/F)^{-1}$ should be sought separately.

1.1.3. Rf magnetron sputtering of conventional polymers

The first reports on rf sputtering of polymers appeared in 1970s. The goals were focused mainly on preparation of fluorocarbon plasma polymer films with good dielectrical and optical properties [5, 6, 7, 8, 9]. In this method, the target to be sputtered is fabricated of a conventional polymer. The target is attached to the biased electrode (often to a magnetron) and the discharge is operated in an rf regime. In the magnetron, the specially-configured magnetic field is used to produce the closed electron paths. This is reached by a ring of permanent bar magnets arranged around a central magnet. Due to drift of electrons along the tunnel axis in crossed electrical and magnetic fields the plasma is confined and is most intense there. Because the discharge is confined in a close vicinity of the target, the working gas is very efficiently ionized. The typical values of the magnetron bias reach hundreds of volts and hence highly energetic fluxes of positive ions bombard the polymeric target, split macromolecular chains to smaller fragments and sputter the latter away from the target. These fragments serve as precursors for plasma polymerization in this case.

Since 1970s, variety of sputtered polymers has been increasing. Interest in this method has been strengthened due to complete elimination of liquid precursors, availability of relatively inexpensive polymeric targets and due to good feasibility with other vacuum technologies. Following poly(tetrafluoroethylene), rf magnetron sputtering of poly(ethylene) [10, 11], poly(propylene) [12, 13], poly(isobuthylene) [14], poly(imide) [15], poly(dimethylsiloxane) [16] and nylon 6,6 [17, 18] was studied. The sputtering was performed either under inert argon atmosphere or in a

mixture of gases (Ar/N_2, N_2/H_2, Ar/H_2) to additionally control the chemical composition of resultant films.

Since polymers usually have poor thermal conductivity, cooling of the target from the magnetron backing plate is difficult. At higher discharge power, intensive ion bombardment may result in significant energy release and, as a result, in heating of the target surface to a temperature at which the polymer starts to decompose thermally and to emit the volatile products of such decomposition. This leads to an abrupt increase of the deposition rate and to significant changes of the properties of resultant plasma polymers. The dual effect of sputtering and thermal decomposition was observed for hydrocarbon polymers [19], poly(imide) [20] and nylon [21]. It was suggested that heating of conventional polymers under rarefied anaerobic atmosphere may be used to obtain the organic vapours without necessary implementation of sputtering. These can be further used as precursors for plasma polymerization processes

1.1.4. Plasma-Assisted Thermal Vapour Deposition

The research of thermal decomposition of polymers started in 1940s. Madorsky et al. [22, 23] examined thermal degradation of a number of polymers such as poly(styrene), poly(isoprene), poly(butadiene), and poly(ethylene) under vacuum at temperatures of 300 – 400 ºC. According to this work, the volatile products of decomposition consisted of fragments that varied in size from a monomer to species having a molecular weight of about 1000 $g \cdot mol^{-1}$. Luff and White proceeded with poly(ethylene) to find that its thermal decomposition has two stages: the first stage starts at 300 ºC while the second stage occurs above 350 ºC [24]. The main difference between the two was in the difference between the activation energies and the molecular weight of the fragments of the evaporated material. Following the works of Luff and White, thermal degradation of various polymeric precursors has been studied [25, 26, 27, 28, 29].

In the mid of 1990s, H. Usui et al. [30] developed an ionization-assisted evaporation method which used the complementary fluxes of electrons to ionize the vapours produced as a result of vacuum thermal ‘evaporation’ of PTFE. The ionized species were then accelerated towards the biased substrates to build a film. The properties of the films were manipulated by controlling the amount and energy of the

ions. In the following work, H. Usui et al. adapted their method to deposition of poly(imide), poly(urea) and poly(urethane) thin films via ionization-assisted polymerization of two bi-functional reactive monomers [31].

Our group has developed a method of Plasma-Assisted Thermal Vapour Deposition which has been applied to poly(ethylene) [32] and poly(imide) [33]. In this method, glow discharge instead of electron fluxes was used to activate the released organic vapours. Glow discharge in argon was maintained by an rf magnetron (Figure 1.3). It was possible to adjust the chemical composition and the cross-link density of the plasma polymers by the power delivered to the magnetron.

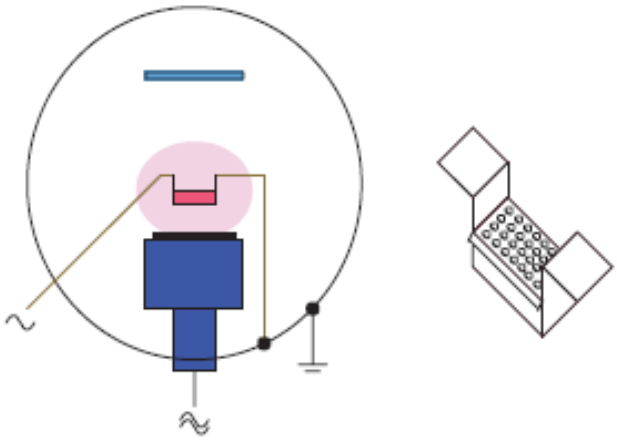

Figure 1.3. The experimental arrangement for fabrication of poly(imide)-like thin films by Plasma-Assisted Thermal Vapour Deposition (adapted from [33]).

1.1.5. Atmospheric pressure plasma polymerization

Most of plasma polymerization processes have been developed at low pressure of up to several hundreds of Pa. The last decades evidenced growing interest to deposition of plasma polymers in atmospheric pressure plasmas as well. Besides the fundamental research, atmospheric pressure plasmas are interesting from the technological perspective for continuous treatment of large-scale objects. Reduced apparatus costs have been also often included in the list of benefits, yet this point is still highly disputable. General requirements include:

- the use of helium or argon for dilution of a carrier gas;
- the implementation of a dielectric insulator between the electrodes in the discharge gap;

- the use of a high frequency, at least higher then 1 kHz.

DBD systems can be made in various configurations. In general, volume DBD and surface DBD are distinguished. Volume DBD discharges operate with the parallel plate-type electrodes covered by a dielectric plate where the electrodes are separated by a gaseous gap. Surface dielectric barrier discharge (SDBD) features the electrodes that are separated by a dielectric layer itself so that the powered electrode (usually patterned) is constructed on the top and exposed to the discharge while the grounded electrode is on the rear side of the dielectric plate [34, 35, 36, 37].

The first thin films deposited by the atmospheric pressure discharge were polymerized from C_2H_4, C_2F_4 and $Si(OC_2H_5)_4$ [38]. The chamber with parallel plate-type electrodes covered by a glass insulator was used for the deposition process. The discharge at frequency of 3 kHz, 15 kHz and 120 kHz was ignited in the gas mixtures of He and the monomers. The plasma–polymerized C_2F_4 and C_2H_4 films were very similar in chemical structure and physical properties to chemically synthesized PTFE and poly(ethylene), respectively.

O. Goossens et al. [39] also reported about the application of atmospheric pressure Dielectric Barrier Discharge (DBD) for polymerization of ethylene. He and Ar mixed with ethylene was used for the depositions. The experimental set-up consisted of two disk-shaped Al electrodes covered by an Al_2O_3 plate.

The application of the atmospheric pressure discharge to fluorinate the inner surface of commercial poly(vinyl chloride) tubes was introduced in a study [40]. The special electrodes were helically wound around a cylindrical glass fed with mixtures of helium and tetrafluoroethylene or hexafluoropropylene. The deposited fluorinated plasma polymers were sufficiently homogeneous with thickness of about 1 µm. The leaching of plasticizers present in the commercial PVC tubes can be also suppressed by these films.

De Geyter et al. [41] investigated the preparation of poly(methyl methacrylate) (PMMA) plasma polymer films from vapours of methyl methacrylate monomer. They found that by controlling the monomer fragmentation in the plasma–assisted process it was possible to prepare the films with similar chemical composition to those obtained by spin coating. Several other works studied plasma polymerization of acrylic acid [42] and organic-inorganic monomers [43].

1.2. Plasma polymers in biomedicine

Plasma polymers have been studied for years and a wide variety of possible applications has been suggested. Biomedicine has been considered as one of the application areas where plasma polymers may be of high relevance.

1.2.1. Plasma polymers as biomaterials

Many definitions exist to the term 'biomaterial'. In a broad sense, "biomaterial is a nonviable material used in a medical device, intended to interact with biological systems" [44]. Biocompatibility is then considered as "the ability of a material to perform with an appropriate host response in a specific application" [45]. By a consensus of experts, a biomaterial must always be considered from the perspective of its final application in its final sterilized form [46].

Biomaterials must meet mechanical and performance requirements. Fulfilment of these requirements depends on the physical bulk properties of the material. Obviously, there exist few materials that simultaneously possess appropriate mechanical properties and are biocompatible. Hence, a recognized strategy for the creation of medical devices is the use of conventional materials (metals, metal alloys, polymers etc) and modification of their surface in such a way that they become biocompatible. For such a strategy, thin films of plasma polymers are particularly suitable as they do not affect the bulk material properties but significantly change the surface morphology and its chemical and physical properties.

The plasma deposited thin films have been explored for biomedical applications since the 1960s. Plasma polymers are advantageous in biomedicine for the following reasons [1, 47]:

- dry processing is clean and efficient;
- coating times are rapid – often seconds;
- coatings are conformal, important for complex geometries;
- treatments can be done on a continuous basis;
- coatings usually exhibit strong adhesion to the substrate;
- monomer costs are relatively low;
- feasibility due to widespread application in microelectronics.

Many chemistries and substrates for deposition process are possible and, therefore, plasma polymers can provide the surface with useful functionalities such as:

- lubricity;
- wettable and non-wettable (hydrophobic) surfaces;
- surfaces that favour adsorption of proteins and adhesion of cells
- non-fouling (protein resistant) and antibacterial coatings;
- barriers to control drug release rates.

An exhaustive review of a vast diversity of possible biomedical applications of plasma polymers is hardly possible within the frames of this thesis. Rather, special attention will be further paid to a specific case of non-fouling materials since fabrication of such surfaces by plasma-based methods was set as a primary goal of the thesis.

1.2.2. Non-fouling surfaces

The term ‘non-fouling’ describes the ability of a material to resist accumulation of a biofilm on its surface. Biofilm is a complex structure composed of microorganisms, cellular material, extracellular polysaccharides and proteins [46]. Obviously, there are many biomedical areas in which accumulation of biofilms should be minimized or, better, eliminated to reduce the risks of inflammation. The examples include haemodialysis membranes, contact lenses, catheters and, particularly, blood-contacting implant devices [48].

A general consensus states that growth of a cellular material is mediated by protein adsorption on surfaces. It means that cells in biological media arrive onto and interact with the surface already occupied by proteins which are significantly smaller and hence much more mobile. Therefore, analysis of the protein adsorption on surfaces may give a clue to understanding of more complex cell/surface interactions.

Adsorption of proteins is driven by a number of factors such as:

- chemical composition of the surface [49, 50, 51, 52];
- hydrophobic-hydrophilic interactions [53, 54, 55, 56];
- electrostatic interactions, pH and the ionic strength of the protein solution [49, 57, 58, 59, 60].

In addition to the above, there are many other factors that to some extend affect (directly or indirectly) the adsorption process, such as: protein concentration,

structural stability of the protein, isoelectric point of the protein, morphology of the surface.

Non-fouling properties have been often suggested to be obtained by use of poly(ethylene oxide). PEO has the structural formula $HO–[CH_2CH_2O]_n–H$ and it is widely used in a variety of applications such as drug delivery, gas chromatography, and microbiology, etc [61]. It is also known to significantly reduce or totally prevent unwanted biological adhesion [62, 63].

The mechanism of non-fouling behavior of PEO remains unclear. Two main factors are usually taken into account. The first is related to specific structuring of water molecules around the C-O-C bonds (hydrogen bonding of water molecules around the ether bonds) so that the proteins are screened from the binding sites in the macromolecular chains (Figure 1.4 a) [64, 65]. The second factor involves steric hindrance implying that flexible and mobile PEO chains act as springs to repulse the approaching proteins back into solution (Figure 1.4 b) [65]. The importance of both factors is still disputed in the literature. Extensive work on self-assembled monolayers for the most part prove reduced protein adhesion with longer polymeric chains used [66, 67]. Nevertheless, other reports state that the packing density of SAMs rather than their length really influences the non-fouling behavior [68].

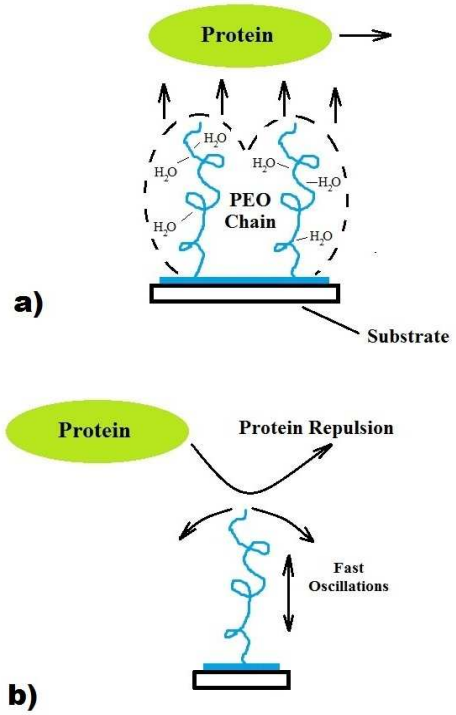

Figure 1.4. The mechanisms of the interaction between proteins and PEO chains on the surface: a) PEO/water structural relationship and b) steric repulsive interaction.

Although good solubility of PEO in water is favorable for drug delivery applications, for fabrication of the non-fouling surfaces it may represent a big issue. Adsorbed physically, PEO leaches from the surface, i.e. it dissolves in aqueous solutions with time. Covalent bonding of PEO chains is required to retain the integrity of the coating over extended periods of time. SAMs of PEO attached covalently to gold or silicon dioxide surface has been shown to exhibit stable low bio-adhesion [69, 70, 71]. The SAM chemistry however is drastically restricted by the material of the substrate. It often involves multi-step and time-consuming chemical pathways as well. Recently, plasma polymerization methods have been proposed to deposit non-fouling PEO-like plasma polymer films.

1.2.3. PEO-like plasma polymers as non-fouling surfaces

As it was discussed earlier, plasma polymerization produces cross-linked organic films. The cross-link density depends on the specific power of discharge. The chemical structure of the precursor is retained in plasma polymers only partially, the extent of the retention being also dependent on the specific power. Thus, the specific power was suggested to be the main variable for deposition of the PEO-like plasma polymers with adjustable cross-link density and concentration of the ether groups.

Lopez with co-workers [72] were the first to show that glow discharge at reduced pressure in vapours of tetraethylene glycol dimethyl ether produced surfaces which were resistant to protein adsorption and cellular attachment. Since the paper by Lopez, numerous works appeared that investigated low pressure plasma polymerization of various ether-bearing precursors under different conditions (Table 1.1). Generally, concentration of the C-O-C groups of 70 % and higher was found to be sufficient for achievement of the non-fouling behavior of the plasma polymers [73, 74]. Retention of the C-O-C structure up to 85 % was obtained by Johnston et al. [75] and Pan et al. [73], up to 75 % by Palumbo et al. [76], up to 73 % by Lopez et al. [72] and Shen et al. [77], and up to 63 % by Denes et al. [78] for different oligoglymes. Sardella and co-workers [74, 79, 80], Favia et al. [81], Bretagnol et al. [82], Cheng et. al. [83] and Muir et al. [84] used diethylglycol dimethyl ether to obtain plasma polymers with up to 72-80 % of ether functional groups. Different vinyl ether compounds were studied by Zhang et al. [85], Wu et al. [86], Chu et al.

[87], Bremmell et al. [88], Beyer et al. [89] and Ademovic et al [90, 91] although without providing quantitative data on the C-O-C group retention. Nevertheless, the XPS spectra provided evidence that the maximal concentration of C-O-C was within the same range of 70-85 % in these cases as well.

Monomer	**Power (W)**	**Maximal retention of C-O-C (%)**	**Reduced protein/cell adhesion**
Oligoglymes, dioxane and crown ethers [75]	5-80 (CW)	85	Fibrinogen
Tetraethylene glycol dimethyl ether (tetraglyme) [73] $CH_3O(CH_2CH_2O)_4CH_3$	5-80 (CW)	85	Laminin
2,5,8,11-tetraoxa-dedocane (triglyme) [76]	2-50 (CW)	75	-
Tetraglyme [72, 77]	5-80 (CW)	73	Fibrinogen, immunoglobulin (IgG), monocytes
Triglyme [78] $CH_3O(CH_2CH_2O)_3CH_3$	100 W (pulsed)	63	Salmonella typhimurium, Staphylococcus epidermidis, Pseudomonas fluorescens
diethylglycol dimethyl ether (DEGME) [74, 79, 80, 81] $CH_3O(CH_2CH_2O)_2CH_3$	5 - 100 (CW)	80	Fibronectin, infinity telomerase immortalized human cells
DEGME [82]	5 (pulsed)	75	Bovine serum albumin (BSA), L929 fibroblasts
DEGME [83]	1-20 (CW)	72	-
DEGME [84]	20 (CW)	58	BSA, lysozyme
Diethylene glycol monovinyl ether (DEGVE) [85] $CH_2=CH(OCH_2CH_2)_2OH$	25-100 (CW and pulsed)	-	BSA, IgG, fibrinogen
Mono- and diethylene glycol vinyl ether [86]	6-50 (CW and pulsed)	-	BSA, fibrinogen
DEGVE [87]	20 W (pulsed)	-	BSA, fibrinogen
DEGVE [88]	-	40	Fibrinogen
Triethylene glycol monoallyl ether [89]	5-50 (CW and pulsed)	-	BSA
Diethylene glycol methyl vinyl ether [90, 91]	0.6-3.6 (pulsed)	-	Fibrinogen, leukocytes

Table 1.1. PEO-like plasma polymers and their non-fouling properties.

A general rule has been deduced that a lower power delivered to the discharge results in less intensive fragmentation of precursor molecules. It results therefore in the fabrication of thin films with better retention of the ether groups which thereby maintain the non-fouling character.

Surprisingly, the deposition of PEO-like plasma polymers by atmospheric pressure discharges has not been considered at all, until very recently. The first reports are dated by 2010, although atmospheric pressure plasma polymerization has been known for at least several decades. Nisol et al. examined atmospheric pressure plasma liquid deposition (APPLD) and atmospheric pressure plasma enhanced chemical vapour deposition of tetraglyme. In the case of APPLD, liquid tetraglyme film was treated by the atmospheric discharge in argon to reach polymerization with up to 85 % retention of the polyether structure. The resultant films exhibited reduced adsorption of bovine serum albumin [92]. Atmospheric pressure PECVD was performed in a mixture of argon and tetraglyme vapours. It showed a 70 % retention of the polyether structure and, accordingly, larger adsorption of albumin. Da Ponte et al. utilized a similar approach with the use of an atomizer to introduce a spray of tetraglyme into Dielectric Barrier Discharge (DBD) operated in helium [93]. After optimization of the voltage and the gas flow rate, the films with 70 % of the C-O-C groups were obtained, however no information on their non-fouling behaviour was provided.

As it was discussed above, the concentration threshold of 70 % of the C-O-C groups was established for the PEO-like plasma polymers to behave non-fouling. The steric factor, i. e. the influence of flexibility and length of the segments between the cross-links, was unattended, simply because these parameters have not yet been reliably assessed for plasma polymers. It is generally accepted that plasma polymer represents a carbonaceous network where short sequences of intact monomer units (as well as other functional groups not available in a precursor but created through random radical recombination) are branched via cross-links. Because of the use of low molar mass volatile monomers as precursors, formation of long macromolecular chains is unlikely under plasma polymerization conditions. On the other hand, long chain PEO units were argued to be unnecessary for the non-fouling plasma polymers and the C-O-C/C-C ratio was regarded as the main parameter affecting the protein adsorption [75, 86, 89]. Wu et al.[86] showed that the precursor with as few as two ether groups yielded the non-fouling PEO-like plasma polymers while the precursor

with only one ether group did not. It should be noted however that adsorption of proteins was analyzed only with respect to the length of the precursor molecule and no direct evidence of the plasma polymer structure was given. Taking into account the above-discussed controversy between the results on PEO SAMs, further examination of the structure-properties relationship of PEO-like materials is required.

2. Experimental

In this work, three essentially different methods were investigated for deposition of PEO-like plasma polymers: rf magnetron sputtering, low pressure plasma-assisted thermal vapour deposition and atmospheric pressure surface dielectric barrier discharge.

2.1. Deposition methods

2.1.1. Magnetron sputtering

Magnetron sputtering of the target fabricated from conventional PEO (Figure 2.1) was performed in a cylindrical vacuum chamber of 0.04 m^3 volume. The target was prepared by melting of conventional PEO granules onto the polyethylene disk with successive hardening of the melt at room temperature.

The chamber was brought to a base pressure of a 1×10^{-3} Pa by rotary and diffusion pumps. The power was delivered to the magnetron by an r. f. generator (Dressler Ceasar, 13.56 MHz) through a matching unit. The experiments were performed with argon used as a working gas at pressure of 2 Pa and flow rate of 5 sccm. The substrates were placed 8 cm above the PEO target. The deposition rate of the plasma polymers was controlled by Quartz Crystal Microbalance (QCM) placed in-plane with the substrates. The substrates were introduced to their working position in the discharge zone via a load-lock system after adjusting and stabilizing of the deposition conditions (Ar pressure and flow rate, discharge power). After the deposition, the samples were removed from the discharge zone to the load-lock chamber where they were kept under vacuum for 30 minutes to complete the recombination processes of active radicals within the films.

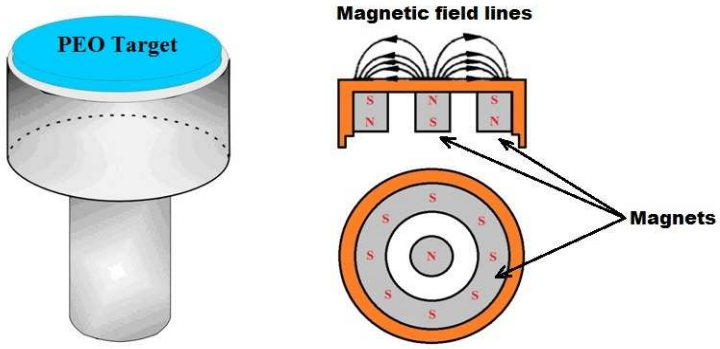

Figure 2.1. The schematic illustration of the planar magnetron with the PEO target.

2.1.2. Plasma-Assisted Thermal Vapour Deposition

The experiments were performed in the same stainless steel reactor which was used for the magnetron sputtering (Section 2.1.1). The copper crucible was placed on two electrically heated molybdenum strips and served as an evaporation source of PEO. The PEO granules were loaded into the crucible. The distance between the substrates and the crucible was fixed at 10 cm. The crucible was placed 4 cm above the 80 mm planar magnetron with a graphite target (Figure 2.2). Graphite was chosen as a low sputter yield material to minimize the contribution of sputtered carbon to deposited films. The magnetron system was cooled by water. For all the experiments, argon pressure and flow rate were set at 1 Pa and 5 sccm, respectively. The deposition conditions were maintained constant during the experiments and their typical values are summarized in Table 2.1.

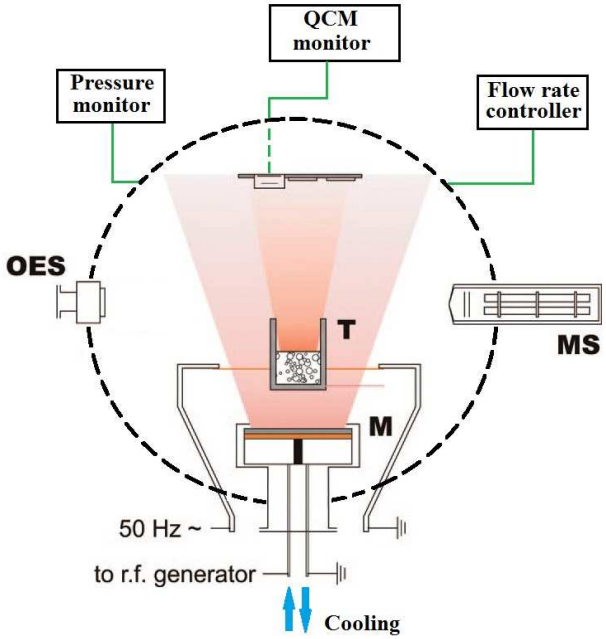

Figure 2.2. The scheme of the experimental arrangement for plasma-assisted thermal vapour deposition of PEO: QCM – quartz crystal microbalance; OES – optical emission spectroscopy; MS – mass spectrometry; T – thermocouple; M – magnetron.

Parameter	Value
Base pressure (Pa)	1×10^{-3}
Ar pressure (Pa)	1
Argon flow rate (sccm)	5
Discharge power (W)	up to 200
Deposition rate (nm/min)	5-25
Deposition time (min)	up to 60

Table 2.1. Typical experimental conditions for plasma-assisted thermal vapour deposition of PEO.

2.1.3. Atmospheric Pressure Amplitude Modulated Surface Dielectric Barrier Discharge

The surface dielectric barrier discharge was ignited at atmospheric pressure in a reactor which included an Al_2O_3 ceramic plate (100 × 100 × 0.635 mm, Al_2O_3 purity 96 %) with metallic electrodes deposited on both sides. The plate with the

electrodes was placed into a polymethylmethacrylate (Plexiglas) chamber with the gas feed input/output ports (Figure 2.3). The nickel electrode exposed to the discharge consisted of 17 parallel metallic strips (1 mm wide, 75 mm long and separated by 3 mm). An induction electrode (74 × 74 mm) covered the entire opposite side of the alumina plate [37]. Figure 2.4 shows the top view of the electrode arrangement.

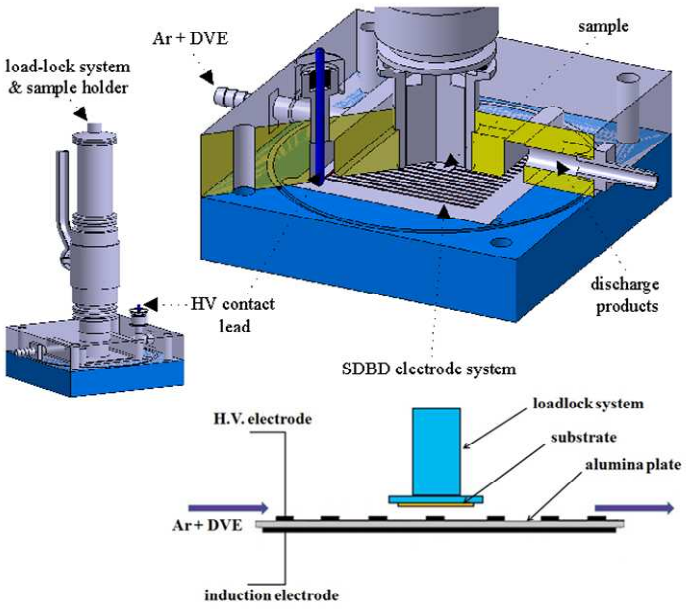

Figure 2.3. The sketch of the experimental set-up for deposition of PEO-like plasma polymers by atmospheric pressure SDBD.

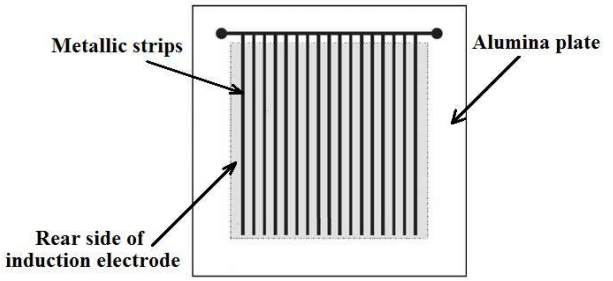

Figure 2.4. The SDBD electrode system.

The discharge was fed with argon/DVE vapors mixture. The flow of argon was fixed by a Bronkhorst HI-TEC mass-flow controller. The liquid monomer was loaded into a glass container, flushed with argon and was kept at a stable room

temperature. The concentration of DVE in Ar was 150 ppm for all the experiments. The concentration of the monomer was determined by measuring the weight difference of the DVE container before and after depositions at fixed Ar flow rate of 1 slm. The substrates were inserted into discharge zone and locked from atmospheric air by a load-lock system. The distance between the substrates and SDBD surface was varied between 1 and 10 mm. The pressure in the chamber was measured by the TPG 260 piezo gauge (Pfeifer Vacuum) and was stabilized at 104 ± 0.7 kPa.

Figure 2.5 shows the block scheme of the whole experimental set-up. The SDBD was powered by an AC power supply composed of a TG1010A Function Generator, a Powertron Model 250A RF Amplifier and a step-up transformer. The applied AC high voltage (u_{AC} = 2.0 – 6.6 kV peak-to-peak, f_{AC} = 5 kHz*)* was amplitude-modulated (modulation frequency f_M = 200-1000 Hz) producing sine-wave T_{ON}/T_{OFF} periods with a variable ($D = T_{ON}/(T_{ON} + T_{OFF})$) duty cycle [37, 94].

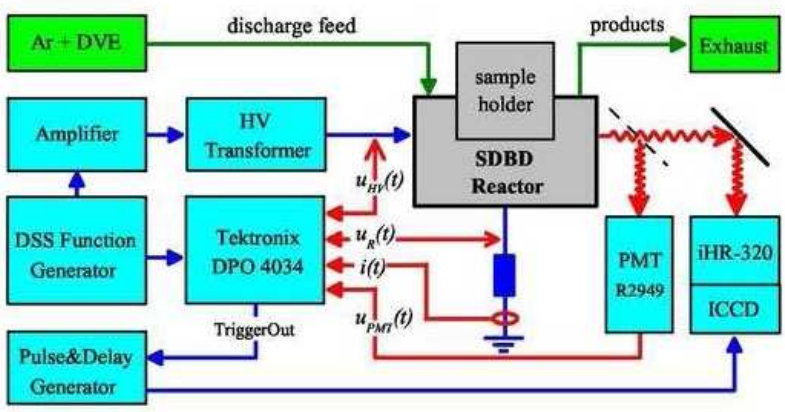

Figure 2.5. The block scheme of the experimental arrangement for the SDBD.

The voltage-charge and voltage-current characteristics of the discharge were recorded using a digitizing oscilloscope (Tektronix DPO4034). A Tektronix P6015 high voltage probe was used to sample the discharge voltage waveforms. A Tektronix P6139A high voltage probe was used to measure the drop on a transferred charge measuring capacitor (C = 0.5 μΦ) which was inserted between the induction electrode and the grounding lead. The typical operating conditions are summarized in Table 2.2.

Parameter	Value
Process pressure of Ar (Pa)	104 ± 0.7
Argon flow rate (slm)	1
Base frequency, f_{AC} (kHz)	5
Modulation frequency, f_M (Hz)	200 – 1000
AC high voltage, u_{AC} (kV)	2.0 – 6.6
Number of AC cycles	1 – 4
Duty cycle, D	0.08 – 0.8
Average discharge power (W)	1 – 6
Distance, d (mm)	3
Deposition time (min)	45

Table 2.2. Typical conditions of deposition of the PEO-like plasma polymers by atmospheric pressure SDBD.

2.2. Characterization methods

2.2.1. Mass spectroscopy

A mass-spectrometer (HAL 301 RC, Hiden Analytical) was used for monitoring of the gas phase composition at plasma-assisted thermal vapour deposition of PEO (Figure 2.2). The analyzed species were ionized in an internal electron impact source with electron energy of 70 eV. The ionized species were filtered by a quadrupole mass filter and detected by a channeltron secondary electron multiplier. The mass spectra of diethylene glycol (DGE) and triethylene glycol (TEG) were also measured for the reference.

2.2.2. Optical Emission Spectroscopy (OES)

An OES apparatus for diagnostics of low-pressure depositions consisted of an optical fiber, an ARC SpectraPro-300i monochromator with the grid and a Hamamatsu photomultiplier R928. The optical fiber was connected to the reactor through a quartz window.

In the case of the atmospheric pressure SDBD, the optical measurements were performed by means of a fast Hamamatsu R2949 photomultiplier (PMT) for surface averaged plasma induced emission (PIE) measurements and an iHR320 spectrometer (Jobin-Yvon) equipped with a DH740i-18U-03 iStar ICCD camera

(Andor) for spectrally resolved emission. The emission signal was detected by fiber through a quartz window on the top of reactor with and without optical filter with respect to wave region.

2.2.3. Ellipsometry

A spectroscopic ellipsometer (Woollam M-2000DI) was used for determination of thickness of plasma polymers deposited on polished silicon. The ellipsometric data were fitted using an effective-medium theory model.

Swelling of the PEO-like plasma polymers in water was measured in a liquid cell. The films of approximately 100 nm thickness were deposited on polished silicon wafers (1.5 × 6 cm) which were then inserted into the liquid cell. The distilled water was used for these measurements and all the swelling experiments were performed at room temperature (25 °C). The single-layer B-spline Kramers-Kronig consistent model in the spectral range 300-1100 nm were used for fitting the absorption coefficient $k(\lambda)$ and the refraction index $n(\lambda)$. Before the measurements, the liquid cell and the samples were left for at least two hours in vicinity of the beaker with water in order to stabilize the temperature.

2.2.4. Nuclear Magnetic Resonance (NMR)

The analysis of the PEO-like plasma polymers both in solid state (solid-state ^{13}C Cross Polarization Magic Angle Spinning) and of their solutions in D_2O (liquid-state ^{1}H and ^{13}C spectra) were performed by an NMR Bruker Avance 500 spectrometer operating at 500.1 MHz. The Magic Angle Spinning (MAS) frequency was 10 kHz, recycle delay 5 s and contact time was set to 1 ms. The spectra were externally referenced to the signal of the carbonyl carbon of glycine.

The relaxation delay for recording the liquid state high-resolution spectra was 10 s. The 16 and 256 scans were used to accumulate ^{1}H and ^{13}C spectra, respectively. The spectra of the PEO-like plasma polymer solutions in D_2O were referenced to the internal standard sodium 2,2-dimethyl-2-silapentane-5-sulfonate (DSS).

2.2.5. Gel Permeation Chromatography (GPC)

Gel Permeation Chromatography (GPC) was used to determine the molar mass distribution of conventional PEO as well as of the soluble fraction of the PEO-

like plasma polymers. These measurements were performed by using a chromatograph (Labio, Czech Republic) equipped with a differential refractometric detector. The 600 × 7.5 mm gel column of porosity 500 Å (Polymer Laboratories) was calibrated with polystyrene standards. The ca 3 % (w/v) solutions of polymers in tetrahydrofuran (THF) used as a mobile phase with a flow rate of 1 ml/min were prepared by intensive stirring with electromagnetic stirrer at room temperature. The fine teflon membrane filter was used to sort out unsoluble (gelled) part of the material. Toluene in low concentration (2 %, v/v) was used as an internal standard.

2.2.6. Atomic Force Microscopy (AFM)

A scanning probe microscope (Ntegra Prima, NT-MDT) with closed-loop sensors was used for measuring the surface topography of the samples in a semi-contact mode under ambient air. Standard silicon cantilevers (NSG10, k = 2 N/m, NT-MDT) were used.

The microscope also allowed performing non direct measurements of the Young's modulus by extracting its values from the force-distance curves via a procedure described in detail by Salerno and Bykov [95]. For this purpose, contact mode cantilevers (ContE-G, typical k = 0.12 N/m, Nanoandmore) were used. First, the deflection detection system of the AFM was calibrated for the force measurements by taking the detector photocurrent/distance curves on a blank silicon reference and transforming them into the force/distance curves. Indentation of silicon tip pressed against silicon substrate can be assumed negligible and therefore the change in the load corresponds directly to the change in cantilever deflection. A requirement for the precise calibration is the knowledge of the spring constant k of the cantilever, which is usually provided by manufacturers with insufficient tolerance. The accurate values of the spring constant were determined from the geometrical dimensions of the cantilevers, resonance frequency and the experimentally measured quality factor by a method of Sader [96]. The cantilevers were vibrated using the semi-contact mode resonance tuning software in the Ntegra Prima microscope (Sader_Normal script, Nova software, built 1.1.0.1851, NT-MDT) to find their resonance frequency and the quality factor. The software script calculates k with the error below 10 % [95]. After the calibration, the force/distance curves were taken with the same cantilever both on the plasma polymer samples and

on blank silicon reference. The samples with 250 nm thickness were used for the measurements. The samples were smooth with RMS roughness below 1 nm (5x5 μm scan size). This allowed excluding influence of roughness on indentation measurements. Five different spots on each sample were probed to check the reproducibility. Approaching curves were used for analysis and the approach speed was set at 40 nm/s. The curves acquired on the plasma polymer and on the silicon reference were shifted with respect to each other so that their points of contact coincided. Then indentation δ of the polymeric film was determined as the difference between the cantilever deflection on the film and on the reference for each value of force F. The Hertz theory of deformation was applied to relate the measured dependence of δ=f(F) to Young's modulus with assumption of pure elastic deformations [97, 98]. For the special case of a parabolic tip pressed against a flat surface, the Hertz theory gives the following expression [99, 100]:

$$\delta = \frac{F^{2/3}}{R^{1/3} E_{tot}^{2/3}} \tag{2.1}$$

Here, R is the radius of the tip and E_{tot} is the reduced Young's modulus given by the elastic properties of the material of the tip and of the surface [100]:

$$\frac{1}{E_{tot}} = \frac{3}{4}\left(\frac{1-\mu_s^2}{E_s} + \frac{1-\mu_t^2}{E_t} \right), \tag{2.2}$$

where μ_t, E_t, μ_s and E_s are the Poisson's ratio and the Young's moduli of the tip and the sample, respectively. The silicon cantilevers used for the measurements are much stiffer than the polymeric samples (E_t=130-185 GPa) [100] and Equation (2.2) can be reduced to:

$$\frac{1}{E_{tot}} = \frac{3}{4}\left(\frac{1-\mu_s^2}{E_s} \right) \tag{2.3}$$

Therefore, the experimentally measured indentation data can be curve-fitted with a function of the form $\delta = \alpha F^{2/3}$ and the values of the Young's modulus can be derived from the obtained values of the factor α, provided that R and μ_s are known:

$$E_s = \frac{3}{4} \frac{\left(1-\mu_s^2\right)}{\alpha^{3/2}\sqrt{R}} \tag{2.4}$$

The nominal tip radii for the ContE-G cantilevers are provided by manufacturer as R<20 nm. More accurate values of R were obtained by performing a reference measurement of a special calibration grid TGT1 (NT-MDT). The grid was scanned with the same cantilever used for the indentation measurements and the radius of curvature was derived from the acquired topography by performing image deconvolution (Image Analysis software, built 3.5.0.2065, NT-MDT). Typical values of R were 11±1 nm.

The data on the Poisson's ratio of plasma polymers, and PEO-like plasma polymers in particular, miss in the literature and some assumptions have to be made. For most of the materials, the Poisson's ratio ranges between 0 and 0.5 [95]. Therefore, the value of μ_s =0.3 was chosen as a good approximation. The uncertainty related to the values of μ results in 20 % error in Equation (2.4). The overall error in the calculation of the Young's modulus given by the uncertainties in spring constant and curvature radius of the cantilevers as well as in the Poisson's ratio of the films is estimated to be 35 %.

2.2.7. X-ray Photoelectron Spectroscopy (XPS) with chemical derivatization

The chemical composition and the structure of the films were determined by X-ray photoelectron spectroscopy (XPS). An Al Kα X-ray source (1486.6 eV, Specs) and a multi-channel hemispherical electrostatic analyzer (Phoibos 100, Specs) were employed. The XPS scans were acquired at constant take-off of 90º. The wide and high-resolution spectra were obtained with pass energy of 40 eV and 10 eV, respectively. The high-resolution XP spectra were fitted with four components. The charge compensation was performed using the position of ether group (C–O–C) at 286.5 eV which is a basic component of the PEO structure. Other peaks correspond to hydrocarbons (C-C, C-H), carbonyl- (C=O) and ester-based (O–C=O) species with relevant band energies reported in Table 2.3.

Chemical groups	**Position (eV)**
C–C, C–H	285.0
C–O–C, C–OH	286.5
C=O	288.0
O–C=O	289.5

Table 2.3. Curve-fitting components of C1s peak.

Furthermore, the chemical derivatization technique was applied for the quantitative evaluation of the OH groups [101, 102]. Trifluoroacetic anhydride (TFAA) was chosen as a chemical reagent for selective tagging of hydroxyl groups in a gas phase at room temperature. The chemical reaction of derivatization process is shown on Figure 2.6.

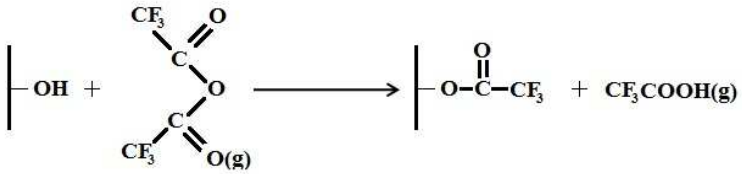

Figure 2.6. The reaction of chemical derivatization of the OH groups with TFAA.

After completion of the reaction, the XPS was applied to determine the concentration of fluorine which was used for calculation of the concentration of the OH groups by Equation 2.5.

$$[OH] = \left[\frac{[F`]}{3} / \left( [C`] - \frac{2[F`]}{3} \right) \right] \times 100\%, \qquad (2.5)$$

where [F`] and [C`] is the concentration of fluorine and carbon determined by XPS after the reaction with TFAA; [F`]/3 is the total number of the OH groups; 2[F`]/3 is the amount of carbon atoms introduced with the TFAA molecules and ([C`] – 2[F`]/3) is a real carbon concentration on the surface.

2.2.8. Fourier Transform Infra-Red Reflection Absorption Spectroscopy (FTIR-RAS)

Fourier Transform Infra Red spectroscopy (Bruker Equinox 55) was performed in a reflectance – absorbance mode. For this purpose, the plasma polymers were deposited onto the gold mirror coated glass substrates. The pure gold-covered glass substrate served as a reference. The resolution and the spectral range of measurements were set at 4 cm^{-1} (400 scans) and 400 – 4000 cm^{-1} respectively for each sample.

2.2.9. Sterilization of the plasma polymers

The films of the plasma polymers were sterilized by three commonly used techniques – UV radiation, dry heat and autoclave. The treatment by UV radiation was performed using a UV-C lamp (SANKYO DENKI G20T10) for the irradiation time of 2 hours. Dry heat sterilization was done at a temperature of 160^{o} by a hot air sterilizer (HS202A) for two hours. The autoclaving was performed at temperature of 120^{o} in de-ionized water for 1 hour by means of a commercial autoclave (Tuttnauer 2540 ELC). The thickness, morphology and chemical composition of the samples before and after sterilization was determined by spectral ellipsometry (Section 2.2.3), AFM (Section 2.2.6) and XPS (Section 2.2.7) respectively.

2.2.10. Cell adhesion

The PEO-like plasma polymers were tested for adhesion of the human MG 63 osteoblast-like cells (European Collection of Cell Cultures, Salisbury, UK) and the Balb/3T3 immortalized mouse fibroblasts. In the case of the MG63 cells, the samples were suspended in Dulbecco's modified Eagle's Minimum Essential Medium (DMEM; Sigma, U.S.A., Cat. N° D5648) with 10 % fetal bovine serum (FBS; Sebak GmbH, Aidenbach, Germany) and gentamicin (40 µg/ml, LEK, Ljubljana, Slovenia). Each dish contained 20 000 cells (i.e., approximately 5 500 cells/cm^2) and 3 ml of the medium. The cells were seeded on three samples for each experimental group and time interval. The cells were cultured in a humidified air atmosphere containing 5 % CO_2 for 1 day at temperature 37 °C. After that, the seeded samples were rinsed with phosphate-buffered saline (PBS; Sigma, USA), fixed with 70 % frozen ethanol (room temperature, 20 minutes) and stained with a combination of two fluorescence dyes, i.e. cell membrane dye Texas Red C2-maleimide (excitation maximum 595 nm, emission maximum 615 nm; Molecular Probes, Invitrogen, USA, Cat. No. T6008; 20ng/ml of PBS) and nuclear dye Hoechst #33342 (excitation max. 346 nm, emission max. 460nm; Sigma, USA; 5µg/ml of PBS) for 2 hours at room temperature. The IX-50 microscope, equipped with a DP 70 digital camera (both from Olympus, Japan, obj. 20x) was used for obtaining the number of cells on the surface which was evaluated on microphotographs.

In the case of the Balb/3T3 immortalized mouse fibroblasts, $1x10^5$ cells were seeded on the plain untreated glass slides (previously cleaned in acetone and

sterilized under UV light) and on the PEO-like polymers (sterilized under UV light), previously put in Petri dishes (100 mm for glass slides and 60 mm for the films) in complete culture medium. After one day, the culture medium was changed removing the old one and adding the fresh one (5 mL). At the last day, the culture medium was removed and 200 µL of staining solution was dropped onto the surface of each slide. The glass slide was immediately removed from the Petri dish and protected with a cover slip. After that the cell growth, their morphology and behavior on the surface were immediately analyzed using the optical microscope and fluorescent microscope ApoTome system ZEISS.

2.2.11. Protein adsorption

Non-fouling of the PEO-like plasma polymers was studied in terms of their resistance to adsorption of blood proteins by measuring a Quartz Crystal Microbalance (QCM) (Maxtek, inc.) resonance frequency shift which directly depends on the mass deposited on the crystal surface. Fibrinogen from bovine plasma, bovine serum albumin (BSA) as well as immunoglobulin (IgG) were selected for the adsorption tests because they are the most abundant proteins in blood. Phosphate Buffered Saline (Dulbecco's PBS) was utilized as the solvent. Only freshly prepared solutions of these proteins were used. Prior to the measurements, the PEO-like film was deposited on the QCM surface. The crystal was then placed into a beaker with 100 ml of pure PBS and left for at least 30 minutes at room temperature in order to stabilize the frequency. After reaching the steady state, 10 ml of 5 mg/ml protein solution was added to the beaker to obtain a final concentration of 50 µg/ml. The kinetic measurement of the protein adsorption was started immediately thereafter. No stirring was used. All the measurements were performed at ambient temperature. The study of the ability of the PEO-like plasma polymers to withstand the accumulation of the fibrin network was performed on the micropatterned samples. Pure silicon (n-type, (100), 1.5×1.5 cm) served as a reference. The fibrin network was formed through polymerization of fibrinogen by thrombin [103]. The patterned samples were prepared by using the copper grids (G2655C and G2016C, Agar Scientific) in two steps. First, a 100 nm thick continuous protein adhesive film (150 W, 30 % of C–O–C) was deposited on silicon. Then, a 100 nm thick protein resistant film (5 W, 75 % of C–O–C) was deposited through the grid attached to the

first layer. After removing the grid, the pattern of the protein-adhesive and protein-resistant areas was obtained. The study of fibrin accumulation included the following stages:

- the samples were immersed into the 15 ml of a 100 $\mu g \cdot ml^{-1}$ solution of fibrinogen in PBS;
- the fibrin gel was created by adding of the 0.9 ml of the 17.9 NIH $units \cdot ml^{-1}$ solution of thrombin;
- the samples were kept in this solution for one hour;
- the fibrin clots were rinsed with PBS and deionized water, dried in air and then analyzed by AFM.

2.2.12. Interaction with blood plasma and blood serum

The irreversible fouling from biological media on substrates coated by the PEO-like plasma polymer films was measured by Surface Plasmon Resonance (SPR) using an instrument based on the Kretschmann geometry and spectral interrogation [104, 105]. PEO-like coatings were deposited on SPR chips. A solution of phosphate buffered saline was firstly injected until a stable baseline (resonant wavelength is achieved). Subsequently, the tested solutions of lysozyme (1 $mg \cdot mL^{-1}$), fibrinogen (1 $mg \cdot mL^{-1}$), undiluted blood plasma and serum were driven for 15 min by a peristaltic pump through four independent channels of a flow cell in which SPR responses were measured simultaneously at 25 ºC. The difference in the resonant wavelength before and after the contact with the protein solutions is directly proportional to the mass of protein adsorbed, i.e. 1nm = 150 $pg.mm^{-2}$.

2.3. Materials

Conventional poly(ethylene oxide) (Sigma-Aldrich, M=1500 $g \cdot mol^{-1}$) was used for magnetron sputtering and plasma-assisted thermal vapour deposition experiments. Argon was used as a working gas. Microscopic glass slides (Marienfeld, Germany, 76 × 26 × 1 mm) were used as substrates for biological tests. Silicon polished wafers (n-type (100), On Semiconductor Czech Republic, a.s.) were used as substrates for XPS, AFM and ellipsometry. Gold-mirror covered microscopic glass substrates (1 × 1 cm) were used for FTIR-RAS analysis. The flat glass plate with the size of 20 × 20 cm was used as to deposit bigger amounts of plasma

polymers for the NMR and GPC studies. Prior to the experiments, all the substrates were ultrasonically cleaned in acetone, alcohol and distilled water with successive drying by a nitrogen flow.

The Cr/Au polished QCM crystals (5 MHz, Maxtek, Inc.) pre-mounted in a crystal-holder (CHC-100, Maxtek) were used for analysis of adsorption of proteins. Copper grids G2655C with 600 mesh thin bars and G2016C with 400 parallel bars (Agar Scientific) with thickness of 3.05 mm were used for preparation of micropatterned samples for the tests on thrombogenicity. The BK 7 (chips) glass coated with 5 nm thick Ti and 50 nm thick gold layers were used for the SPR analysis of the interaction of PEO-like plasma polymers with blood components. The chips were acquired from the Institute of Photonics and Electronic, Academy of Science of the Czech Republic.

All the chemicals including di(ethylene) glycol vinyl ether (DVE) (purity 98 %), fibrinogen from bovine plasma, bovine serum albumin (BSA), bovine immunoglobulin (IgG), thrombin from bovine plasma, Dulbecco's PBS were purchased from Sigma-Aldrich, Inc.

Human MG 63 osteoblast-like cells (European Collection of Cell Cultures, Salisbury, UK) and Balb/3T3 immortalized mouse fibroblasts were used for *in vitro* study of cell adhesion on the PEO-like plasma polymers.

3. Results and Discussion

3.1. Magnetron sputtering

During the sputtering of the PEO target, two distinct regions were observed. At the 20 W power, the deposition rate was constant at 8 nm/min in the first minutes of the experiment. After 9 min, the temperature of the target reached 45 ºC due to heat dissipation from the ion bombardment. At this point, the deposition rate significantly increased as a result of thermal co-evaporation of melted PEO.

For the analysis of these regimes, two types of the samples were prepared. The first series of the samples (referred to as sample 1) was obtained during the first 6 min of the sputtering. The second series of the samples (referred to as sample 2) was deposited for 2 min after the start of the co-evaporation process. The sample 2 was preliminary covered by the shutter until the onset of the co-evaporation.

Only the carbon and the oxygen atoms were present in the deposited plasma polymer films, as revealed by the XPS analysis. The wide spectrum of XPS shows 60 % of C and 40 % of O for the sample 1 and 64 % of C and 36 % of O for the sample 2. The C1s high resolution XPS spectra detected the drastic difference between the samples 1 and 2. The high content of hydrocarbon bonding environment can be found in the sample 1 (Figure 3.1a) with a small amount of the ether groups (only 17 %). The presence of highly oxidized carbon functionalities such as the carbonyl-based species (14 %) and esters (5 %) was also detected. In the case of the sputtering in co-evaporation regime (sample 2), the higher retention of the PEO structure was observed (Figure 3.1b). The content of the C–O–C/C–OH chemical groups reached 54 %, the concentration of the hydrocarbons reduced down to 27 % whereas the amount of carbonyls and esters stayed the same for both samples.

The confirmation of the XPS results was obtained by the FTIR analysis as well (Figure 3.2a and b). The detailed assignment of the FTIR spectra will be given further in the section 3.2.3. Briefly, the spectra consist of the absorption bands around 3400 cm^{-1} (OH stretching), 2900 cm^{-1} (CH_x stretching), 1720 cm^{-1} (C=O stretching), 1610 cm^{-1} (C–C stretching), the absorption region between 1450 and 1250 cm^{-1} belonging to various deformation vibrations of CH_x groups, and the band at 1110 cm^{-1} (C–O–C stretching). The enhanced intensity of hydroxyls and unsaturated carbon species were detected on the FTIR spectra of the sputtered film

(Figure 3.2a). In this case, the high extent of disorder in the film was indicated by the broadening of the absorption bands throughout the spectrum that is a known effect for plasma polymers.

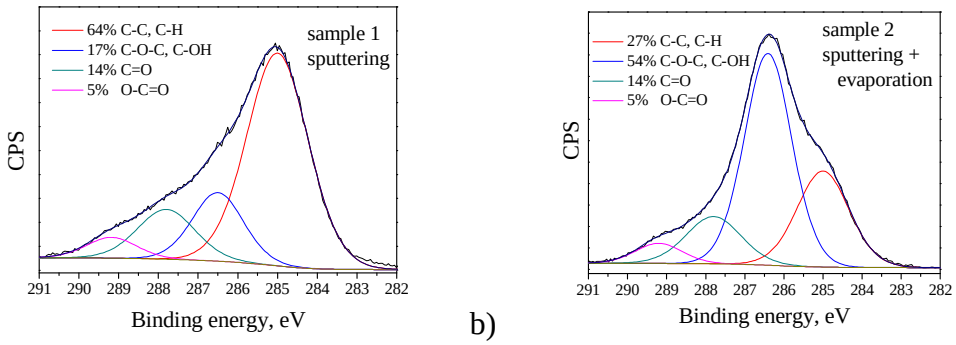

Figure 3.1. The C 1s XP spectra of the PEO-sputtered plasma polymers: a) sputtered without co-evaporation and b) with co-evaporation.

In contrast to the sputtered film, the spectra of the films deposited in the co-evaporation regime (sample 2) show the strong absorption form the C–O–C functional groups. The signal from OH, C=O and C=C species is reduced in this case as compared to absorption of ethers (Figure 3.2b). Nevertheless, even in the case of the co-evaporation regime the retention of the C-O-C groups was not sufficient and never reached 65-70 % required for the non-fouling behaviour. Moreover, sputtering in the co-evaporation regime was accompanied with splashing of the microdroplets of melted PEO from the target. This significantly deteriorated the homogeneity of the resultant films. Therefore, a new deposition strategy was chosen where melting of PEO was conducted in a separate crucible while the magnetron was used to maintain the discharge (see next Section).

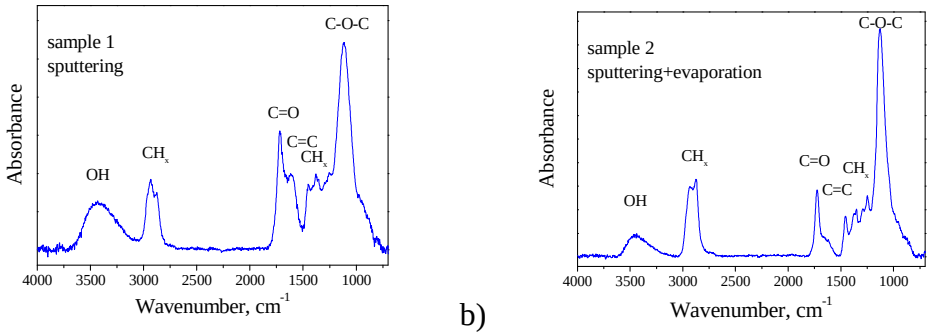

Figure 3.2. The FTIR spectra of the sputtered PEO-sputtered plasma polymers: a) sputtered without co-evaporation and b) with co-evaporation.

3.2. Plasma-assisted thermal vapor deposition

3.2.1. Deposition rate

The temperature of the crucible with PEO granules was controlled by electrical current and the deposition rate was measured by the shift of the resonance frequency of QCM. Thickness of the deposits for each specific temperature was determined by spectroscopic ellipsometry (see Section 2.2.3). The deposition rate was then recalculated from the values of QCM frequency shift as a function of temperature (Figure 3.3). PEO started to melt in the crucible at about 60 ºC and this was visualized through a chamber window. However, the first deposits were not detected until 260 ºC. The mass spectra did not reveal the changes in the gaseous phase composition until 260 ºC either. Starting from 260 ºC, the deposition rate increased with temperature almost exponentially and reached 25 nm/min at 320 ºC.

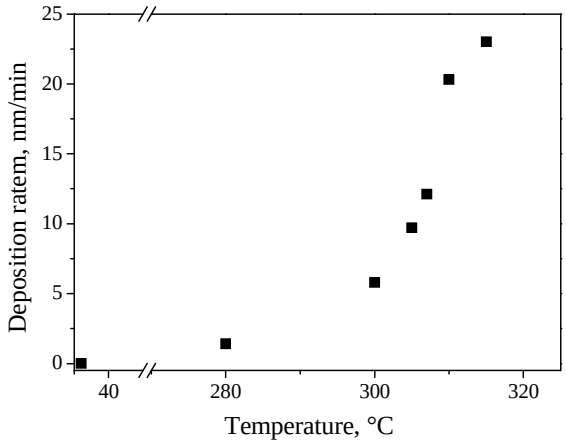

Figure 3.3. The deposition rate of the polymeric film as a result of vacuum thermal decomposition of PEO.

3.2.2. The mechanism of vacuum thermal degradation of PEO

The mass spectra of the gaseous phase in the chamber were taken under 1 Pa argon pressure with crucible being at room temperature and at 320 ºC (Figure 3.4). The spectrum acquired at room temperature (black color) consists of the species with $m/z < 45$ in which the most abundant species are Ar^+ and Ar^{2+} with $m/z = 40$ and 20.

Expectedly, the components of residual air are detected through the *m/z* =14 and 28 (N_2), 16 and 32 (O_2), 18 (H_2O) and 44 (CO_2).

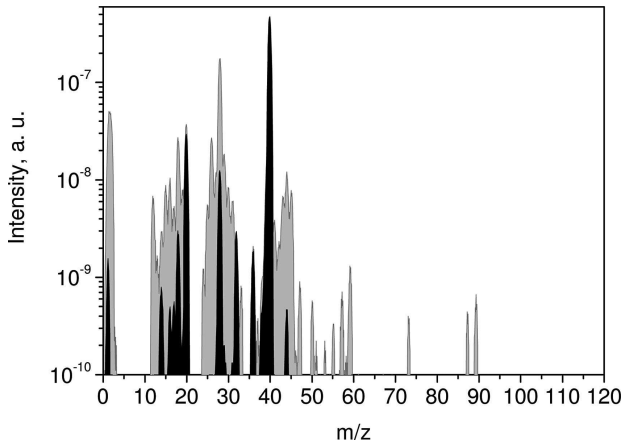

Figure 3.4. The mass spectral analysis of vacuum thermal decomposition of PEO (Ar, 1Pa): black, PEO at 25 ºC; gray, PEO at 320 ºC.

When the temperature of the crucible with PEO was raised up to 320 ºC the mass spectrum (gray color) significantly changed. Since the pressure of argon was held constant, the intensity of the lines with *m/z* = 40 and 20 did not changed within the experiments. Furthermore, the leak into the chamber from the outer atmosphere was checked to be constant before and after the deposition. Therefore, all the changes detected in the mass spectra can be attributed to emission of the volatile fragments from the PEO melt.

The mass spectrum is characterized by the drastic changes in intensity of the lines with *m/z* = 1–2, 12–18, 24–34, 44, and above. The signal of hydrogen increased almost 2 orders of magnitude that can be explained by the cleavage of the CH and OH bonds of the PEO molecules. The lines of the C, CH_x, OH, and H_2O species with *m/z* =12–18 are also enhanced but not as much as hydrogen. The strong increase of the *m/z* = 28 can be assigned to emission of C_2H_4 and CO. The set of the lines around *m/z* = 44 is attributed to a number of the fragments of the PEO backbone such as CH_2CH_2O, CH_3COH, CH_3–O–CH_3, and CH_3–CH_2–OH or to CO_2. The spectrum is also remarkable for the presence of higher *m/z* species which belong to the fragments with more than one monomer unit.

The evolution of the individual peaks in the mass spectra was monitored continuously with heating. The dependence of intensity of hydrogen, CO/C_2H_4, and

H_2O on the temperature of the PEO melt is shown in Figure 3.5. Other species are not shown for simplicity reasons. All the intensities were normalized to Ar, *m/z* = 40. After reaching 260 ºC, most of the mass spectral bands increase with respect to argon except for H_2O. The strongest increase is apparent for the CO/C_2H_4 peak while the signal from H_2O stays at a constant level throughout the entire temperature range. Thus, thermal degradation of PEO proceeds with the scission of the polymeric chains and elimination of volatile species with a wide distribution of molecular weights.

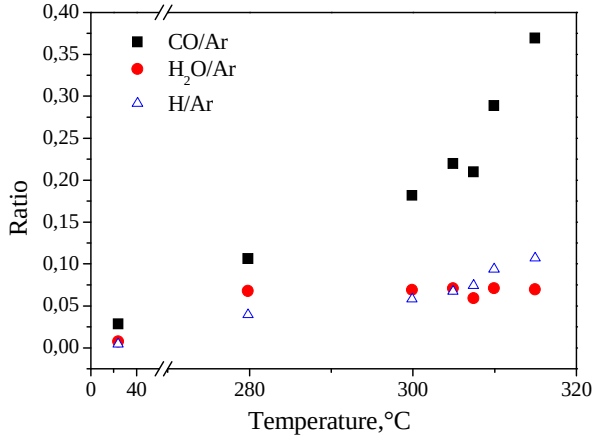

Figure 3.5. The evolution of the individual peaks of the mass spectral bands with the temperature of the PEO melt.

The next mass spectra were taken in the similar arrangement but without argon in the chamber. After evacuating the system down to 10^{-3} Pa the heating was started. The pressure in the chamber was set at 1 Pa when the temperature reached 320 ºC. The mass spectrum was composed, in this case, of the emitted fragments of PEO and residual gases (Figure 3.6a). The spectrum of residual gases obtained at 25 ºC is also shown here for reference.

A wide spectrum of the emitted fragments of PEO with the highest *m/z* = 112 is seen in Figure 3.6a. One should bear in mind that diverse fragmentation pattern measured by the detector in the mass spectrometer is given by two stages of fragmentation of PEO: decomposition of the polymer in the crucible by the influence of elevated temperature and fragmentation of evaporated species of unknown composition in the ionization source of the mass spectrometer. Consequently, an uncertainty exists about the origin of the ions. In mass spectrometry, a conventional way to indentify the unknown compound is to compare its spectrum with that of the

compound of defined composition. For correct identification, it is necessary to find the proper reference. In our case, starting from *m/z* = 44 the spectrum consists of a series of the lines similar in shape and with the maxima separated by Δm/z =14 or 16, which is reasonable to assign to the -CH_2- and -O- residues of the polymeric backbone (Table 3.1). This assumption can be further supported by comparison of the bond energies. The dissociation energy of the C-O-C and C-C-O bond is lower compared to C-H and hence it is generally expected that decomposition of PEO starts with the random scission of the backbone bonds. Therefore, assuming that the volatile fragments are composed of the combination of -CH_2- and -O- residues, their molecular structure can be guessed by comparison against the mass spectra of ethylene glycol homologues of known composition. For this purpose, di- and triethylene glycol (DEG and TEG, M = 106 and 150 g·mol^{-1}, respectively) were used (Figure 3.6b and c).

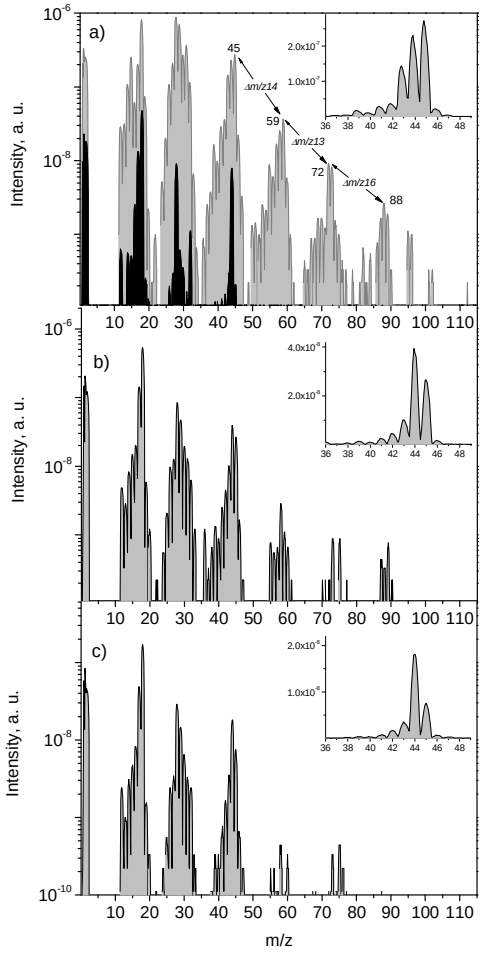

Figure 3.6. The mass spectra of the gaseous phase in the vacuum chamber without Ar: a) PEO at 25 ºC (black) and at 320 ºC (gray); b) TEG at 40 ºC; c) DEG at 25 º C.

The mass spectral bands are centered at *m/z* = 2, 18, 28, 44, 58, 73 for DEG. The same pattern is observed in the case of TEG with additional band appearing at *m/z* = 89. Since the spectra remain almost unchanged with increasing mass in the homologous series (di- and triethylene glycol), it indicates that the fragmentation phenomena occur in the same manner regardless of the molecular mass of the monomer. The mass spectra of DEG and TEG are almost identical to the pattern observed for evaporation of PEO. Such affinity proves that the gaseous phase in the vacuum chamber during experiments with PEO is mainly composed of PEO oligomers with a different number of monomer units.

Species	**Calculated** ***(m/z)***	**Detected maxima** ***(m/z)***
-CH_2–CH_2–O-	44	45
-CH_2–CH_2–O–CH_2-	58	59
-CH_2–CH_2–O–CH_2–CH_2-	72	73
-CH_2–CH_2–O–CH_2–CH_2–O-	88	88
-CH_2–CH_2–O–CH_2–CH_2–O–CH_2-	102	103

Table 3.1. Assignment of the most intensive mass spectral lines at vacuum thermal decomposition of PEO.

The mass spectra of the ethylene glycols on the Figure 3.6 b) and c) do not show the species with *m/z* > 102. It does not necessarily mean, however, that such fragments are not present in the chamber volume as the mass spectra of ethylene glycols do not show the species of higher m/z either. This fact can be explained by the long distance between the detector and the evaporation source which restricts the transport of heavy particles to the ionization chamber. Furthermore, transmission function of the quadrupole is mass-dependent, and its poor sensitivity to ions of higher mass also restricts their detection.

The presence of the low mass species in the spectra of DEG and TEG indicates that the fragmentation of the monomers occurs in the ionization source of the spectrometer. Therefore, the mass spectrum of evaporated PEO, which is also rich in light masses, hardly represents accurately the actual fragmentation induced purely by thermal means. Nevertheless, unlike the ethylene glycols, the spectrum of PEO shows the strongest peak at *m/z* = 28. This means that the CO and probably the

C_2H_4 species are released not only as a result of fragmentation phenomena in the mass spectrometer but also due to thermal degradation of the original polymer.

The difference between the ethylene glycol homologues and PEO can be also observed at higher *m/z* in intensity of the species with $M - n$ (n = 1, 2, 3, …), where M is *m/z* of the most intensive peak of the individual bands. For the ethylene glycols, the amount of the species with $M - n$ is much smaller than that of the M peak (see also the insets of Figure 3.6a–c). Furthermore, for evaporated PEO the wider distribution of *m/z* is detected and there intensity is stronger. This fact indicates that formation of such species may not be originated exclusively in the ionization chamber of the mass spectrometer but they are also emitted into the chamber volume at the evaporation process. The species with *m/z* several units less than a simple sum of CH_2 and O are attributed to the fragments which are strongly dehydrogenated; this is also supported by the strong signal from hydrogen at *m/z* = 1 and 2. Cleavage of a hydrogen atom leaves a free radical or, if two hydrogen atoms are removed from the neighboring carbons, the recombination of the radicals with formation of the double C=C bond is possible. Nevertheless, such dehydrogenated species are in minority with respect to PEO oligomers. For example, the intensity of the left-hand side shoulder of the band centered at *m/z* = 59 is rapidly decreasing as it is shown on the Figure 3.6a. It is also worth noting that the maxima of the bands of evaporated PEO are located at the m/z which exceed by 1 those calculated for a mere combination of the CH_2 and O species. This means that capture of hydrogen atoms by oligomeric fragments also takes place. The contribution from higher isotopes (^2H, ^{13}C, or ^{17}O) can be ruled out here as their natural abundance in the corresponding elements is low [106]. Taking into account the appearance of both the dehydrogenated species and the species with excess of hydrogen, radical termination by disproportionation can be suggested as the possible mechanism of thermal decomposition of PEO. In this mechanism, a radical at the end of one chain attacks a hydrogen atom in the other chain [1]. As a result, a hydrogen atom is transferred to the first chain whereas a double C=C bond is created in the other (Figure 3.7). The presence of the C=C functional groups in the deposited films was confirmed by FTIR spectroscopy (see section 3.2.3).

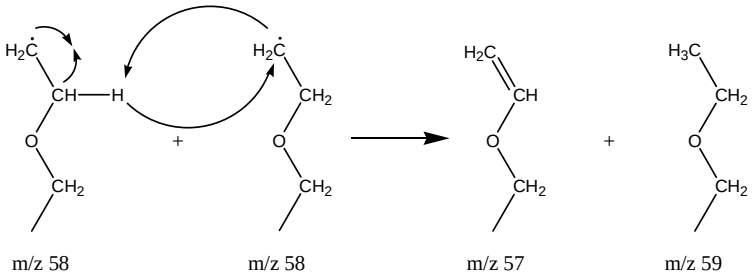

Figure 3.7. The mechanism of radical termination by disproportionation.

The films deposited by pyrolysis of conventional polymers were frequently reported in the literature as being “waxlike” since such films are mainly composed of the lower molecular weight fragments of original macromolecules [24, 107]. Different post-deposition treatment methods were suggested to increase the cross-linking within the films, including UV irradiation and annealing [108]. Ionization-assisted evaporation was also considered to ionize the volatile fragments by electron impact and direct them onto negatively biased substrate [30, 31].

In this work, the stream of the species released by thermal decomposition of PEO was allowed to pass through a zone of the glow discharge. Figure 3.8 shows the mass spectra of the chosen species with the bands centered at *m/z* = 2, 28, and 59. These patterns were taken in two regimes: without plasma and with 5 and 60 W plasma turned on. The application of the glow discharge leads to ablation of hydrogen from the macromolecular fragments by electron impact and, as a result, to increase of atomic and molecular hydrogen concentration. The amount of the species with *m/z* = 28 increases insignificantly. These most probably correspond to the CO molecules as their presence was confirmed by independent OES measurements (see below). For the species with higher masses, the reverse behavior is observed where even 5 W power discharge results in the decrease of their amount. The species with *m/z* > 60 were not detected when the plasma was on. It can be explained by the enhanced fragmentation of the higher mass species.

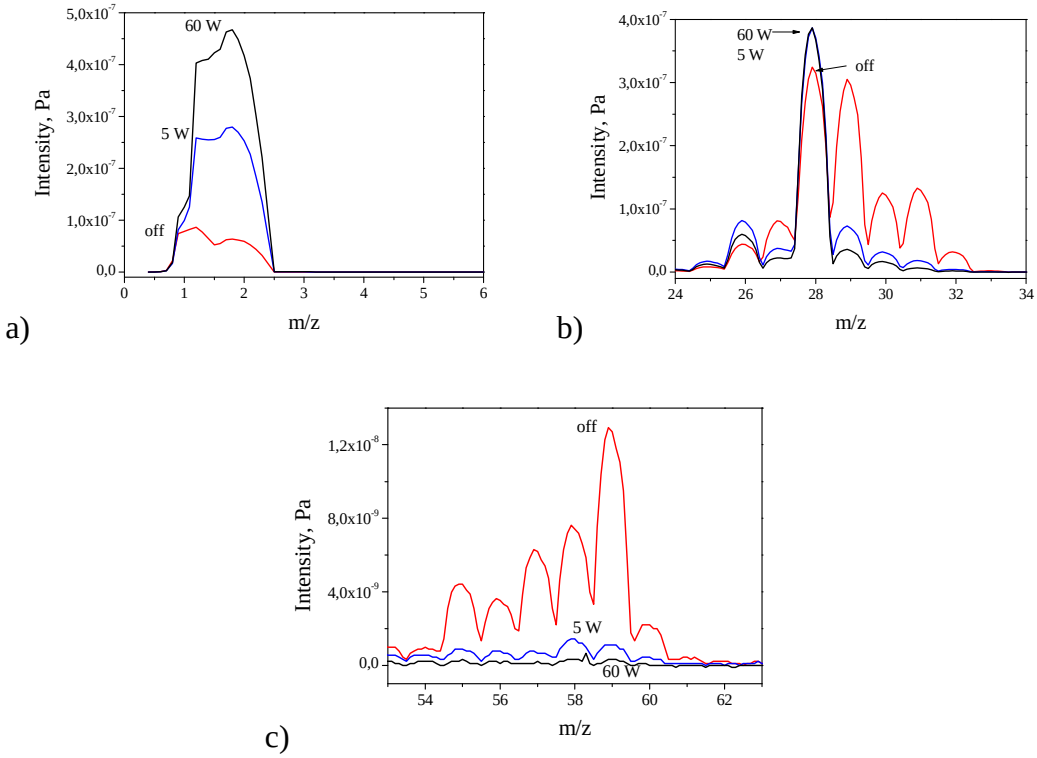

Figure 3.8. The mass spectra of evaporated PEO acquired with and without plasma: a) *m/z* = 2, b) *m/z* = 28, c) *m/z* = 59

Further characterization of the gas phase composition was performed by OES. The OES spectra were acquired in two regimes:

- with argon as a working gas;
- without argon.

In the last case, the discharge was ignited only in the vapors of the volatile products of thermal decomposition of PEO. Both spectra (Figure 3.9) were acquired during the same experiment under the same conditions (temperature of the PEO melt, pressure, and power of the discharge) so that the only difference was the composition of the gas phase.

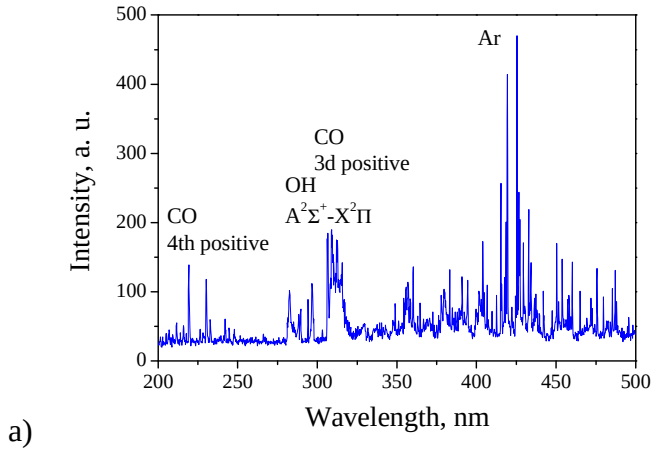

a)

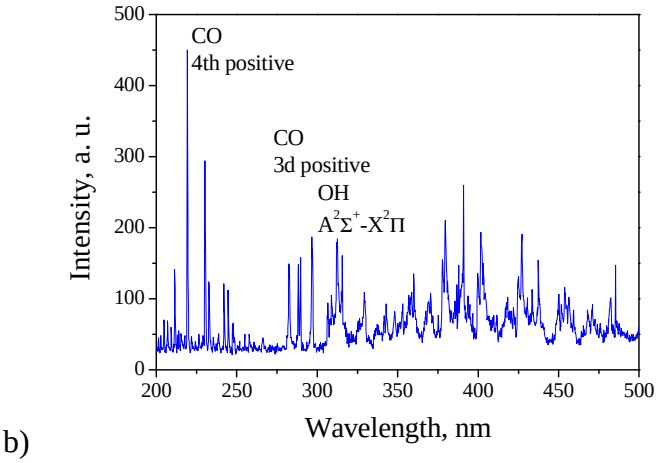

b)

Figure 3.9. The optical emission spectra of the glow discharge ignited at 50 W power in vapors of PEO a) with and b) without Ar.

In spite of the fact that the interpretation of the OES is often complicated by a large number of the available species, in our case several bands can be definitely assigned according to [109]. For example, emission of the fourth positive ($A^1\Pi^+ - X^1\Sigma$) and the 3^d positive ($b^3\Sigma - a^3\Pi$) systems of CO with the probable contribution of the Cameron and 5B bands was indentified. The OH groups were identified through the $A^2\Sigma^+ - X^2\Pi$ system. The lines of neutral argon were present only in the spectrum of the discharge with argon whereas they vanished when the argon inlet was shut off. The emission of CO is significantly enhanced in the case of deposition without argon as it can be seen from a comparison of the line of CO at 219.2 nm against the line of OH at 308.8 nm (Figure 3.9). The concentration of the OH groups is not much influenced by the action of plasma. It was shown above that the concentration of water molecules is not influenced by the temperature of the PEO melt either (Figure

3.5). Apparently, neither thermal degradation nor fragmentation by electron impact leads to the enhanced release of the OH/H_2O species. This contrasts with thermal degradation of other oxygen-containing polymers such as, for example, poly(vinyl alcohol), which contains hydroxyls as side groups bonded to a hydrocarbon backbone and which degrades with elimination of water [110, 111, 112, 113].

3.2.3. Chemical composition

X-ray Photoelectron Spectroscopy (XPS)

The plasma polymers deposited at a constant rate (5 nm/min) with various discharge powers (form 1 W to 200 W) significantly differ in their composition. The XPS analysis shows a trend of increasing carbonization with increasing power of discharge (Figure 3.10). The films deposited without application of plasma and with plasma at lower power contain approximately 62.0 % of C and 38.0 % of O with C/O ratio of 1.63 (without accounting for hydrogen, undetectable by XPS). For conventional PEO used as the precursor, the same values were obtained which are somewhat lower than expected from the structural formula calculations (66.7 % C and 33.3 % O). With increasing power of discharge, the carbon content increased up to 68.0 % while the oxygen content reduced to 32.0 %. This is consistent with the above mass spectroscopic data showing intensive formation of carbon monoxide in the gas phase with increasing power. CO is effectively pumped out of the reactor leaving the resultant films deficient in oxygen.

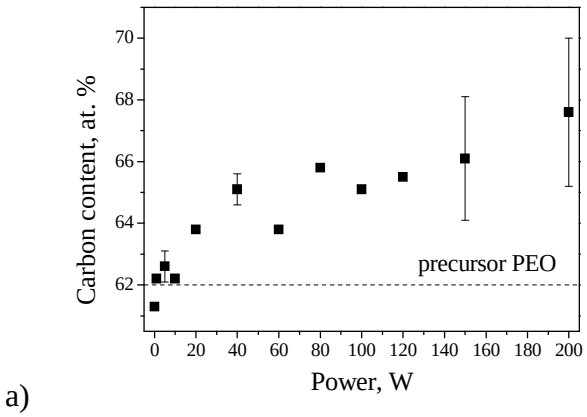

a)

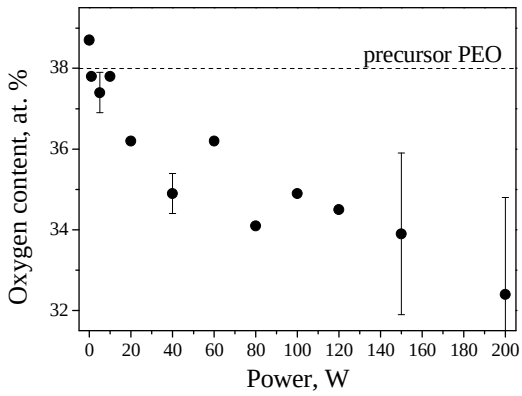

b)

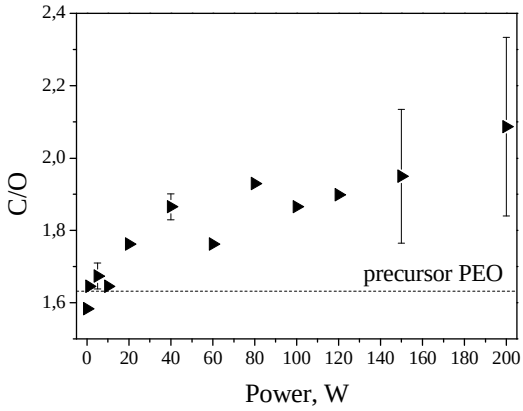

c)

Figure 3.10. The elemental composition of the PEO-like plasma polymers in dependence on power of discharge: a) the carbon content; b) the oxygen content; c) the ratio of carbon to oxygen.

Figure 3.11 shows the evolution of the high-resolution C1s XPS spectra of the films prepared with increasing power of discharge as well as that deposited without plasma. Similar to the magnetron sputtered films, the spectra can be deconvoluted into four components located at 285.0eV (C-C, C-H), 286.5eV (C-O-

C), 287.8eV (C=O) and 289.0eV (O-C=O). However, stronger abundance of the peak at 286.5 eV was achieved by plasma-assisted thermal vapour deposition as compared to magnetron sputtering. Strictly speaking, the component at 286.5 eV can be contributed by the hydroxy- and epoxy groups as well. The tests on chemical derivatization of the OH groups with TFAA showed that only 1 – 2 % of carbon atoms were bound with hydroxyls in the films evaporated without plasma and 5 – 7 % for the films deposited with plasma. The insignificance of epoxy groups has been also proved by the FTIR analysis (see the next Section). Therefore, the component at 286.5 eV is assigned hereafter mainly to ethers.

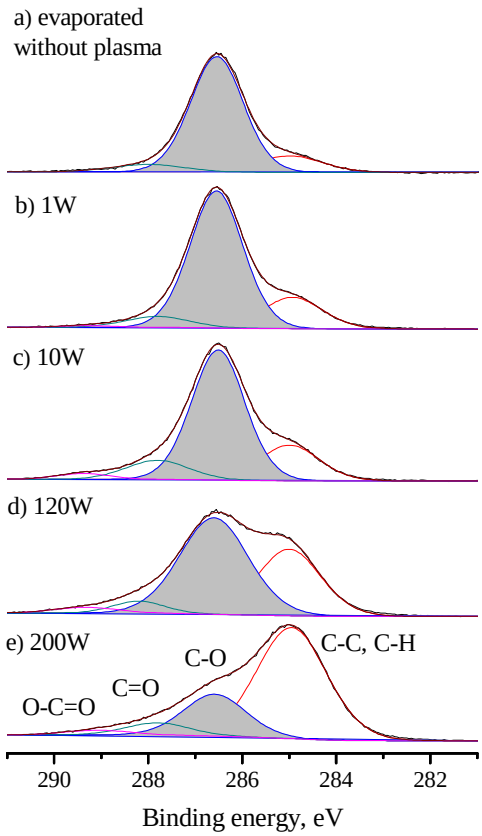

Figure 3.11. The evolution of the C1s XPS spectra of the PEO-like plasma polymers as a function of the discharge power: a) evaporated without plasma; b) 1W; c) 10W; d) 120W; and e) 200W.

For the films deposited without plasma, 80 % retention of the C–O–C groups and only 14 % of the C–C/C–H was detected. These values are very close to those of

original PEO used as the precursor (88 % of the ether and 6 % of the aliphatic hydrocarbons). The increase of power is accompanied by increasing of the hydrocarbon component whereas the concentration of the C–O–C groups is decreased. Such changes are minimal at the powers below 10 W for which the concentration of the ether groups is still about 75 %. At higher power of discharge the peak of the C–C/C–H components dominates the spectra. For example, at 200 W the concentration of aliphatic hydrocarbons reaches 55 % and ether components reduce to 34 %. Such behaviour is attributed to intensive fragmentation of the released PEO oligomers at higher power with successive re-arrangement of the fragments into a hydrocarbon network deficient with the ether groups. Incorporation of other species such as C=O (9 ± 2 %) and O–C=O (3 ± 2 %) is not significantly influenced by the power of discharge.

Fourier Transform Infra-Red Spectroscopy (FTIR)

FTIR analysis offers additional information on the chemical composition of the resultant films. Figure 3.12 shows the FTIR spectra of the PEO-like plasma polymers prepared with and without plasma. The spectrum of original PEO precursor is shown for comparison as well.

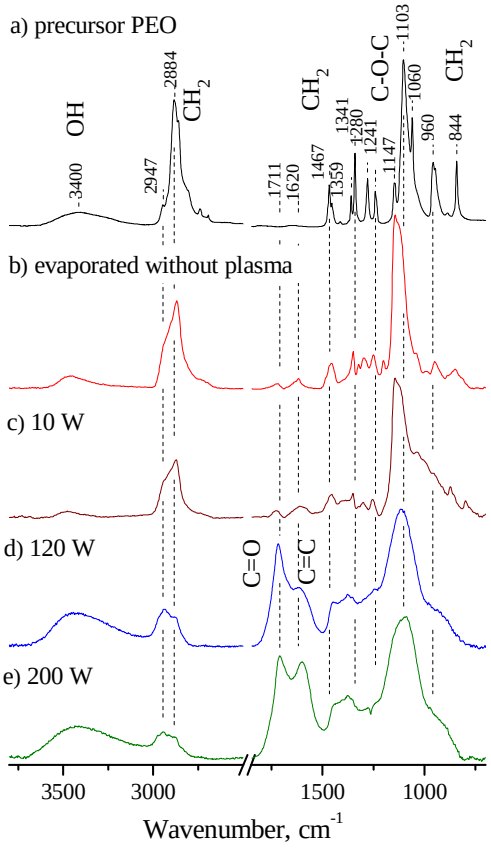

Figure 3.12. The FTIR analysis of the PEO-like plasma polymers as a function of the discharge power: a) precursor PEO; b) evaporated without plasma; c) 10 W; d) 120 W; e) 200 W.

The spectrum of conventional PEO (Figure 3.12a) contains the stretching vibrations of the hydroxyls (≈ 3400 cm^{-1}) and CH_2 groups (weaker asymmetric stretching at 2947 cm^{-1} and very strong symmetric at 2884 cm^{-1}), a number of the deformation vibration bands of the CH_2 groups including the asymmetric bending at 1467 cm^{-1}, the wagging doublet at 1359 cm^{-1} (symmetric wagging coupled with the stretching of the C–C bond) and 1341 cm^{-1} (asymmetric wagging), twisting at 1280 cm^{-1} (symmetric) and 1241 cm^{-1} (asymmetric), and two rocking bands at 960 cm^{-1} (symmetric rocking coupled with the stretching of the C–C bond) and 844 cm^{-1} (asymmetric rocking). For the ether structure, a very strong asymmetric stretching vibration at 1103 cm^{-1} is observed. The smaller side peaks at 1147 and 1060 cm^{-1} correspond to the coupling of the ether structure with the stretching of the C–C bond

and with the symmetric rocking of the CH_2 group, respectively. All the band positions and assignments for the precursor PEO and for the plasma polymer films are summarized in Table 3.2.

Mode assignment*	**Band position (cm^{-1})**		
	Precursor PEO	**Evaporated without discharge**	**Evaporated with discharge at power 1 → 200 W**
νOH	3200 – 3600	3200 – 3600	3200 – 3600
$\nu_{as}(CH_2)$	2947	2945	2946 → 2946
$\nu_{s}(CH_2)$	2884	2870	2870 → 2879
ν(C=O)	-	1724	1724 → 1711
ν(C=C)	-	1620	1618 → 1602
$\delta_{as}(CH_2)$	1467	1460	1458
$w_{s}(CH_2)$ + ν(CC)	1359	1350	1352
$w_{as}(CH_2)$	1341	-	-
$t_{s}(CH_2)$ + $t_{as}(CH_2)$	1280	1300	1286
$t_{as}(CH_2)$	1241	1250	1247
ν(CC) – ν_{as}(COC)	1147	-	-
ν_{as}(COC)	1103	1146	1100
ν_{as}(COC) + $r_{s}(CH_2)$	1060	1042	-
$r_{s}(CH_2)$ – ν_{as}(COC)	960	949	-
$r_{as}(CH_2)$	844	849	-

*The assignment follows the ref. [114] with ν=stretching, δ=bending, w=wagging, t=twisting, r=rocking.

Table 3.2. The FTIR band positions and assignment for the PEO-like plasma polymer films.

All the measurements were performed at room temperature which was below the crystalline/amorphous phase transition temperature (≈60 ºC) usually observed for PEOs. As expected, the sharp character of the bands and their positions measured for the precursor PEO (Figure 3.12a) correspond within 2 cm^{-1} to those reported for crystalline phase [114, 115, 116]. The spectrum of the film prepared without plasma (Figure 3.12b) retains the feature of the band positions measured for the precursor PEO (Figure 3.12a). It also supports the mass spectral findings (see Section 3.2.2) showing that thermal degradation of PEO proceeds with random scission of the backbone and that oligomeric fragments released into the gas phase are mainly

composed of the repeating (–CH_2–O–) unit. Nevertheless, the spectrum of evaporated film exhibits shifts and broadening of the adsorption bands as compared to the precursor PEO (see also Table 3.2). This was attributed to transition from the crystalline to amorphous phase at which various molecular structural conformations may give rise to a wider distribution of intermolecular interactions [116]. The differences between the evaporated film and the precursor PEO can be observed in the entire range of wavelengths. The ν_{as}(COC) vibrations are shifted from 1103 cm^{-1} characteristic for crystalline phase to 1146 cm^{-1} characteristic for amorphous phase. The rocking $r_s(CH_2)$ vibrations at 960 cm^{-1} and the twisting $t_{as}(CH_2)$ vibrations at 1241 cm^{-1} shift to 949 and 1250 cm^{-1} respectively. The wagging doublet $w_s(CH_2)$ at 1359 cm^{-1} and $w_{as}(CH_2)$ at 1341 cm^{-1} merges into one band at 1350 cm^{-1}. Such behavior of the rocking, twisting and wagging vibrations of the ether methylene units was previously observed and explained also by transition from crystalline to amorphous state [115, 116]. By analogy, the changes in the band positions observed here indicate the loss of order in the evaporated film. This can be explained by higher mobility of the lower molar mass PEO fragments arriving on the substrate surface which allows their easier adoption of various configurations. As a result, the evaporated film has the essentially amorphous structure, in contrast to the crystalline PEO precursor.

Two new absorption bands can be found in the spectrum of the evaporated film. They are assigned to the carbonyl-based species (1724 cm^{-1}) and to the unsaturated C=C bonds (1620 cm^{-1}). Neither is present in the precursor and may appear as a result of quenching of the radicals through radical termination by disproportionation, as it was shown in the Section 3.2.2, or due to post-deposition oxidation with air. Nevertheless, the C=O and C=C groups are in minority with respect to others and the chemical composition of the evaporated film is very close to that of the PEO precursor.

The drastic changes of the FTIR spectra were observed when applying the glow discharge. The spectrum of the film evaporated at 10 W power looks similar to that prepared without plasma (Figure 3.12b and c). Nevertheless, the bands in the CH_2 wagging and twisting region become broader whereas the rocking CH_2 vibrations merge into broad spectral features appearing as a lower wavelength shoulder of the ν_{as}(COC) band. At higher powers, the ν_{as}(COC) band becomes even broader and the intensity of the C=O and C=C bands significantly increase (Figure

3.12d and e). Broadening of the FTIR bands is characteristic for plasma polymers, especially for those prepared at higher power of discharge. The term "macromolecule" is not well justified in the case of such plasma polymers because the intensive fragmentation at higher powers leads to increase of the lower molar mass fraction in the gas phase (see Section 3.2.2.). As a result, a highly crosslinked matrix is formed on the surface where the chains between cross-links are rather short (see Section 3.2.5). The diversity of possible conformations and inter-chain interactions results in a broad absorption spectral band.

The FTIR spectra, in agreement with the XPS/chemical derivatization data (see above), also show the increase of absorption of the hydroxyl groups with increasing the discharge power. However, the agreement between the XPS and FTIR data is not complete. For example, the significant enhancement of the C=O absorption was detected by FTIR whereas the XPS analysis indicated their stable content regardless of the power. This disagreement may be explained by different analysis depth of FTIR (entire bulk of the film) and XPS (several outermost nanometers). Apparently, the polymeric matrix retains a certain degree of flexibility to rearrange itself and to adopt the configuration of the lowest surface energy with non- polar hydrocarbon chains exposed and polar groups turned into the bulk.

Influence of specific power on the properties of the plasma polymers

Application of plasma significantly complicates the evaporation process because the energy balance within the plasma zone depends not only on wattage delivered from the generator, but on the amount of species to be polymerized as well. This means that the changes induced in the films prepared at different evaporation rates cannot be accounted for by the power alone but specific power per mass unit of precursor should be rather considered. This phenomenon was discussed first by Yasuda [3], who suggested a parameter W/FM, where W is power of discharge (watt), F is monomer molar flow rate ($mol \cdot s^{-1}$), and M is monomer molar mass ($kg \cdot mol^{-1}$). Thus, W/FM is expressed in terms of $J \cdot kg^{-1}$. Accordingly, an increase of F is equivalent to a decrease of W for a certain monomer. The W/FM parameter was also used by Johnston et al. [75] to adjust the conditions of constant power delivery per unit mass of ether-bearing precursors of different molar mass. In the case of evaporation of PEO, the monomer molar mass is uncertain because the gas phase

consists of a variety of species with a broad molar mass distribution. Nevertheless, the overall mass flux can be easily measured by QCM. The first series of the PEO-like plasma polymers was prepared at constant QCM frequency shift of 20Hz·min^{-1}, which corresponded to 5–8 nm·min^{-1} deposition rates. The deviation of the deposition rate relates to the different density of the films which increased with the power of the discharge (see further below). The constant QCM frequency shift therefore corresponds to the constant mass deposited over the substrate per unit time. However, the films of different thickness are produced according to a Sauerbrey equation:

$$\Delta f = -C_f \cdot \Delta m = -C_f \cdot \rho S h \qquad (3.1)$$

where Δf is the QCM frequency shift (Hz), C_f is the sensitivity factor of the crystal, Δm is the mass deposited per unit area (ng·cm^{-2}), ρ is the density of the film, S is the deposited area, and h is the thickness of the film. For the calculation of mass flux by equation (3.1), the sensitivity factor is necessary which can be found in the literature. However, the standard values of C_f are given on an assumption that a rigid material is deposited on QCM and that its acoustic properties are identical to quartz. In our case, especially for the films deposited at lower powers and higher evaporation rates, significant viscoelastic losses can be expected which should be accounted for. This significantly complicates the determination of C_f [117]. Therefore, the gravimetrical method was used to establish the mass flux and the film density. For this purpose, the samples were deposited onto aluminum foils of known area for a certain period of time. Then the weight and the values of the film thickness determined independently by ellipsometry were used for calculations. The mass flux in this case is expressed in kg·m^{-2}·s^{-1} and specific power, that is, power related to mass flux, has the dimension of J·m^2·kg^{-1}. Figure 3.13 shows the density of the PEO-like plasma polymers and the percentage of the ether groups in dependence on specific power which was calculated for different values of delivered power and the mass flux. The film density increases from about 1000 to 2600 kg·m^{-3} and the concentration of the C–O–C groups decreases from 80 to 27 % with increasing the specific power. The values obtained for different mass fluxes at given specific power coincide well within the experimental error. Therefore, the same value of the film density and the C–O–C content can be obtained at different discharge powers and mass fluxes. For example, the film with 1 500 kg·m^3 density and 40% of the ethers can be fabricated either at 80

W power and 17 ng·cm-2·s-1 mass flux or at 200 W power and 44 ng·cm-2·s-1 mass flux. Thus, the deposition rate of PEO-like plasma polymers can be increased with equivalent increase of both discharge power and mass flux to obtain the same value of the film density and the C-O-C content. This strategy was further utilized to prepare the samples for GPC and NMR analysis (see Section 3.2.4).

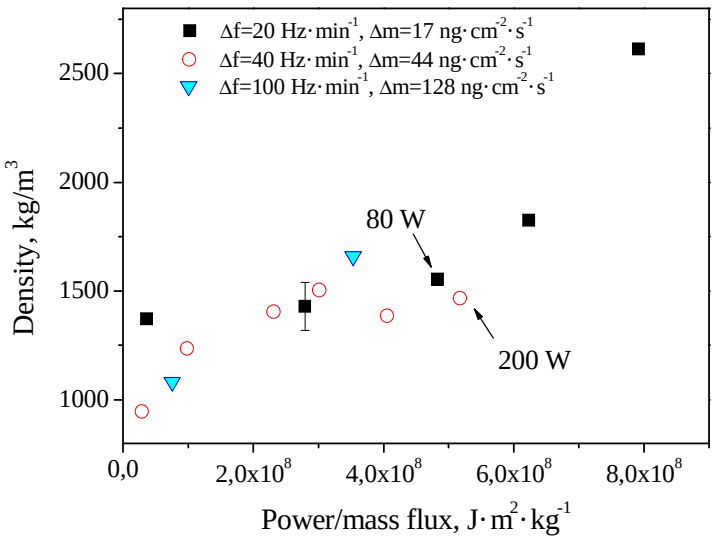

a)

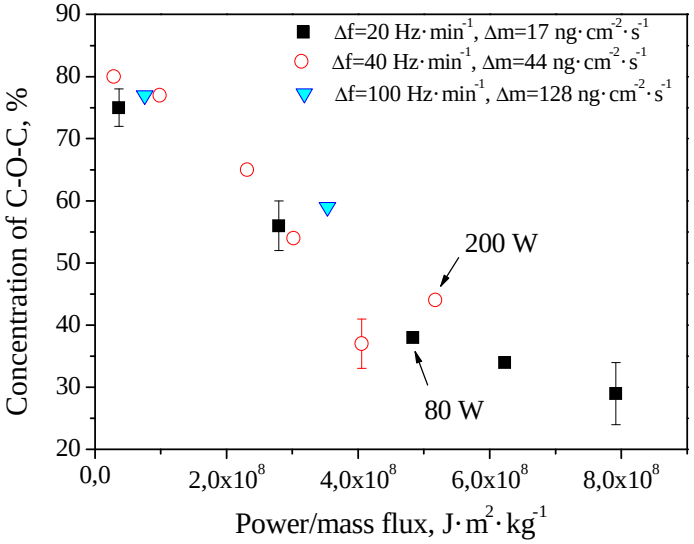

b)

Figure 3.13. Density a) and concentration b) of the ether groups of PEO-like plasma polymers in dependence on the specific power of the discharge.

3.2.4. Structure

Gel Permeation Chromatography (GPC)

The molar mass distribution of conventional PEO and the films evaporated with and without plasma were determined by GPC as shown in Figure 3.14. The PEO precursor shows a very narrow distribution of molar mass centered at 1500 $g \cdot mol^{-1}$. The PEO film evaporated without plasma is composed mainly of the oligomers with lower molar mass with the peak maximum shifted to 1050 $g \cdot mol^{-1}$. The left-hand side asymmetry indicates wider distribution of lighter species (Figure 3.14b). The molecules with molar mass down to 300 $g \cdot mol^{-1}$ can be resolved in this case. The values obtained by GPC may not reflect exactly the real molar mass due to both smearing of the GPC signal by the column and a possible branching of macromolecules via radical recombination during the film growth. In GPC, macromolecules are separated in accordance with their hydrodynamic volume in solution when passing through a microporous gel. The large molecules do not permeate the pores and pass the column faster then the small molecules with volume size lower or comparable to the pores of gel. Therefore, small macromolecules require longer elution time. A correlation between the elution volume and the molecular weight is then made on assumption that the structure of the compared macromolecules is similar. In the case of PEOs, the linear macromolecules may be directly analyzed and compared whereas the branched macromolecules of smaller molar mass can produce a signal equivalent to that of larger linear molecules [118]. Thus, the molar mass distribution measured by GPC for the evaporated film may be overestimated to some extent and the presence of even lower molar mass cannot be excluded. The same consideration is especially valid for the films deposited with activation by plasma because glow discharge is known to enhance cross-linking within the films. The PEO-like plasma polymer films were deposited at a higher mass flux corresponding to 100 $Hz \cdot min^{-1}$ QCM frequency shift which made the specific power relatively low. For example, the films deposited at 1, 5 and 150 W with 100 $Hz \cdot min^{-1}$ evaporation rate correspond in chemical composition to those which might be deposited at 0.2, 1 and 35 W with 20 $Hz \cdot min^{-1}$ evaporation rate.

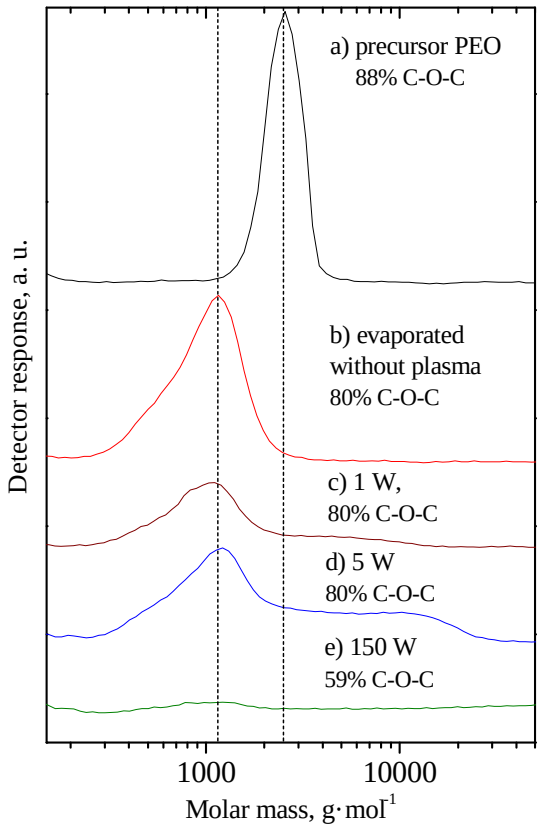

Figure 3.14. The GPC molar mass distribution of the soluble phase of the PEO-like plasma polymers: a) precursor PEO; b) the film evaporated without plasma; c) at 1 W; d) at 5 W; and e) 150 W. The mass flux corresponds to 100 Hz·min^{-1} (QCM).

The corresponding values of the concentration of the C–O–C bonds detected by XPS are also given in Figure 3.14. As it was shown previously, the concentration of the ether groups decreases with increasing the discharge power. However, for the films deposited at 1 and 5 W such decrease cannot be distinguished and their chemical composition is very similar to that of the film evaporated without plasma, at least within the error of the XPS fitting. Nevertheless, the difference in chemical structure and physical properties of these plasma polymers can be observed (Figure 3.14a-e). The film evaporated without plasma is completely soluble in water and tetrahydrofuran while the plasma polymers are only partially soluble in both solvents. The solubility of the plasma polymers decreases with increasing of the discharge power (see Section 3.2.5). The film deposited at 150 W was almost

insoluble and retained 97 % of its thickness after 1 day soaking in water. Reduced solubility of the plasma polymers is manifested in decreasing intensity of the GPC signal which is correlated to a smaller amount of macromolecules released into the solution. As to the 150 W film, a very weak signal supports the observed stability of this film in polar solvents.

The GPC curves are also remarkable for their polydispersity. It is most definitly seen for the 5 W film where the main peak at 1050 $g \cdot mol^{-1}$ is accompanied by a broad shoulder spreading up to $3x10^4$ $g \cdot mol^{-1}$. (Figure 3.14 d). This value should also be taken with reserve considering the branched structure of the solute. Nevertheless, plasma enhanced deposition of the macromolecular species with molar masses significantly exceeding that of the precursor PEO was undoubtedly detected.

This finding is inconsistent with the earlier studies that addressed the mass distribution of species in PEO-like plasma polymers deposited from volatile precursors bearing ether groups by Secondary Ion Mass Spectroscopy (SIMS) [75, 77, 80, 82, 90]. In these studies, an established consensus claims that increased plasma powers lead to an increase of low molar mass ($m/z < 103$) and to a decrease of higher molar mass ($m/z > 103$) molecules because of intensive fragmentation of the precursor. The highest mass detected by the SIMS reached m/z = 130-160 [77, 80, 82, 90] while Johnston et al. [75] reported masses up to m/z = 300 for oligoglymes, dioxanes and crown ethers used as precursors. The low values of the highest mass detected in these works in comparison with the evaporated PEO-like plasma polymers presented here may be explained both by discrimination over higher masses inherent for SIMS, and more likely by the absence of longer macromolecular chains in the films deposited from volatile precursors.

Based on these findings, the structure of the films deposited by evaporation of PEO can be viewed as follows. The film evaporated without plasma is in fact a blend of oligomeric species with a wide distribution of molar masses starting from 300 $g \cdot mol^{-1}$ (or smaller) and never reaching that of the precursor PEO (1500 $g \cdot mol^{-1}$). The low extent of cross-linking makes this film completely soluble in water and THF. The films deposited with plasma are essentially heterogeneous systems where the network formed via random radical recombination coexists with the polydisperse soluble phase with molar mass distribution much wider than that of original PEO. The ratio between the network and the soluble phases can be controlled by specific power of discharge so that increasing power favors polymerization of the lighter

species and increases the average molar mass of sol. Furthermore, the lower specific power produces films with good retention of the C-O-C bonds and low extent of cross-linking whereas the higher specific power enhances the hydrocarbon content and cross-linking within the films and makes them more rigid.

Nuclear Magnetic Resonance (NMR) Spectroscopy

Further important knowledge of the structure of PEO-like plasma polymers was obtained by NMR. The solid-state ^{13}C CP/MAS NMR spectra are shown in Figure 3.15.

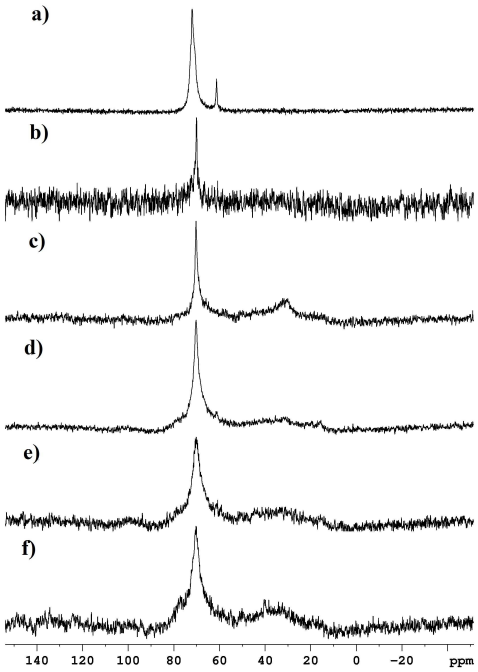

Figure 3.15. The solid state ^{13}C CP/MAS NMR spectra of the PEO-like plasma polymers in dependence on the discharge power: a) precursor PEO; b) the film prepared without plasma; c) 10 W; d) 50 W; e) 150 W and f) 200 W. The mass flux corresponds to 100 Hz·min^{-1} (QCM).

The spectrum of the PEO precursor consists of the broad peak at 71.9 ppm and the narrow peak at 61.2 ppm (Figure 3.15a) which can be assigned to amorphous and crystalline phases of PEO, respectively. The peak corresponded to the crystalline PEO structure was not detected in the spectra of the plasma polymers. However, they showed the additional CH_2 and CH_3 resonances in range of 10 – 50 ppm. The strong broadening of the main O–CH_2 peak was observed at increasing power of discharge

(Figure 3.16). This indicates a broader distribution of the macromolecular structures reflected in dispersion of chemical shifts. Figure 3.15 and Figure 3.16 are consistent with the previous XPS and FTIR data. In addition, the availability of the C=C double bonds or/and unprotonated carbons in the corresponding samples (Figure 3.15d and e) was evidenced by presence of the peak located at approximately 100 ppm.

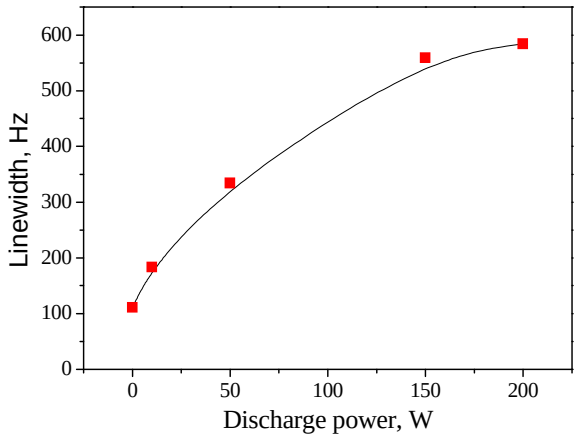

Figure 3.16. The linewidth of the main NMR signal of PEO at different discharge power.

The liquid-state proton ^{1}H NMR spectra were obtained for D_2O solutions of the PEO-like films deposited with and without plasma (Figure 3.17). The signal at 3.69 ppm belongs to the O-CH_2 groups and the residual signal from HDO solvent molecules is located at 4.73 ppm. As discussed before (see above), the plasma polymers were partially or almost completely insoluble depending on the discharge power applied. The band of the PEO units decreases in intensity with increasing discharge power reflecting reduced solubility of the plasma polymers and decreased amount of the soluble chains with detectable O-CH_2 groups. Mobility of the PEO units involved in insoluble chains is reduced to such an extent that corresponding lines are too broad to be detected in the high-resolution spectra. Such remarkable line broadening was previously observed for thermoresponsive polymer solutions [119].

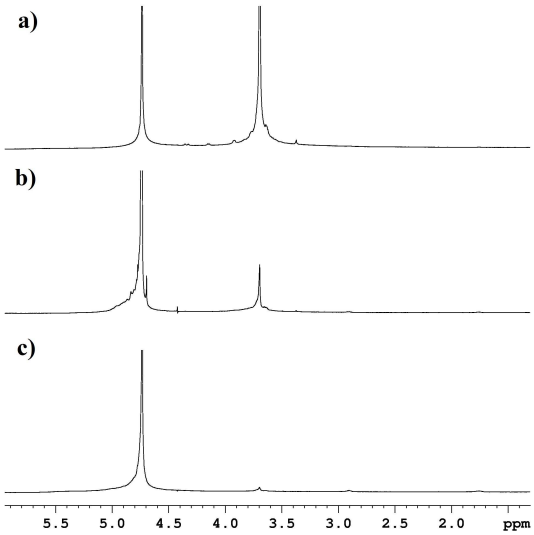

Figure 3.17. The liquid state ^{1}H NMR spectra of the PEO-like plasma polymers prepared at different power of discharge (measured in solution with D_2O): a) the film evaporated without plasma; b) 10 W and c) 50 W.

3.2.5. Swelling phenomena

As mentioned previously, a close chemical resemblance between the plasma polymers deposited at low specific powers and conventional PEO was observed. Therefore, other features relevant to PEO can be expected to be revealed as well. Conventional PEO is a very well known hydrogel and one of its peculiarities is swelling, i. e. the ability to absorb water with considerable increase of polymer volume. PEOs are generally physical hydrogels, i. e. its individual chains are not bound to each other chemically but through the molecular entanglements. Upon swelling, the macromolecules unfold, disintegrate and the polymer eventually dissolves completely. On the contrary, plasma polymers are covalently cross-linked networks and therefore their swelling behavior can be different.

The kinetics of thickness change of the PEO-like plasma polymers in contact with water was investigated by spectroscopic ellipsometry. The films with thickness of approximately 100 nm were prepared on the polished silicon wafers (Section 2.2.3). The samples were introduced into the liquid cell, the ellipsometer settings were tuned and the first data acquisition was performed in a dry state to obtain the initial dry thickness, d_0. Then distilled water was poured into the liquid cell through a

syringe and the time depended measurements were immediately started. The measurements were performed until the equilibrium conditions were reached, i. e. until the thickness of the films stopped changing. As a result, the equilibrium swelling thickness (d_1) was determined. Finally, the liquid cell was drained, the excess of water was removed from the samples by a gentle nitrogen flow and the samples were dried under 1×10^{-3} Pa vacuum for three hours to remove the water bound within the films. Subsequently, the final film thickness (d_2) was measured. The polymer volume fraction was calculated as the d_2/d_1 ratio.

Power (W)	**Initial dry thickness, d_0 (nm)**	**Equilibrium swelling thickness, d_1 (nm)**	**Thickness after vacuum drying, d_2 (nm)**	**Polymer volume fraction, φ_p**
1	150	320	90	0.28
2	122	161	61	0.38
3	110	139	76	0.55
4	132	158	113	0.72
5	135	160	120	0.75
10	137	150	132	0.88
30	132	139	129	0.93

Table 3.3. The results of the swelling/dissolving experiments performed on the PEO-like plasma polymer films.

Table 3.3 summarizes the data of the swelling experiments. The changes of the film thickness during swelling/dissolution in distilled water are shown in the Figure 3.18. The thickness of the films deposited at 10 W increases only by several percent during the first minutes of contact with water and then it remains constant. After vacuum drying, the thickness is several nanometers smaller as compared with initial dry value. The polymer volume fraction reaches the value of $\varphi_p = 0.9$.

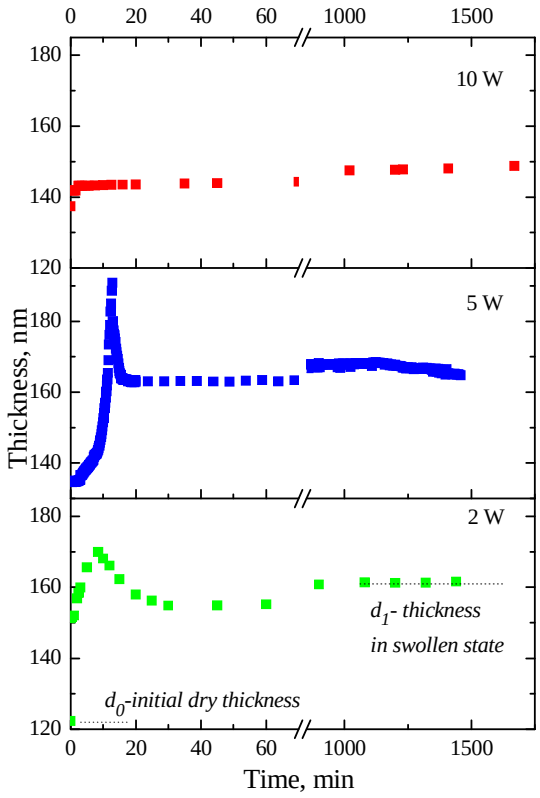

Figure 3.18. Kinetics of swelling of the PEO-like plasma polymers deposited at different discharge powers as measured by ellipsometry.

The swelling behavior is different for the plasma polymer films prepared at lower discharge power (2 and 5 W). In the first 10 minutes of the films contact with water, their thickness significantly increases. This is followed by a decrease during the next 10-20 minutes when the thickness reduces to a value which still exceeds the initial dry thickness. Subsequently, thickness increases very slowly and eventually reaches the equilibrium.

Such swelling behavior of the films can be explained if the sol/gel structure of the plasma polymers is considered. As shown by GPC and NMR, the PEO-like plasma polymers, in particular those deposited at low specific powers, contain a considerable amount of unbound macromolecules with molar mass reaching 3×10^4 $g\cdot mol^{-1}$. As a result, the unbound chains become solvated and tend to leave the film by out-diffusion processes upon contact with water. This should lead to a decrease of the film thickness. Nevertheless, the dissolution is relatively slow as it is hindered by macromolecular entanglements. On the contrary, in-diffusion of small water

molecules proceeds more rapidly and it is reasonable to assume that water penetrates fast into the entire volume of thin film. Since ether groups attract the molecules of water and bind them by hydrogen bonds, osmotic pressure develops in the bulk of thin film which stimulates unfolding of the polymeric segments and results in an increase of plasma polymer volume. The overall changes of the film thickness are therefore governed by two concurrent processes of swelling (in-diffusion of water, unfolding and relaxation of the macromolecular segments in the gel) and dissolution (out-diffusion of unbound macromolecules of sol).

As shown on the Figure 3.18, the film thickness increases fast during the first several minutes. This can be attributed to the dominance of the swelling phenomena when dissolution of the sol is hindered by close packing and physical entanglements of neighboring chains. With expansion of thin film volume, the mesh size of the gel increases which results in more effective release of the sol fraction. The maxima on kinetic curves correspond to the moment when swelling of the gel is counterbalanced by dissolution of the sol. Nevertheless, the thickness does not decrease to the initial dry value due to the swollen state of the gel. The final stage is characterized by insignificant increase of the thickness due to slow relaxation of the macromolecular segments within the network which re-orient themselves to find thermodynamically most favourable conformations.

The described behavior is very well observed for the films prepared at low discharge powers (<10 W) whereas the films deposited at higher powers (>10 W) are more resistant to swelling/dissolution. This can be attributed to increased cross-linking density and decreased flexibility of the macromolecular chains. For quantitative estimation of the cross-link density in the plasma polymers the Flory-Rehner theory of gels was employed. In macromolecular physics, cross-link density is one of the key parameters describing the polymeric networks. It is usually related to the average molar mass between cross-links (M_c). Plasma polymers deposited from the low-molar-mass precursors are generally highly cross-linked since their individual segments are composed of small precursor fragments. M_c can hardly be determined in this case. However, plasma polymers prepared as a result of vacuum thermal vapour deposition are built from much longer oligomers and therefore classical theories of polymeric networks can be attempted to characterize them. For the determination of M_c, swelling experiments are often used in which a polymer is kept in a thermodynamically good solvent to reach its equilibrium volume. Then, the

Flory-Rehner theory of gels can be applied [120]. Flory and Rehner were first to suggest that free energy of gel can be divided into two independed terms. The first is the mixing term which is determined by the strength of the interaction between polymer chains and solvent molecules. The elastic term accounts for elongation of polymer chains in the swelling process. One of the outcomes of the Flory-Rehner theory is a relationship for M_c (Equation 3.2):

$$\frac{1}{M_c} = \frac{2}{\overline{M}_n} - \frac{\ln(1-\varphi_p)+\varphi_p+\chi\varphi_p^2}{\rho_p V_s\left(\varphi_p^{1/3}-\varphi_p/2\right)} \tag{3.2}$$

In this equation, the $\overline{M}_n$ is the number average molar mass (g·mol^{-1}) of the initial macromolecular chains before cross-linking; φ_p is the polymer volume fraction of the swollen network; ρ_p is the polymer density (g/cm^3); V_s is the molar volume of the solvent (cm^3·mol^{-1}); χ is the Flory-Huggins interaction parameter between the polymer and the solvent.

In this work, $\overline{M}_n$ was determined from the experiments without plasma. The films in this case consist of the uncross-linked oligomers with $\overline{M}_n$ = 1045 g·mol^{-1} as determined by GPC (Section 3.2.4).

The polymer volume fraction of the swollen network, φ_p, can be found as a ratio of thickness of the vacuum-dried samples to the equilibrium swelling thickness ($\varphi_p = d_2/d_1$) which was obtained by ellipsometric measurements (Table 3.3).

The polymer density (ρ_p) was determined gravimetrically as described in (Section 3.2.3). It was found that for the films prepared at discharge powers below 40 W ρ_p averaged around 1.4 g/cm^3. Therefore, for the range of powers between 1 and 30 W used in the swelling measurements, the value of ρ_p was chosen to be 1.4 g/cm^3. The molar volume of deionized water used as a solvent is V_s=18 cm^3·mol^{-1}.

Possible values of the Flory-Huggins interaction parameter (χ) for PEO/water systems were reviewed by Lin and co-workers [121]. The value χ=0.43 was reported for φ_p < 0.2 whereas for the higher polymer volume fractions χ reached the value of 0.66. In our case, the exact dependence $\chi(\varphi_p)$ is unknown and therefore the average value χ=0.55 is used for the calculations, discussion of possible uncertainties given where relevant.

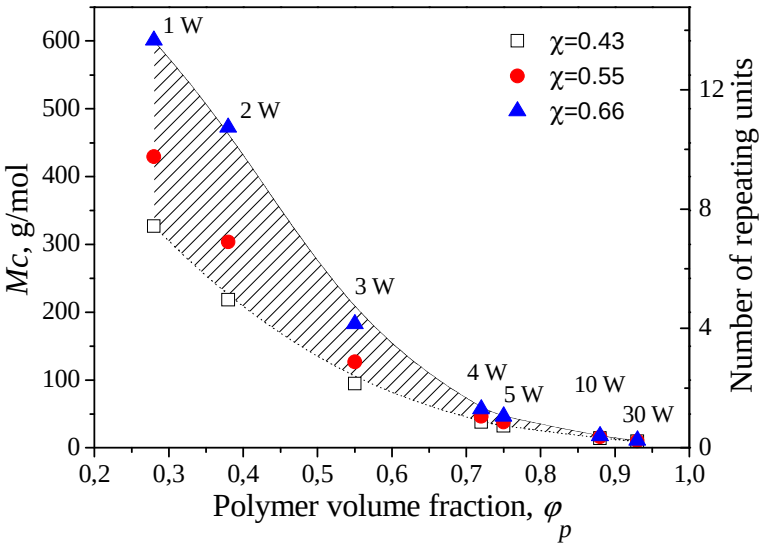

Figure 3.19. Average molar mass between cross-links in the PEO-like plasma polymers vs polymer volume fraction for the different values of the Flory-Huggins interaction parameter, χ.

Figure 3.19 shows the values of M_c calculated by Equation 3.2 from the swelling data (Table 3.3) with the average value of the Flory-Huggins interaction parameter χ=0.55 as well as for minimal χ=0.43 and maximal χ=0.66 values. The patterned area indicates the values that M_c may adopt with differentχ. The right-hand y-axis is related to the average number of repeating units between cross-links obtained by dividing M_c by the molar mass of the repeating unit, M_r=44 g·mol^{-1}. Apparently, the cross-link density increases (M_c decreases) with increasing of the discharge power. At increasing power, the plasma contains a larger amount of free radicals which act as cross-linking centers during the film growth.

The Flory-Rehner theory provides an important tool to describe the cross-link density in quantitative terms. The average molar mass between cross-links for the film prepared at 1 W with volume fraction φ_p= 0.28 (Table 3.3) reaches 430 g·mol^{-1} correspond in average to 10 monomeric units. It is worth noting here that for plasma polymers this number is very large and it is hardly unattainable for the films deposited from low-molar-mass precursors. On the other hand, for classical macromolecular physics, this number represents significantly cross-linked networks.

With increasing discharge power, the number of monomeric units between cross-links decreases and the films become less soluble and less swelling. For the

films deposited at 10 and 30W the corresponding values of M_c are 15 and 10 g·mol^{-1}, respectively. These appear to be unrealistic being comparable, for example, with atomic mass of carbon. It has been widely accepted that the Flory-Rehner theory dealing with the Gaussian chain model overestimates the elastic energy required for unfolding of the chains and does not describe correctly highly cross-linked systems [122, 123]. The Gaussian chain model assumes that the macromolecular sections between the cross-links are sufficiently long not to be influenced by the cross-link junctions [124]. A number of bond vectors exceeding 100 is usually taken as a measure of validity of the Gaussian chain distribution [121, 124, 125]. For highly cross-linked polymers, the number of bond vectors can be significantly smaller and such systems should be analyzed using non-Gaussian distribution models. The Flory-Rehner theory was modified by Peppas and co-workers to account for the non-Gaussian effects [124, 125]. The following relationship was obtained:

$$\frac{1}{M_c} = \frac{2}{M_n} - \frac{(\ln(1-\varphi_p) + \varphi_p + \chi\varphi_p^2)(1-\frac{\varphi_p^{2/3}}{N})^3}{\rho_p V_1(\varphi_p{}^{1/3} - \varphi_p/2)(1+\frac{\varphi_p^{1/3}}{N})^2}, \tag{3.3}$$

where N is the number of links per chain between two cross-links. N is defined as:

$$N = \frac{\lambda M_c}{M_r} \tag{3.4}$$

Here, λ is the number of links per repeating unit which is 3 for CH_2–CH_2–O– [125], M_r is the molar mass of the repeating unit (M_r=44 g·mol^{-1}). By substituting Equation (3.3) to Equation (3.4) the latter can be reduced to a cubic function which may be solved analytically by using, for example, the Cardano's method to obtain M_c.

$$aM_c^3 + bM_c^2 + cM_c + d = 0 \tag{3.5}$$

Figure 3.20 gives the values of M_c calculated by the classical Flory-Rehner theory and by the Peppas-Lucht model with correction for non-Gaussian chain distribution. As expected, for the films prepared at lower discharge powers (with long macromolecular segments between the cross-links) close values of Mc are obtained by both models. For example, for the film deposited at 1 W the Peppas-Lucht model calculates the value of M_c=430 g·mol^{-1} which is identical to that derived from the Flory-Rehner model. For the other films, the Peppas-Lucht model gives larger values of M_c as compared to the Flory-Rehner, and the difference between both increases with shortening of the macromolecular chains. For the highly cross-

linked films (higher power), M_c approaches the value of 47 g·mol^{-1} which corresponds approximately to one monomeric unit between the cross-links. It is also remarkable that decrease of M_c with discharge power is not linear.

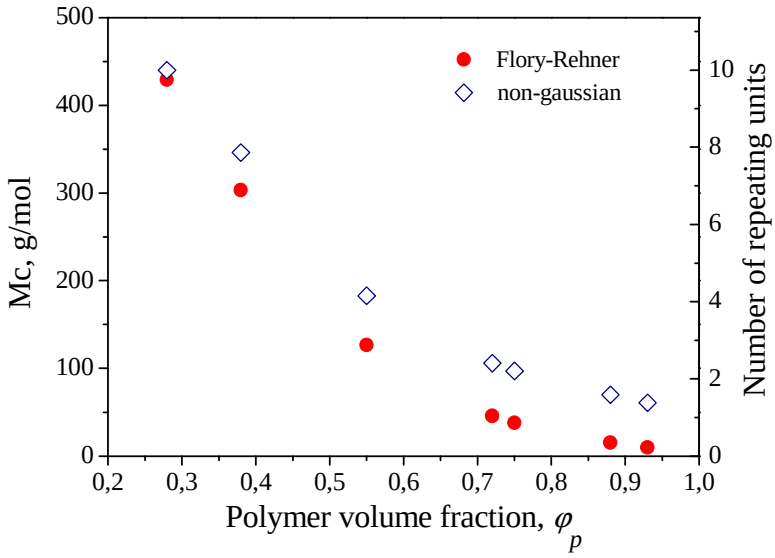

Figure 3.20. Average molar mass between cross-links calculated for gaussian (Flory-Rehner) and non-gaussian (Peppas-Lucht) chain distribution (χ=0.55).

Figure 3.20 gives the values of M_c calculated by the classical Flory-Rehner theory and by the Peppas-Lucht model with correction for non-Gaussian chain distribution. As expected, for the films prepared at lower discharge powers (with long macromolecular segments between the cross-links) close values of Mc are obtained by both models. For example, for the film deposited at 1 W the Peppas-Lucht model calculates the value of M_c=430 g·mol^{-1} which is identical to that derived from the Flory-Rehner model. For the other films, the Peppas-Lucht model gives larger values of M_c as compared to the Flory-Rehner, and the difference between both increases with shortening of the macromolecular chains. For the highly cross-linked films (higher power), M_c approaches the value of 47 g·mol^{-1} which corresponds approximately to one monomeric unit between the cross-links. It is also remarkable that decrease of M_c with discharge power is not linear. The most prominent changes are observed for the powers <5 W where a significant variation of the cross-linking density is detected. In this region, the increase of the power from 1 W to 5 W leads to the proportional five-fold shortening of the macromolecular chains from 430 to 80 g·mol^{-1}. However, M_c decreases much slower in the region of powers

between 5 W and 30 W. It can be assumed that at such powers the conversion of precursors in plasma already reaches the high values and further increase of power does not result in significant increase of the number of active species.

3.2.6. Film elasticity

The rubber elasticity theory correlates the cross-linking density in polymeric networks with their elastic properties. For plasma polymers, such interrelation is also recognized, usually in terms of increasing stiffness of the films with increasing power of discharge. The indentation data with the Hertzian curve fits are shown in Figure 3.21. The curves were acquired on the samples analogous to those studied in the swelling experiments (Section 3.2.5). All the measurements were performed in a single run with the same cantilever and the same settings of the AFM to avoid any inconsistency.

Two important conclusions can be drawn upon examination of the indentation curves. First, the Hertz model fits well the indentation curves and this proves that the assumption of the parabolically shaped tip was a good approximation. Deconvolution of the tip apex also confirmed the proximity of its convex shape to the parabolic one.

Second, only elastic behavior is observed even for the highest deformations reached. Generally, when the cantilever applies a critical pressure on the sample a yielding point is detected on the indentation curve which indicates the onset of plastic deformation. After the yield, significantly higher values of the deformation are obtained than those predicted by the Hertz model [100]. In our experiments, no yielding occurs at loads below 10 nN even for the softest plasma polymers. It means, for example, that the 1 W film completely recovers its thickness after 60 nm deformation induced by the tip. With increasing power, the cross-link density and stiffness of the samples increase and, as a result, the same load produces smaller deformations. For example, the indentations below 1 nm were obtained for the film deposited at 30 W.

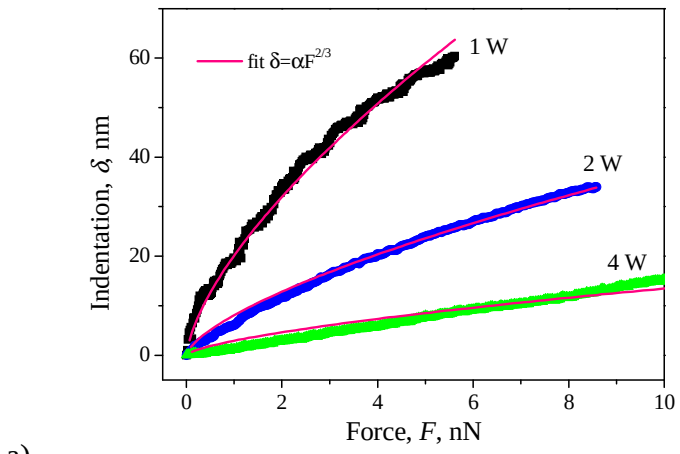

a)

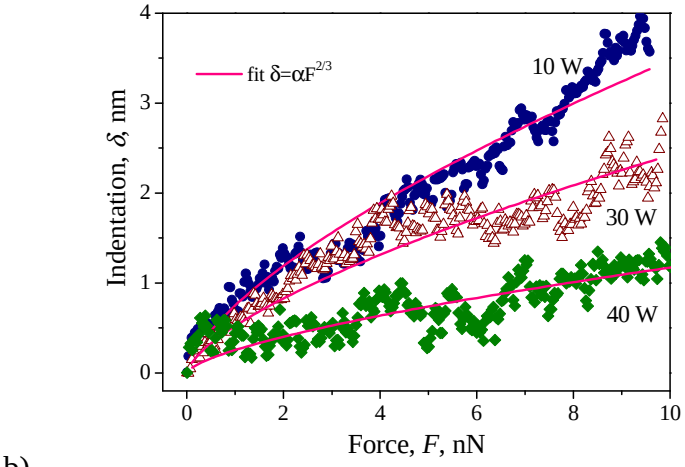

b)

Figure 3.21. The indentation curves acquired on the PEO-like plasma polymers (the cantilever ContE-G, k=0.15 N/m, radius of curvature 11 nm).

Figure 3.22 shows the values of the Young's modulus calculated from the fitting results by Equation (3.6) in dependence on the discharge power. It is worth noting that glass transition temperature, T_g, of PEOs (linear and cross-linked) is reported at about -40 °C and below [121, 126, 127], and therefore the samples measured at room temperature are in the rubbery plateau region. The data for three types of samples are shown in Figure 3.22. The as-deposited PEO-like plasma polymers with 250 nm thickness are represented by red solid squares. Their indentation curves were shown in Figure 3.21. Thicker deposits were also prepared and tested to check the influence of the rigid substrate on the indentation results. The green triangles in Figure 3.22 correspond to the as-deposited films with 800 nm

thickness whereas the blue circles correspond to the same films soaked in water for 24 hours and vacuum dried afterwards.

The most abrupt changes of modulus can be observed for the powers between 1 and 10 W where the values of *E* change by three orders of magnitude. For the 250 nm films, *E* increases from 2 to 300 MPa whereas the thicker films give 2–3 times smaller values. This can be attributed to attenuated influence of the hard substrate. Nevertheless, the general trend of a steep increase of *E* with power is fulfilled for them as well.

The indentation measurements on the as-deposited films offer the information on the elastic properties of the entire sol/gel heterogeneous networks. The samples were soaked in water overnight and then dried under vacuum to remove the soluble part from gel. Thus, the conditions used in the swelling experiments were exactly reproduced. The values of the Young's modulus of gels in dry state were obtained 3-4 times higher than those before soaking in water. Apparently, absence of unlinked, elastically inactive oligomers is responsible for such effect.

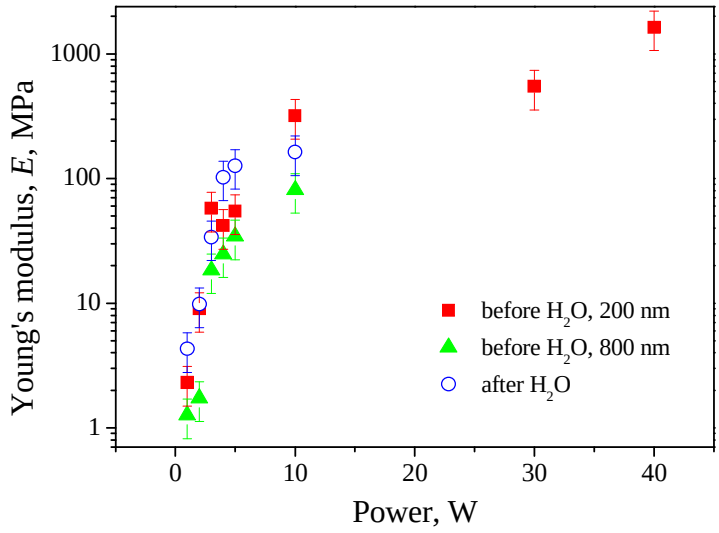

Figure 3.22. The Young's modulus of the PEO-like plasma polymers of different thickness calculated from the indentation results.

The value of *E*=4 MPa calculated for the 1 W film agrees well with the range 1-50 MPa [127] and 0.5-4.8 MPa [128] reported for differently cross-linked bulk PEOs, and also correlates with *E*=2 MPa typically observed for elastomers in the rubbery plateau region [129]. Increasing the cross-linking density results in increased

number of elastically active junctions and, as a consequence, the Young's modulus of PEO increases.

From the rubber elasticity theory, the relationship between the Young's modulus and the cross-link density for the small strains can be obtained as follows:

$$\upsilon_e = 3ERT = \rho / M_c, \qquad (3.6)$$

where υ_e is the number of active network chain segments per unit volume or, in other words, the cross-link density, mol/cm^3; E is the Young's modulus of the rubbery plateau region which is the case here; R and T are the gas constant and the absolute temperature, respectively [129]. The values of E calculated from the swelling experiments and from the indentation measurements are summarized in Table 3.4.

Power (W)	**υ_e Swelling, 10^{-3} (mol/cm^3)**	**M_c Swelling (g·mol^{-1})**	**υ_e Indentation, 10^{-3} (mol/cm^3)**	**M_c Indentation (g·mol^{-1})**
1	3	440	0.6	2423
2	4	346	1	1064
3	8	183	5	308
4	13	106	14	102
5	14	97	17	82
10	20	70	22	64
30	23	61	-	-

Table 3.4. The cross-link density of PEO-like plasma polymers calculated from the swelling and indentation measurements.

For the films prepared at discharge power above 4 W, good agreement between the two methods was observed. However, for the smaller powers the values of M_c obtained by indentation measurements were larger. It was reported that the values obtained from the two methods may differ by a factor of 2 [129]. Indentation measurements are generally less relaxed than equilibrium swelling data, i. e. the time of mechanical impact is shorter than the relaxation time required for a polymer to respond to the external stress by thermal motion. Therefore, higher values of the Young's modulus are usually obtained and this leads to underestimation of M_c (see

Equation 3.6). In our case, the acquisition time of the loading and unloading curves at the cantilever speed of 40 nm/s corresponded to the frequency of about 0.2 Hz which seems to be sufficiently small to avoid significant overestimation of E (underestimation of M_c). Surprisingly, the indentation values of M_c exceed those of swelling, in particular for the low-power films. The disagreement can be hypothetically explained by the availability of intra-molecular loops which do not contribute to the elastic behaviour of the gels, the so-called "wasted cross-links" [130]. Rubbery plateau modulus of cross-linked PEOs was shown to decrease from about 50 MPa to 1 MPa with increased concentration of elastically ineffective loops [131]. Therefore in our work, loops and dangling macromolecular ends are suggested to be responsible for high values of M_c obtained from the indentation measurements of the low-power films.

3.2.7. Sterilization

The key objective of research on biomedical use of plasma polymers is related to identification of the conditions to produce the films with required bio-responsive properties. Obviously, the films should also withstand a sterilization process. The resistance of plasma polymers towards common sterilization processes was, however, overlooked in the literature, and only a few studies exist devoted to this topic [132, 133]. In some cases, vulnerability to sterilization may be detrimental for the successful use of plasma polymers. Therefore, prior to studies of protein adsorption and cell adhesion, this thesis has focused on stability of PEO-like plasma polymers in water and on their tolerance to different sterilization methods.

XPS was acquired on the as-deposited samples as well as after their soaking in water and vacuum drying. Figure 3.23 shows the dependence of concentration of the ether groups on the discharge power. In agreement with Section 3.2.3, an increase of the power results in a progressive decrease in retention of the C-O-C groups. Interaction with water does not lead to chemical changes at least within the accuracy of deconvolution fitting.

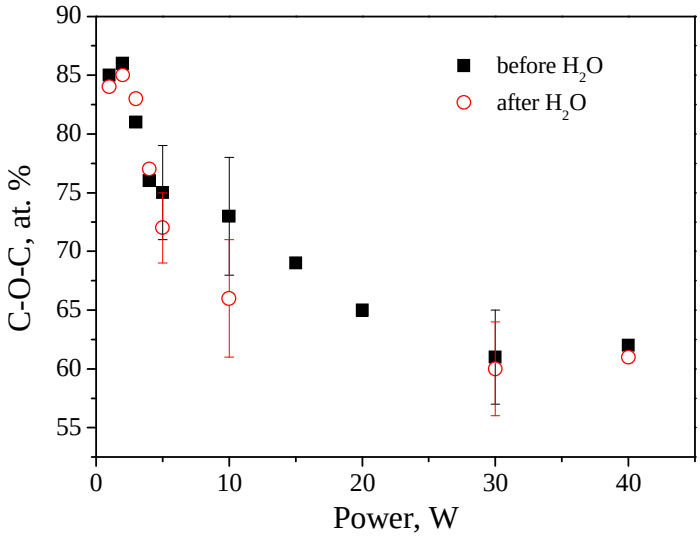

Figure 3.23. The XPS concentration of the ether groups in the PEO-like plasma polymers before and after soaking in water.

The films deposited at 5 W were used to study the effect of sterilization on the properties of the PEO-like plasma polymers. The first parameter to study was variation of the thickness of the plasma polymers depending on the sterilization method used. Comparison of the films before and after sterilization shows that only UV radiation did not change the thickness of the films (Figure 3.24). Both autoclave and, even to more extent, dry heat caused reduction of the film thickness, which suggests thermal instability of the PEO-like plasma polymers. This finding is of high importance, especially for ultrathin coatings of several nanometer thickness which are required, for instance, for novel optical affinity biosensors. In this case, reduction of the thickness may expose the underlying substrate which can subsequently interact with biological samples and give false signals.

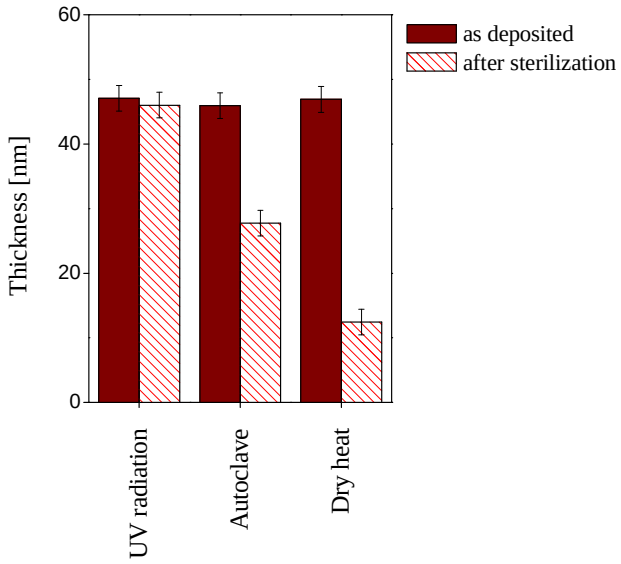

Figure 3.24. Thickness of the PEO-like plasma polymers before and after sterilization.

The AFM analysis did not show any changes in surface topography after the sterilization. The roughness of the films remained very smooth with the root mean square roughness being below 1 nm.

The high resolution C 1s XPS spectrum of the non-sterilized sample consist of the dominant peak corresponded to the C-O-C bonds (77 %), followed by the C=O bonds (12 %) and the C-C/C-H bonds (11 %). The concentration of these three chemical components remained almost unaffected when the samples were exposed to UV radiation. This was also confirmed by the water contact angle (WCA) measurements that gave 36^{o} and 37^{o} for the non-sterilized and UV radiated samples, respectively (Figure 3.25a and b).

After autoclaving, the film shows good retention of the PEO-like character as well. The concentration of the C-O-C bonds reduced to 72 % whereas the fraction of the C-C/C-H bonds increased up to 14 % (Table 3.5). Higher fraction of hydrophobic C-C/C-H bonds caused the small increase of WCA to the value of 46^{o} (Figure 3.25c). Such minimal chemical changes were expected as ethers do not normally hydrolyze.

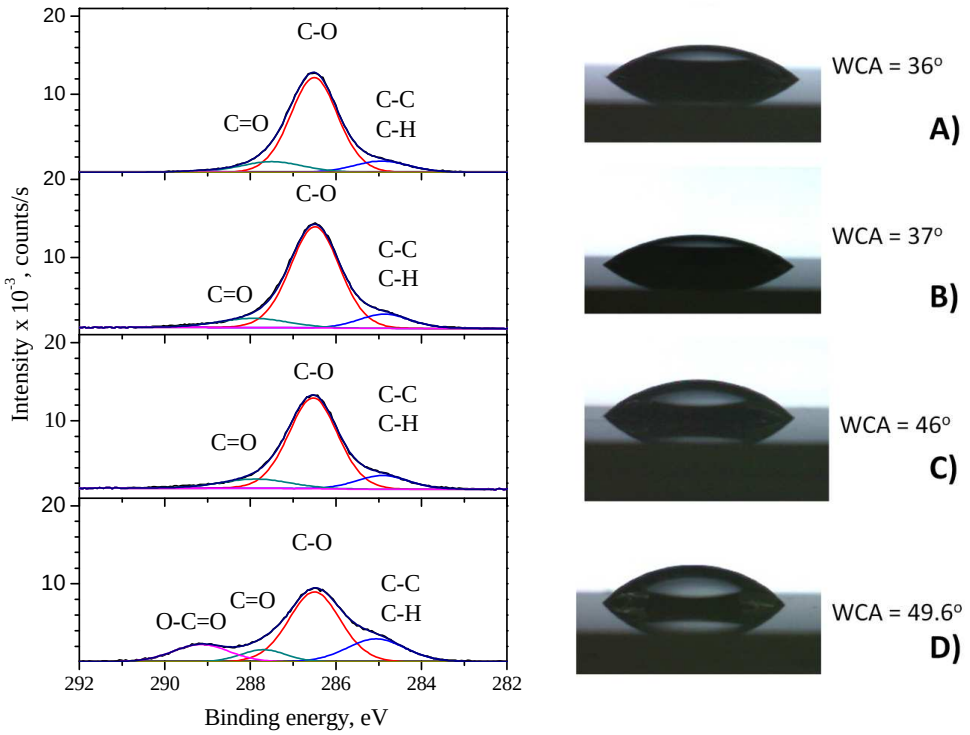

Figure 3.25. The high resolution C 1s XP spectra of the PEO-like plasma polymers (left) and water droplets on their surface. A) non-sterilized sample B) the sample sterilized by UV radiation C) the autoclaved sample D) the sample treated by dry heat

	C-C, C-H %	**C-O-C, %**	**C=O, %**	**O-C=O, %**
Non-sterilized	11	77	12	-
UV radiation	12	77	11	-
Autoclave	14	72	14	-
Dry heat	21	55	9	15

Table 3.5. The XPS analysis of the non-sterilized and sterilized PEO-like plasma polymers.

Despite the small changes of chemical composition, the loss of mass after autoclaving for the PEO-like plasma polymers was significant. Since hydrolysis can be ruled out, another mechanism should account for the observed loss of the material. We have shown that PEO-like plasma polymers films prepared by plasma-assisted evaporation are heterogeneous systems in which a cross-linked network co-exists with a mixture of oligomers with very broad molar mass distribution (Section 3.2.4). The oligomers are not bonded chemically to the network but are held within by

physical entanglements. Upon contact with water, such macromolecules leave plasma polymer by diffusion. In particular, the PEO-like plasma polymer film prepared at identical conditions as those used here lost about 12 % of its thickness simply by out-diffusion of the unlinked species away from the film. In the sterilization experiments, the film was autoclaved, i. e. brought in contact with water vapours. Nevertheless, the elevated temperature is responsible for intensification of the macromolecular dynamics and unbonded oligomers, especially of lower molar mass, get higher probability to disentangle and to escape from the plasma polymer.

The film sterilized by dry heat lost about 70 % of its thickness (Figure 3.24). In this case, the C-O-C content decreased to 55 % and it was accompanied by an increase of the C-C/C-H bonds (21 %) and formation of the O-C=O bonds (15 %). Significant change in the O/C ratio was also observed with oxygen content increased at the expense of carbon and the O/C raised to the value of 0.73. Formation of the O-C=O bonds is also consistent with the findings of Han with co-workers who found esterification of PEO by the random chain scission mechanism during thermal degradation in air [134]. In agreement with the chemical changes, an increase of WCA to the value close to 50^{o} was observed. (Table 3.5 and Figure 3.25d).

3.2.8. Cell adhesion

The following step of the study included evaluation of resistance of the plasma polymers to cell adhesion without and with application of different sterilization processes. Figure 3.26 and Figure 3.27 show that the MG63 cells do not adhere to the non-sterilized films. The UV treatment does not influence the ability of the films to withstand the accumulation of cells either. This was also confirmed by the experiments with the Balb/3T3 immortalized mouse fibroblasts which showed significantly reduced adhesion of these cells to UV-treated PEO-like plasma polymers (Figure 3.28).

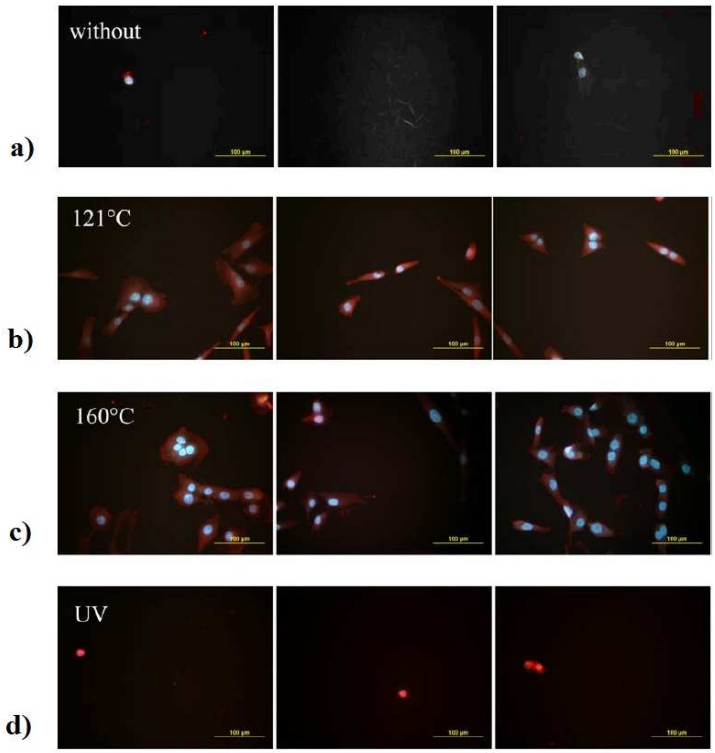

Figure 3.26. The development of the osteoblast-like cells on the PEO-like plasma polymers: a) without sterilization; b) after autoclaving process; c) after dry heat sterilization; d) after UV sterilization.

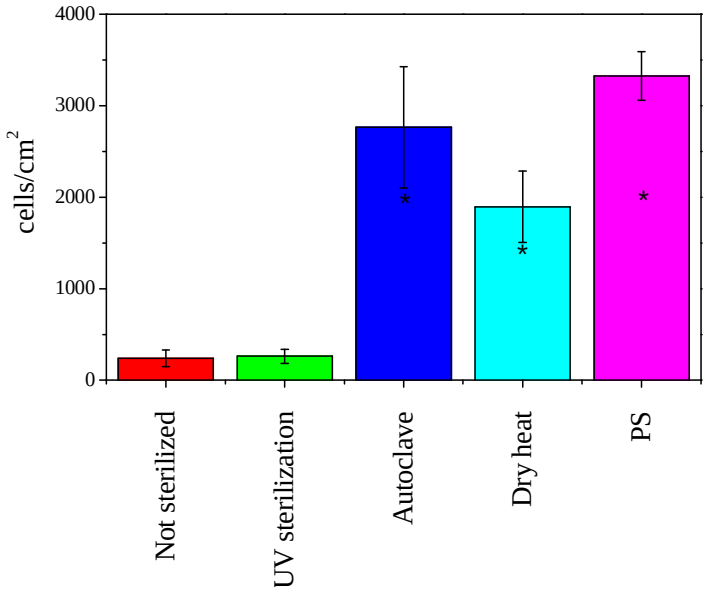

Figure 3.27. The number of adhering MG63 cells 1 day after seeding on PEO-like plasma polymers sterilized by different methods. The number of cells adhering to reference polystyrene dish (PS) is given for comparison.

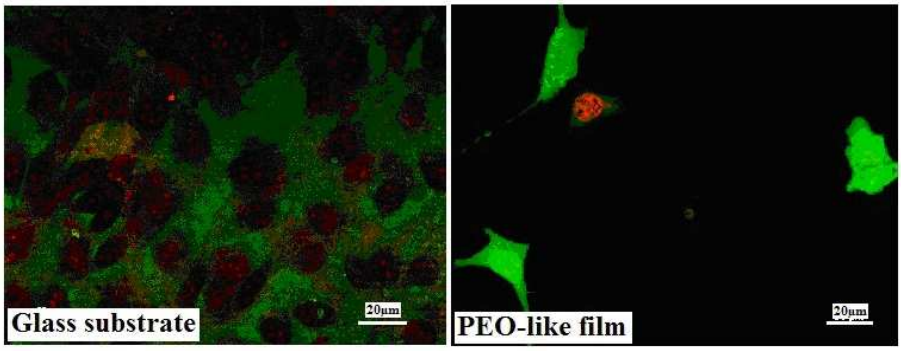

Figure 3.28. The cell growth on the surface of glass and PEO-like plasma polymer as seen by fluorescent microscope ApoTome system ZEISS (green - alive and red – died).

The autoclaved and the dry heated samples lost the non-fouling character and the number of cells adhering to them approached the value observed for the polystyrene dish. These results are consistent with alterations of the chemical composition of the films: the loss of the ether bonds results in enhancement of the cell adhesion.

To conclude, the autoclaving and dry heat sterilization methods were found to be destructive for the PEO-like plasma polymers and should be avoided. Therefore, for further biological tests only UV sterilization was used.

3.2.9. Protein adsorption

Single protein adsorption

One of the most remarkable properties of PEO is its ability to resist protein, cell and bacteria adhesion, i. e. its nonfouling properties. PEO-like plasma polymers deposited at low discharge power by PECVD of volatile precursors were also found to exhibit the nonfouling properties. Reduced or none protein adhesion was confirmed for blood proteins, mainly BSA and fibrinogen [72, 73, 75, 77, 80, 84-91], several types of cells [72, 77, 79, 80, 82, 91] and bacteria [78] (see Table 1.1). All the works agree on a general trend of enhancement of nonfouling behaviour with retention of the C-O-C structure. In this thesis, BSA, IgG and fibrinogen were chosen to study protein adsorption in the case of PEO-like films prepared by plasma-assisted thermal vapour deposition.

The films of 75 nm thickness were deposited onto QCM crystals at the powers of 5 and 150 W and at constant evaporation rate (Δf = 20 Hz·min^{-1}, Δm = 17 ng·cm^{-2}·s^{-1}). Respectively, 75 % and 30 % concentration of the C-O-C bonds was obtained. The above results showed that the XPS and FTIR spectra of both types of the films taken before and after soaking in water were identical.

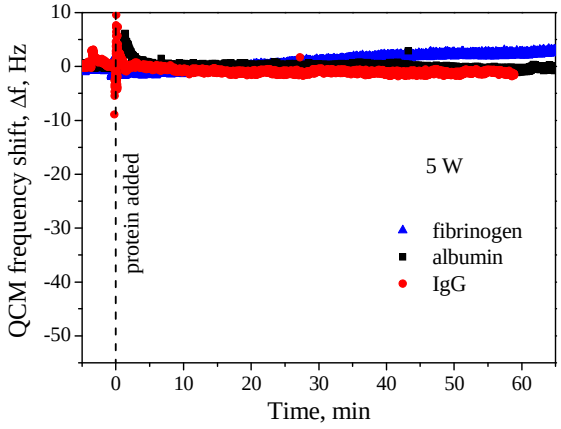

a)

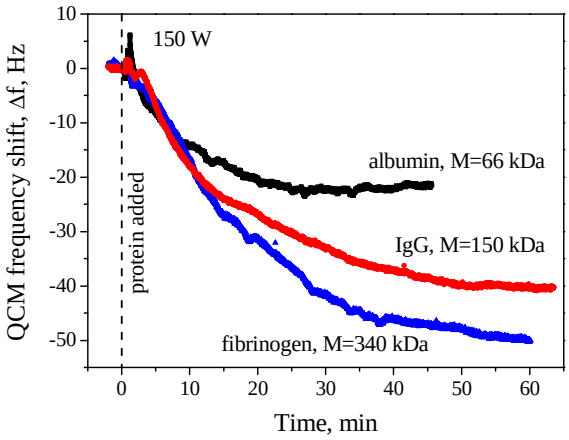

b)

Figure 3.29. The kinetics of protein adsorption as measured by QCM for the PEO-like plasma polymers deposited a) at 5 W power and b) at 150 W.

In the case of 5 W plasma polymers, good non-fouling properties were observed with respect to all proteins via insignificant QCM frequency shift (Figure 3.29a). Nitrogen was not found by the XPS analysis after multiple rinsing of the films with water and this further proves their resistance to irreversible protein adhesion. The 150 W films demonstrated fast accumulation of proteins on the surface (Figure 3.29b). The values of QCM frequency shift were proportional to the molar mass of the protein. For example, the lightest albumin induces 22 Hz frequency shift

whereas the heaviest fibrinogen produces the 50 Hz shift. XPS detected nitrogen after rinsing the films with water which indicates the irreversible character of the protein adsorption on the 150 W films. The detected 50 Hz frequency shift agrees with that previously published for adsorption of fibrinogen on $–CF_3$ terminated SAM [135]. This may indicate that amount of adsorbed fibrinogen is not affected by the surface hydrophilicity.

Fibrinogen as the protein producing the largest QCM frequency shift was used for further analysis to find the critical concentration of the ether groups required for nonfouling properties. The kinetics of fibrinogen adsorption on different PEO-like plasma polymers and on the reference uncoated crystal (gold surface) are shown in Figure 3.30. The non-fouling properties were found for all the samples deposited at power 20 W and below. Such range of powers corresponded to the concentration of ether groups above 65 %. Only two representative curves (82 and 84 % C-O-C) from this range are given in Figure 3.30, others are not shown as they are identical. A slight frequency shift of 5 Hz per 30 minutes is seen in the case of the films with 65 % of the C-O-C groups, however such shift is still comparable to the experimental error caused by the normal drifts in the measuring circuit. Eventually, distinct fibrinogen adsorption can be observed on the 30 W film with 61 % of C-O-C, and even in this case it is lower than on the reference gold surface.

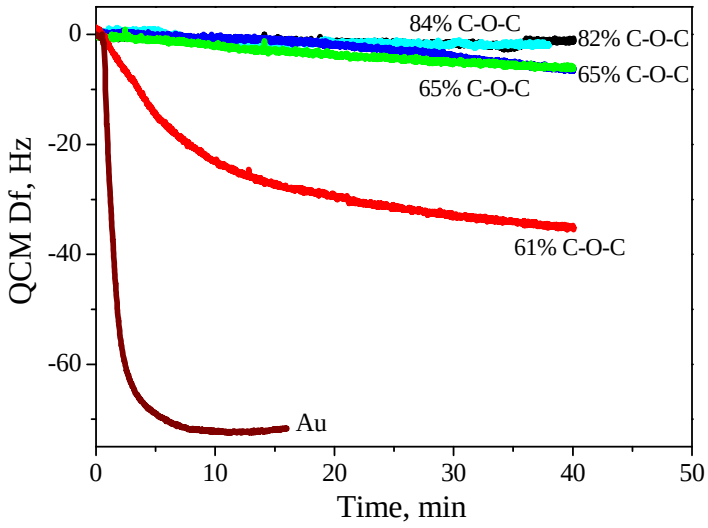

Figure 3.30. The kinetic curves of fibrinogen adsorption on the PEO-like plasma polymers with different retention of the ether groups.

The results obtained by ellipsometry (swelling experiments), AFM (indentation measurements), QCM (fibrinogen adsorption) and XPS (chemical composition) are summarized in Figure 3.31 where open diamonds correspond to the average number of repeating monomer units between the cross-links determined by Equation 3.3, solid squares correspond to the Young's modulus and the shaded box defines the area where adsorption of fibrinogen occurs.

It can be seen that even highly cross-linked films withstand adsorption of fibrinogen provided the concentration of the C-O-C groups exceeds 65 %. For example, the samples prepared at 10 and 30 W have close values of the Young's modulus and cross-link density which approaches to 1 monomeric unit between the cross-links. Nevertheless, the 10 W sample resists fibrinogen adsorption while the 30 W one does not. Remarkably, the sample deposited at 30 W reveals deficiency in the C-O-C groups in comparison to the 10 W counterpart. Thus, chemical composition is the key parameter that influences the non-fouling behavior of the films.

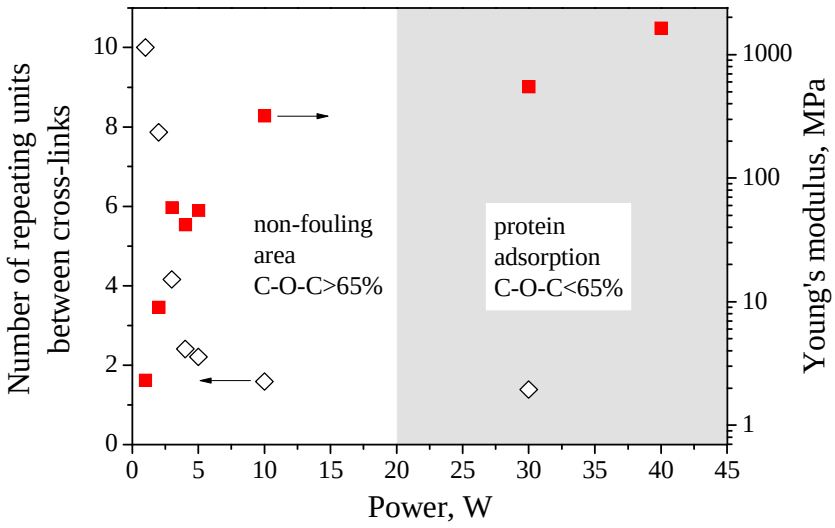

Figure 3.31. Correlation between the number of monomeric units between cross-links, the Young's modulus and the resistance to fibrinogen adsorption of the PEO-like plasma polymers prepared at different discharge power.

The necessity of long PEO chains to achieve non-fouling behavior is an issue frequently raised in the area of self-assembled monolayers (SAM) and polymer brushes. It has been usually reported that longer PEO chains of SAM are more

resistant to protein adsorption [63, 136]. Two-three repeating ethylene oxide units were shown to be sufficient for SAM to reduce protein adsorption, although the authors claimed that longer chains were more effective [136]. However, at least one paper proved that reduced bacteria attachment did not depend on the length of PEO chains [137]. Our findings also question the necessity of long PEO chains as PEO-like plasma polymers with as little as one monomeric unit between cross-links prove protein-resistant provided they contain more than 65 % of the ether groups.

Our results are consistent with the assumption suggested for plasma polymers prepared from the low-molar-mass precursors that shorter PEO chains may also produce the non-fouling effect [75, 86]. Apparently, the fragmentation of the low molar mass precursors in the plasma with successive random recombination of free radicals may hardly lead to the formation of long macromolecular chains. Nevertheless, significant incorporation of the C-O-C groups under mild plasma conditions is possible to render the films good protein resistance. For example, the experiments on pulse plasma polymerization of low-molar-mass molecules produced non-fouling surfaces from the precursor containing two ethylene oxide monomer units whereas the monomer containing only one did not prevent accumulation of proteins [86]. In the latter case, however, retention of the C-O-C groups was poor even under mild plasma conditions and this seemed to be a primary factor determining the failure of such films.

Johnston with co-workers [75] found that the films deposited from monoglyme (one ethylene oxide unit in the precursor) strongly adsorbed fibrinogen. The concentration of the C-O-C groups in this film was only 55% and this correlates well with the results of Wu [86]. The concentration of more than 70 % of the ether groups was reached for the films deposited from the higher molar mass precursors which showed significantly reduced (but non-zero) protein adsorption [75]. In contrast to our results, Johnston with co-workers observed that protein resistance was enhanced with increasing chain length of the precursor. The disagreement may be explained if the thickness of the studied films is taken into account. Johnston did not provide the exact information on the thickness of their films; however it can be estimated from the XPS data. Silicon signal from the glass substrates was detected which limits the thickness by several nanometers at most. In such ultra-thin films, the mobility of the chains may be significantly impeded by the proximity of a hard

substrate and the film/protein interaction may differ from that observed on thicker plasma polymers.

In general, both common features and differences can be revealed between plasma polymers prepared by plasma-assisted thermal vapour deposition of PEO and those deposited from low-molar-mass precursors. In a certain range of specific powers, for example the powers more than 5 W in Figure 3.31, both types of films are very close. The chains of about two monomeric units are present between the neighbouring junctions. This value reduces to one for higher powers. Even highly cross-linked plasma polymers with about one repeating unit between the cross-links behave as protein resistant provided the concentration of the C-O-C groups exceeds 65-70 %. Both types of the films may contain insignificant soluble fraction and may slightly swell in water as well. The soluble fraction of the "evaporated" films consists of linear PEO oligomers with a wide distribution of molar masses (up to $3x10^4$ $g \cdot mol^{-1}$). Such information is missing for the plasma polymers from volatile precursors; however, high values of molar mass can hardly be expected for them.

The range of powers below 5 W in Figure 3.31 is a region which separates plasma polymers deposited from volatile precursors and conventional polymers, and which is occupied by the "evaporated" films. In this region, slight variation of the discharge power results in manifold changes of the cross-link density, the Young's modulus, the solubility and the swelling ability of the films without strong influence on their close chemical resemblance to PEO. This type of the plasma polymers is close to so-called bimodal polymers which consist of networks of low-molar-mass and high-molar-mass components [129]. Such plasma polymers may be attractive in applications where controlled release of PEGylated drugs is required or for modification of CO_2 gas separation membranes where controlled flexibility and mesh size of PEO network is necessary [125, 127].

Formation of fibrin network

Nonfouling surfaces are of paramount importance in areas where protein adsorption should be avoided such as haemodialysis membranes, contact lenses, catheters and particularly in blood-contacting implant devices [48]. It has been reported that conventional PEO is nonthrombogenic which means it does not induce or promote the clotting of blood [138]. The detailed mechanism of blood clotting can

be found elsewhere [139]. Briefly, the development of thrombus is a complex cascade of reactions involving at least 12 blood proteins. It is triggered by adsorption of blood proteins with successive adhesion and activation of platelets. The final stage of this cascade involves cleavage of fibrinogen molecules by thrombin with the formation of fibrinopeptides which further polymerize into a fibrin gel. Fibrin together with trapped platelets forms tough and insoluble clot.

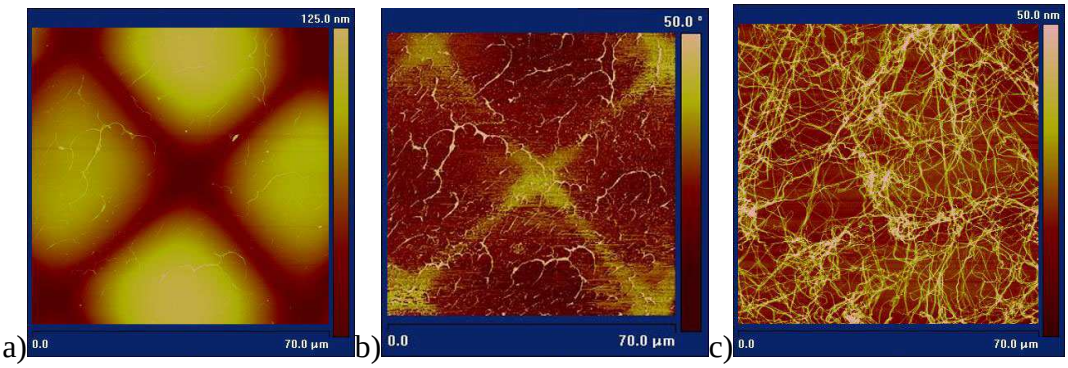

Figure 3.32. The AFM images of fibrin network on different surfaces: a) the topography image on the patterned PEO-like plasma polymer; b) the corresponding phase image on the patterned PEO-like plasma polymer; c) the topography image on the silicon substrate.

In this work, polymerization of fibrinogen into fibrin via activation by thrombin was studied to investigate nonthrombogenicity of PEO-like plasma polymers. The plasma deposition parameters were identical to those reported for the protein adsorption studies. The 100 nm thick continuous protein adhesive film (150 W, 30 % of C-O-C) was deposited onto the silicon substrate. After that, the 100 nm thick protein resistant film (5 W power, 75 % of C-O-C) was deposited over through the grid mask. Thus, the patterned samples with alternating fouling and non-fouling areas were prepared. The topography AMF image of the patterned sample subjected to solution where fibrinogen and thrombin were mixed is shown on the Figure 3.32a. The light areas correspond to the protein resistant areas whereas the dark crossing bars correspond to the underlying protein adhesive film. Fibrin fibers of maximum 25 nm height are hardly visible on the topography image at such scale and therefore a corresponding phase contrast image is also given in Figure 3.32b. Scarce adhesion of separate fibrin fibers can be discerned here. For comparison, the pure silicon substrate immersed in the same batch with the PEO-like plasma polymer sample is

shown in Figure 3.32c. A dense fibrin network has developed in this case. This confirms superior resistance of the PEO-like plasma polymers to formation of clots. It is interesting to notice that fibrin adheres similarly to the plasma polymers with different retention of the C-O-C structure. Figure 3.32b shows uniform distribution of fibrin over both protein resistant and protein adhesive areas without any preferential orientation. It can be attributed to swelling of poorly cross-linked 5 W plasma polymers. In swollen state, the protein resistant areas expand and prevent the biomolecules from reaching narrowed underlying bars of the protein adhesive film.

3.2.10. Interaction with blood

The analysis of interaction of PEO-like plasma polymers prepared at different discharge powers with human blood plasma and blood serum was performed by an SPR method (Section 2.2.12). The results of these measurements are summarized in Table 3.6.

As it was shown in Section 3.2.9 the ability of PEO-like coating to resist protein adsorption decrease with increasing discharged power. Here, adsorption from single protein solutions (lysozyme and fibrinogen) was also very low or undetectable for the films prepared at 3 and 5 W discharge power. Adsorption increased for the 10 W film, yet it was still much weaker than on the reference gold sample. An important observation can be made when comparing the results of adsorption from blood plasma and blood serum. Significant accumulation of proteins (though 2-3 times lower than on the reference gold) was detected on each type of the films. Obviously, adsorption of proteins from complex biological media is much more adverse and does not obey the same trends as adsorption from single protein solutions.

Power of discharge, (W)	**Lysozyme, (pg/mm^2)**	**Fibrinogen, (pg/mm^2)**	**Blood plasma, (pg/mm^2)**	**Blood serum, (pg/mm^2)**
3	53.0	0.0	1692.0	1231.5
5	9.0	0.0	1537.5	1170.0
10	429.0	201.0	1252.5	1051.5
Reference gold	1207.0	3208.0	3073.0	2910.0

Table 3.6. Protein adsorption on the PEO-like plasma polymers detected by SPR.

Summary

Rf magnetron sputtering did not prove to be efficient for production of PEO-like films as strong fragmentation of macromolecular chains resulted in poor retention of the ether groups in the plasma polymers. Plasma-Assisted Thermal Vapour Deposition is advantageous as it offers better control of the film properties via specific power which can be adjusted independently by the evaporation rate and by the power delivered to the magnetron.

PEO macromolecules depolymerize thermally when exposed to elevated temperature under vacuum. Thermal degradation of PEO proceeds with random scission of the backbone and with a release of volatile species of diverse composition. The low molar mass fraction consists of atomic and molecular hydrogen, C, CH_x, OH, H_2O and CO species. The higher molar mass fraction is composed of oligomers of the macromolecular chain that differ in the number of (-CH_2-O-) units. Furthermore, oligomers with a lack and with an excess of hydrogen are present in the gas phase suggesting that radical termination by disproportionation is responsible for this phenomenon.

The films deposited from the emitted oligomeric species have chemical composition very close to parent PEO. Ether groups constitute about 80 % of carbon atoms. The molar mass distribution of the oligomers that constitute the evaporated film is shifted to lower masses as compared to the precursor PEO and ranges from approximately 300 to 2500 $g \cdot mol^{-1}$. Such films are completely soluble in aqueous solutions and this restricts their use for modification of surfaces to be in contact with biological media.

Employment of plasma to activate emitted oligomeric fragments leads to their further fragmentation and formation of free radicals which take part in plasma polymerization reactions on the surface. The resultant films are heterogeneous mixtures of macromolecular chains with much broader molar mass distribution entangled within a polymeric network. Such films exhibit a hydrogel-type behavior. Differently cross-linked films were prepared in which the number of repeating monomeric units between cross-links ranged from 1 to 10 whereas chemical composition was close to conventional PEO. These films are intermediates between conventional polymers and plasma polymers deposited from low-molar-mass precursors. The changes of cross-link density resulted in significant changes of

sol/gel ratio, solubility, swelling behaviour and mechanical properties of the films. The films with as few as 1-2 repeating units between the cross-links and with >65 % retention of the ether groups resisted adsorption of fibrinogen, adhesion of cells and development of fibrin network. Thus, retention of the C-O-C groups >65 % was found to be a key factor influencing the non-fouling properties of the plasma polymers.

In case sterilization of the PEO-like plasma polymers is required, only UV radiation can be used without a risk of loosing the non-fouling properties.

3.3. Atmospheric pressure amplitude modulated AC SDBD

Low pressure plasma-assisted thermal vapour deposition was found effective for preparation of stable PEO-like plasma polymers with required properties. In recent years, a scientific urge was addressed to deposition of plasma polymers by atmospheric pressure plasmas as well. It is therefore of high academic as well as of technological interest to investigate the applicability of atmospheric pressure discharge for fabrication of the PEO-like films and to compare the results with the low-pressure plasma.

Our research is focused on the properties of plasma polymers produced at atmospheric pressure by amplitude-modulated surface Dielectric Barrier Discharge (SDBD). The use of amplitude modulation was inspired by the works with low pressure plasma polymerization of ether-bearing precursors which showed that plasma chemistry can be tuned by pulsing the discharge at low duty cycles [85-91]. The use of unsaturated precursors such as those bearing the vinyl structure may favour the pulsed plasma polymerization. In this case, in addition to the radical-radical recombination the radicals may take part in conventional molecular polymerization reactions involving opening of the unsaturated bond and chain propagation. During the plasma off-time this process is facilitated due to an absence of ion bombardment and, generally, pulsed plasma polymerization produces films with enhanced retention of precursor's structure [140]. In our work, di(ethylene glycol) vinyl ether (DVE) with chemical structure $H_2C=CH(OCH_2CH_2)_2$-OH was chosen as the monomer containing a vinyl bond, which might favour chain propagation steps when interacting with free radicals in the discharge. The aim of this part of the research was to evaluate non-fouling properties of atmospheric pressure PEO-like plasma polymers and to demonstrate correlations in plasma chemistry processes between pulsed low-pressure and amplitude-modulated SDBD atmospheric pressure discharges.

3.3.1. Diagnostics of AC SDBD

Electrical parameters

The discharge power was measured by acquiring the electrical characteristics of the SDBD at various deposition conditions. Figure 3.33 shows the typical waveforms of the discharge voltage (u_{HV}), voltage on a measuring capacitor (u_C) and the PMT signal in pure argon and Ar/monomer mixture for AC high voltage u_{AC} = 2.2 kV_{p-p}, modulation frequency f_M = 1 kHz, and argon flow Φ = 1 slm.

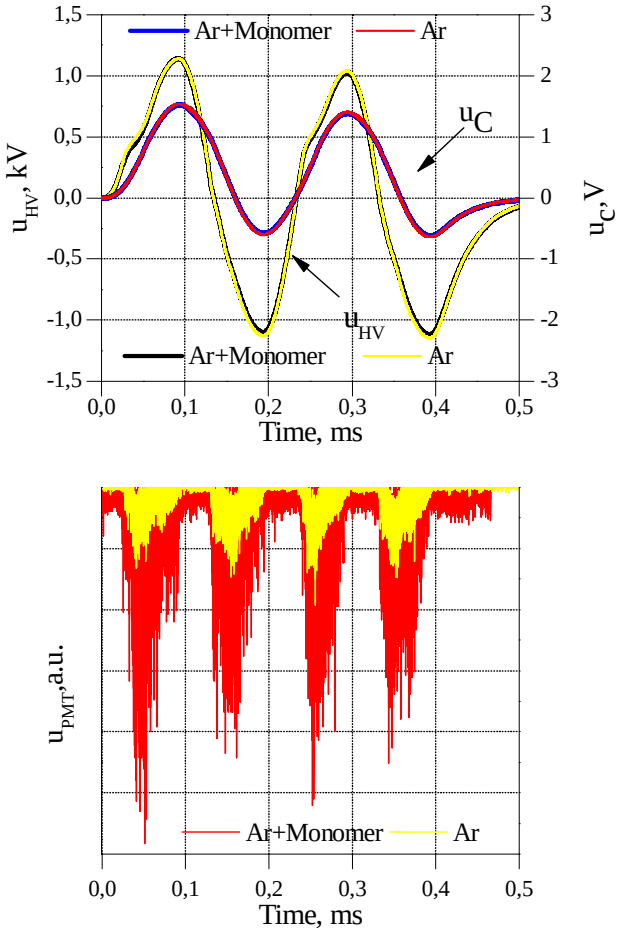

Figure 3.33. Typical electrical and optical characteristics of the SDBD discharge in pure argon and in argon/monomer vapours for u_{AC} = 2.2 kV_{p-p} (peak-to-peak), T_{ON} = 0.4 ms, D = 0.4, Ar flow rate Φ = 1 slm.

The characteristics were used to obtain voltage – charge (Lissajous) figures (Figure 3.34). These were used to evaluate energy dissipation during the T_{ON} period at given AC cycle and, consequently, the average discharge power as follows:

$$E = P \times T \tag{3.7}$$

$$P = \frac{1}{T}\int_T p(t)dt \tag{3.8}$$

Here, E is energy delivered to the discharge, T is the time period which consists of the sum of T_{ON} and T_{OFF}, P is power of discharge averaged over one period and $p(t)$ is instantaneous power of the discharge [141].

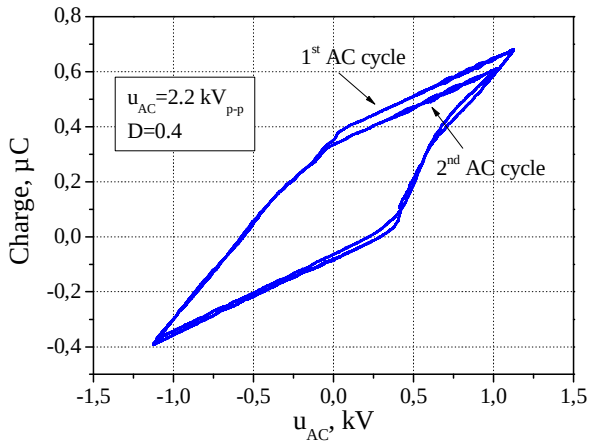

Figure 3.34. The voltage – charge Lissajous figures for the SDBD in Ar; u_{AC} = 2.2 kV_{p-p}, T_{ON} = 0.4 ms.

The instantaneous power is given by voltage and current of the discharge (Equation 3.9)

$$p(t) = u(t) \times i(t) \tag{3.9}$$

,where current is:

$$i(t) = \frac{dq}{dt} = C\frac{du_C}{dt} \tag{3.10}$$

In equation 3.10, $u(t)$ is voltage of discharge determined as $u(t) = u_{HV} + u_C \approx u_{HV}$ because $u_{HV} >> u_C$; u_{HV} and u_C is high voltage and voltage on a measuring capacitor, respectively (Figure 3.33); C is a condenser capacity.

The instantaneous discharge power is therefore:

$$p(t) = u(t) \times i(t) \approx u_{HV}(t) \times C \frac{du_C}{dt} = u_{HV}(t) \times \frac{dq_C}{dt}, \qquad (3.11)$$

where q_C is the charge appearing on the capacitor per unit of time. Knowing the values of $u_{HV}(t)$, $u_C(t)$, C and substituting Equation (3.11) into Equations (3.7) and (3.8) average energy and power delivered to the discharge can be obtained.

With u_{AC} increasing from 2.0 to 6.6 kV_{p-p}, the energy dissipation during the T_{ON} changed from 0.5 to 3.0 mJ for 1 AC cycle pulse and from 1 to 5.5 mJ for 2 AC cycle pulse, respectively (Figure 3.35). The discharge driven in pure argon and argon with DVE admixtures showed similar dissipated energy with u_{AC} close to 2.0 kV_{p-p}. For voltages approaching the upper u_{AC} limit (6.6 kV_{p-p}) the discharge energy dissipated in argon/DVE mixture was about 5 % lower with respect to that in pure argon.

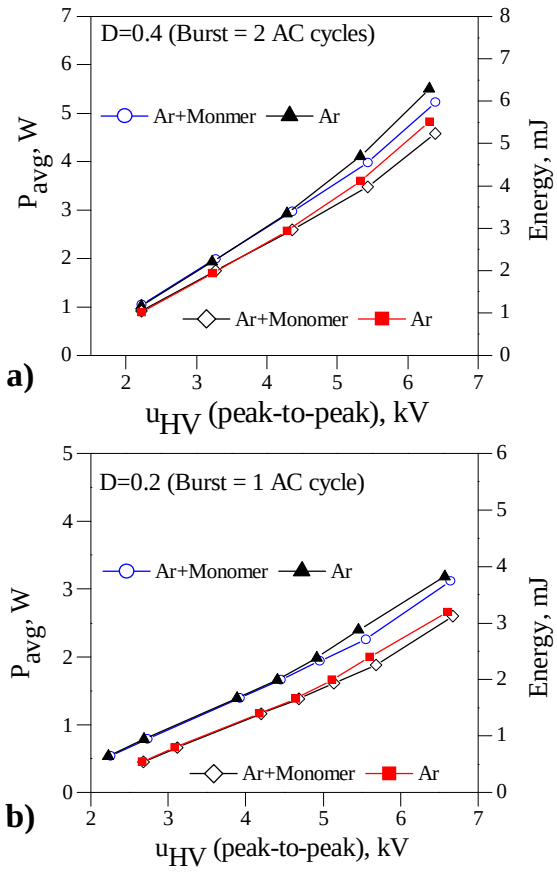

Figure 3.35. Average energy (a) and power (b) delivered to the discharge in pure argon and in argon with DVE vapours during the T_{ON} period as a function of AC high voltage peak-to-peak amplitude for two different duty cycles (D = 0.2 and 0.4, Ar flow rate Φ = 1 slm, f_{AC} = 5 kHz, f_M = 1 kHz).

Optical Emission Spectroscopy

Plasma induced emission (PIE) spectra produced by micro-discharges exhibits strong emission of Ar lines and band emission produced by OH, N_2, CH and CO species originating from the DVE fragments or from carrier gas impurities such as N_2, O_2, H_2O (Figure 3.36). The typical time-averaged emissions of SDBD were obtained with and without the DVE monomer admixtures. The hydroxyl radicals were detected by characteristic OH ($A^2\Sigma$–$X^2\Pi$) emission at 310 nm. The CH and CO bands were observed in the region from 360 to 450 nm and only in the case of argon/DVE mixture. The strongest argon lines were observed in the 650–900 nm range due to $3s^23p^54p \rightarrow 3s^23p^54s$ transitions. In pure argon, weak emission of N_2 ($C^3\Pi_u \rightarrow B^3\Pi_g$) second positive system was also observed.

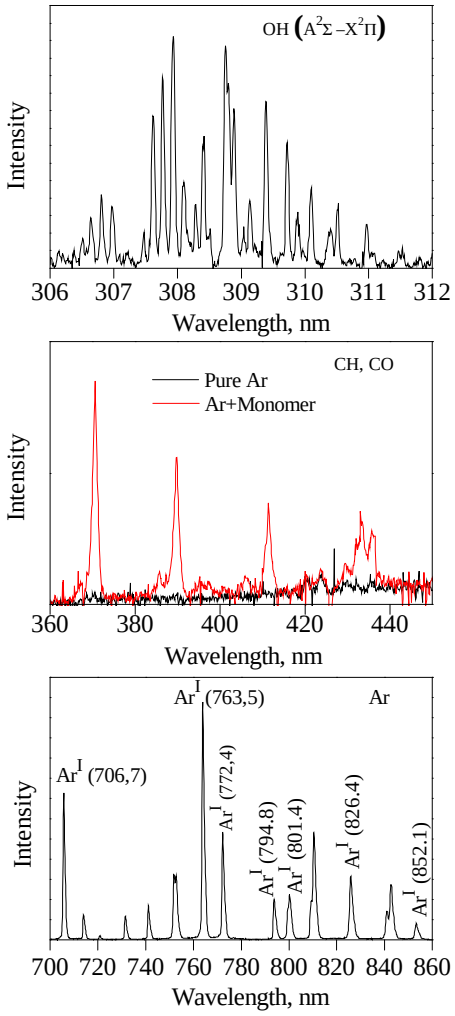

Figure 3.36. Typical emission spectra of the SDBD in argon with DVE vapours averaged over first positive half period. Ar flow rate Φ = 1 slm, u_{AC} = 2.2 $kV_{p\text{-}p}$, f_{AC} = 5 kHz, f_M = 1 kHz, D = 0.4.

Figure 3.37 shows the 3D graphs of the time-resolved PIE spectra of OH and Ar emissions obtained for T_{ON} period composed of two consecutive AC cycles. On assumption that emission of argon is controlled by the direct electron impact excitation processes, noticeable variations of Ar emission intensities reveal active discharge periods within a given AC cycle.

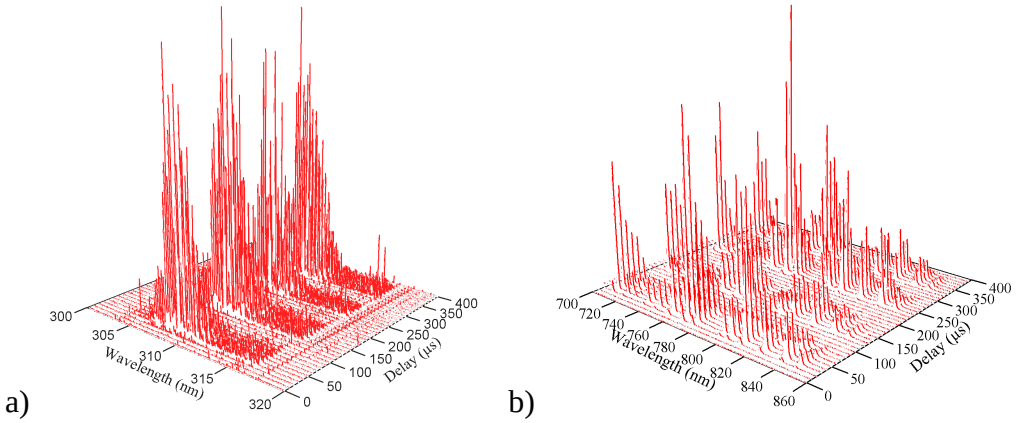

Figure 3.37. Time evolution of a) OH and b) Ar^{I} emissions in argon/DVE discharge feed (Ar flow rate Φ = 1 slm, u_{AC} = 2.2 $kV_{p\text{-}p}$, f_{AC} = 5 kHz, f_M = 1 kHz, D = 0.4).

3.3.2. Optimization of the deposition parameters

Efficiency of plasma polymerization is strongly dependent on a number of parameters including power of the discharge, flow rate of Ar/monomer mixture, the distance between the substrates and the electrodes etc [94]. The influence of a specific parameter on the film properties was found by performing a set of depositions with varying one of the inspected parameters while keeping all other parameters constant. The deposition rate and retention of the PEO-like character were considered. Similar to the low-pressure depositions, the PEO-like character of deposited films was detected through the peak of ether group located at 1123 cm^{-1} (Figure 3.38). The shoulder at 1086 cm^{-1} may also be assigned to the stretching vibrations of ether group, yet coupled with the deformation vibrations of the CH_2 group. Other chemical groups identified in the IR spectrum of deposited films were OH (3430 cm^{-1}), CH_2 (2944, 2882 cm^{-1} and a number of smaller peaks between 1500 and 900 cm^{-1}) and C=O (1726 cm^{-1}).

First, the distance between the electrode and the substrates was changed from 1 to 4 mm with a step of 1 mm whereas argon flow rate (Φ = 1.0 l/min), AC driving

voltage amplitude (u_{AC} = 2.2 kV) and discharge duty cycle (D = 0.4) were held fixed. The maximal deposition rate of 1 nm/min was obtained at 2 and 3 mm distance. At a larger distance, the substrates were out of the zone of the discharge and the deposition rate decreased. At a smaller distance, slower deposition rate was also detected which was given by partial ablation of deposited material from the substrate surface mainly due to enhanced photolysis by UV/VUV radiation.

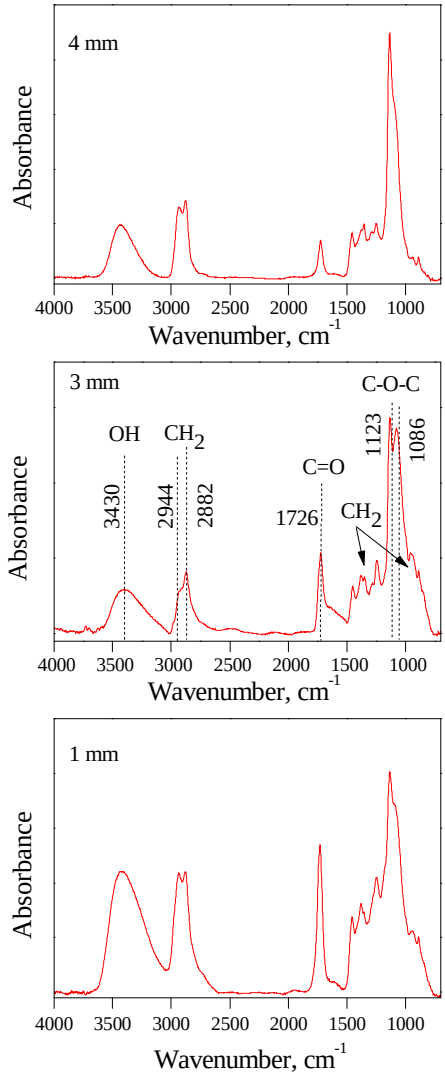

Figure 3.38. The FTIR-RAS spectra of PEO-like plasma polymers deposited at different substrate-SDBD electrode distances (Ar flow rate 1 slm, u_{AC} = 2.2 kV_{p-p}, D = 0.4).

The plasma polymerization mechanisms are essentially fast step-growth processes. The discharge induced fragmentation of original monomer molecules results in the formation of dissociation products including free radicals.

Consequently, free radicals take part in specific chemical reactions such as chain propagation and termination through recombination [1, 4]. A random polymeric network with short cross-linked chains is created due to the diversity of reactive species in the discharge. The degree of cross-linking then depends on the discharge properties.

In the case of SDBD with argon used as a carrier gas, the formation of plasma polymers on the substrate is likely based on the following dominant processes: (i) electron impact reactions, (ii) photolytic reactions and (iii) modification of the film surface induced by VUV/UV radiation [1, 4, 142, 143, 144]. The electron impact interactions with the DVE molecules produce various radicals. Photochemical processes (photodissociation, photolysis, or photodecomposition) and modification of the film surface are induced by VUV/UV photons (120-250 nm) produced by argon excimer molecules [144]. With photon energies of about 5-10 eV, this wavelength region is very important for photolysis processes. Such UV radiations can split most chemical bonds (*e.g.* C-C and C-O (3.5-4 eV), C-H and O-H (4-5 eV), C=C (6-6.3 eV) and C=O (8-8.5 eV) etc.) and, consequently, promote further chemical reactions in the afterglow/deposition zone. An interaction of high energy photons with deposited film can (i) reduce the deposition rate by the resputtering process, (ii) cause a loss of non-fouling film properties or (iii) modify the surface of the film by increasing the degree of cross-linking [1, 4, 142-144, 145, 146, 147, 148]. Last but not least, interaction of Ar($^3P_0$) and Ar($^3P_2$) metastable species carying more than 11 eV with polymer film surface should be considered.

At the shortest SDBD-substrate distance (1mm) the film deposition might be impeded by active discharge processes and by the flux of VUV/UV radiation. With increasing distance from the SDBD surface, the influence of active discharge species and VUV/UV photons decreases. The formation of the plasma polymer film is determined mainly by the transport of active species from the zone of discharge. The vinyl bonds available in the precursor molecules may further promote polymerization via their opening upon interaction with free radicals coming from the SDBD. Then, the ethylene glycol structure stays to some degree intact due to the reduced action of destructive VUV/UV radiation. This assumption is supported by detected changes in chemical composition of the films. At increasing electrode-substrate distance better retention of the PEO character can be observed on the FTIR spectra which is indicated by a significant enhancement of the C-O-C and by reduction of the C=O

bands (Figure 3.38). The maximal retention of the C–O–C groups was obtained at distances of 3 and 4 mm. Therefore, the distance of 3 mm was chosen for all further experiments.

In the next experiments, the flow rate of argon was varied between 0.5 and 2.0 l/min (D = 0.4, f_{AC} = 5 kHz, f_M = 1 kHz). The deposition rate increased with the flow rate to the value of about 1 nm/min at Φ =1.0 l/min and it did not change significantly thereafter. Such behaviour agrees with low pressure plasma polymerization where the region of maximal deposition usually separates the power deficient (high flow rate of monomer) and the monomer deficient (low flow rate of monomer) areas.

The flow rate of argon basically controls the residence time of monomer molecules in the discharge zone and also the gas temperature. The influence of this parameter on the character of deposited films is enhanced at low argon flow rates. The flux of active radicals was evidently insufficient for initiating the plasma polymerization processes delivered by an Ar flow of 0.5 slm. Consequently, the produced films were very thin and the intensity of signal on FTIR spectrum looked exceedingly weak (Figure 3.39). At higher flow rates, the efficiency of the film formation increases and the FTIR spectra reveal better signal-to-noise ratio.

Note also that at an Ar flow rate of 2 slm the intensity of the C=O absorption increased compared with the Ar flow of 1 slm. It can be suggested that at the highest flow rates radical induced polymerization through the vinyl bonds (responsible for better retention of the C-O-C structure) is hindered due to a shorter interaction time between the monomer molecules and free radicals.

Therefore, the flow rate of argon of 1.0 l/min was chosen for further experiments. At this value, the concentration of DVE in Ar was measured to be 150 PPM. All the data reported below were obtained at this concentration of DVE.

In the above considerations, the deposition rate was regarded as average thickness of the film related to time of deposition. However, the films were not deposited homogeneously over the entire substrate surface. The SDBD is formed on the edges of the electrode stripes and it is essentially inhomogeneous. The substrates are therefore exposed to the areas of discharge alternating with the areas where the discharge is absent. Such pattern is revealed on the substrates as a profile with interlacing areas of bigger and smaller thickness.

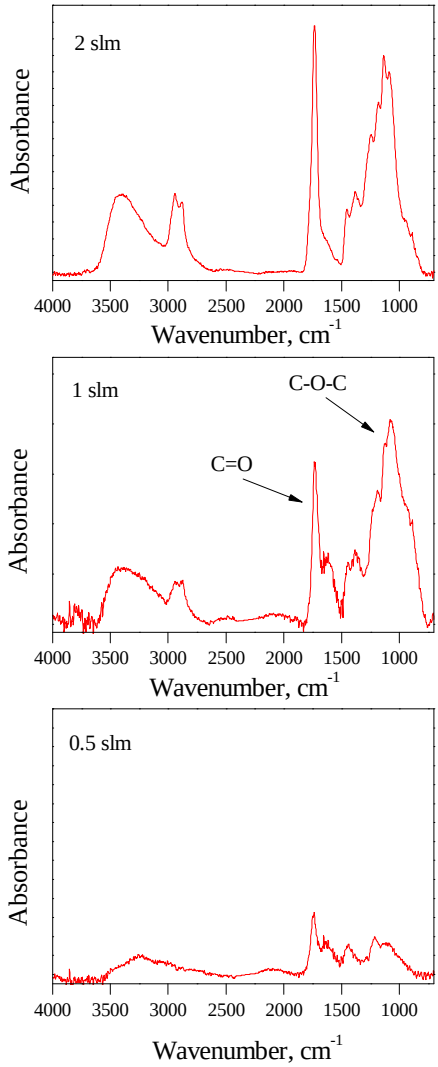

Figure 3.39. The FTIR-RAS spectra of the PEO-like plasma polymers deposited by SDBD at different flow rates of argon (distance 3 mm, u_{AC} = 4.9 kV_{p-p}, D = 0.4).

3.3.3. Influence of average power and pulsing

Reportedly, the chemical composition of PEO-like plasma polymers deposited from DVE vapours under low pressure conditions is strongly affected by the power of discharge and by duty cycles employed [85-87]. One of the aims of this thesis was to investigate how significant these effects are in the atmospheric pressure SDBD.

Under the constant substrate-target distance and flow rate of the Ar/DVE mixture, the deposition rate decreases with average power. For example, Figure 3.40 shows the average thickness of the films deposited for 45 minutes at the average

power changing from 1 to 6 W and with other parameters held constant (Table 3.7). The smallest power of 1 W yields the most effective deposition while at higher powers the deposition is much slower. This effect is apparently also related to partial ablation of the deposited material back to the gas phase. In low pressure plasmas, the mean free paths of the species are sufficiently large to rule out their diffusive transport to the substrate. The film formation is restricted by reaction kinetics in the gas phase and on the surface as well as by ion bombardment of the surface. Activation of precursor molecules in the gas phase proceeds predominantly via inelastic collisions with energetic electrons and by UV radiation. Under constant supply of the monomer, the electron density increases with power and, as a consequence, the number of active species also increases. This results in an increase of the deposition rate. The deposition rate saturates at high degree of conversion of precursor as further increase of power does not yield more active species unless the supply of the monomer is increased [4]. This behaviour is not completely true for some monomers, especially those containing fluorine and oxygen, where the deposition rate may decrease with power due to enhancement of chemical etching phenomena [4].

Parameters	**Data**							
f_M (Hz)	1000							
Cycles per T_{ON}	2				1			
T_{ON} (msec)	0.4				0.2			
T_{OFF} (msec)	0.6				0.8			
D	0.4	0.4	0.4	0.4	0.2	0.2	0.2	0.2
u_{AC} (kV)	2.2	3.7	4.4	6.4	2.7	4.5	5.0	6.6
Average power (W)	1.0	2.0	3.0	6.0	0.8	1.7	1.9	3.1
C–O–C (%)	67	53	45	29	64	46	43	38

Table 3.7. The experimental parameters of the SDBD depositions with variable average power.

At atmospheric pressure, the mean free path is very small while the gas flow is significant and the film growth is most probably limited by diffusion of active species from the bulk of plasma to the surface. Furthermore, at the electrode-substrate distance of 3 mm chosen here the substrates are actually located out of the

active discharge zone which was estimated not to exceed 0.5 mm from the electrode surface. Therefore, the direct influence of plasma on growth of plasma polymer can be neglected here. As it can be seen in Figure 3.40, ablation dominates over polymerization with increasing power and this effect is attributed mainly to the action of UV/VUV radiation discussed above.

The deposition rate of about 1 nm/min measured in this work is comparable with the results obtained at low pressure at similar average powers (3-5 nm/min [86], 1.65 nm/min [87], 3 nm/min [89]) but it is much lower than that reported by Da Ponte with co-workers for atmospheric pressure plasma deposition (up to 37±2 nm/min) [93]. Higher deposition rate can be expected if heating the precursor is applied.

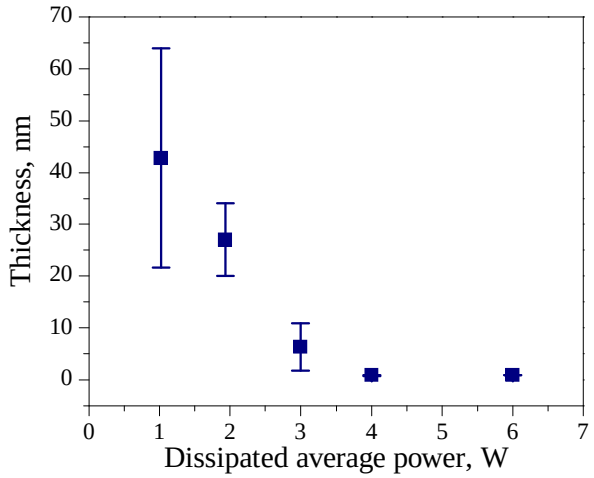

Figure 3.40. The thickness of deposited PEO-like plasma polymers at different SDBD average power (Ar flow rate Φ = 1.0 slm, electrode-substrate distance 3 mm, f_{AC} = 5 kHz, f_M = 1 kHz, D = 0.4).

Figure 3.41 shows the C 1s XPS and FTIR spectra of the PEO-like films. As in the case of low-pressure films, the XPS C 1s spectra were fitted with four components at 285.0 eV (C-C and C-H groups), 286.5 eV (C-O-C and C-OH groups) 288.0 eV (C=O groups) and 289.0 eV (O-C=O groups). With decreasing the average power from 6 to 1 W, the second component at 286.5 eV increases from 29 % to 67 % and other components vary inversely. At the average power of 1 W the C 1s spectrum is similar to low pressure plasma polymers although the retention of the C-O-C groups is worse than 75-80 % found for the latter.

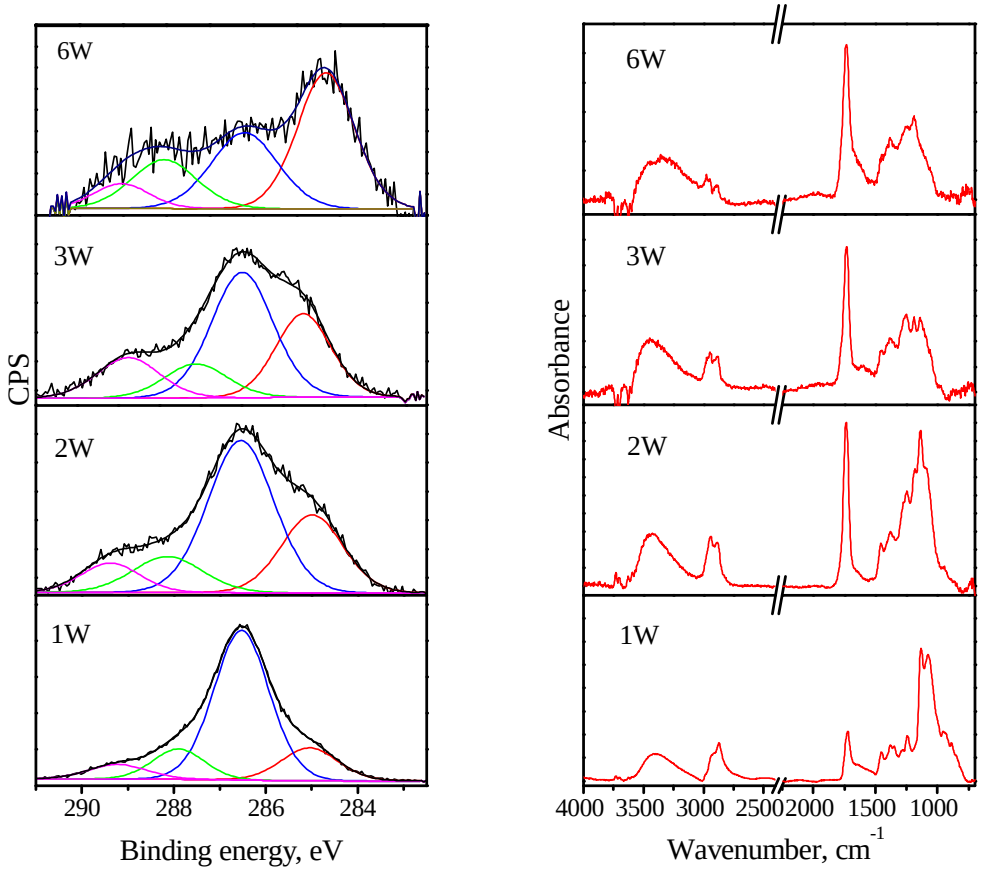

a) b)

Figure 3.41. The C1s XP spectra a) and FTIR spectra b) of the PEO-like plasma polymers deposited by atmospheric pressure SDBD at different average powers (the experimental details are given in Table 3.7).

Such changes are further reflected in the FTIR spectra. Remarkably, the vinyl groups present in the original molecules are hardly to be detected here. The stretching vibrations of the C=C group in the DVE molecule absorb at ~1620 cm^{-1} [86]. Here, this peak is absent or overlapped by absorption of carbonyl-based species which are not originally present in the precursor. Furthermore, in vinyl ethers the asymmetric and symmetric CH_2 stretching vibrations of the CH_2=CH- groups are located at 3120 cm^{-1} and 3045 cm^{-1}, whereas those of the –CH_2- groups are found at lower wavelengths at 2930 cm^{-1} and 2880 cm^{-1}, respectively [149]. The FTIR spectra in Figure 3.41b give ~2900 cm^{-1} for the CH_2 groups which implies that hydrocarbons in the plasma polymers are bound predominantly as single-bond methylene species. Significant conversion of the C=C groups indicates that in atmospheric pressure SDBD radical polymerization of DVE via opening of the vinyl bond is effective as

well as in low pressure PECVD [85-87]. Moreover, the presence of the carbonyl-based species confirms fragmentation and successive rearrangement of the chemical structure of the precursor molecules. At the average power of 6 W, absorption of the C=O species dominates the spectrum, hydroxyls are also very strong and the band of the C-O-C groups is poorly resolved and overlaps with various deformation vibrations of the CH_2 groups. The character of the spectrum bears a strong resemblance to highly cross-linked plasma polymers where collective interactions among a variety of closely packed species result in broadening and merging of individual bands. With decreasing average power, the C=O and OH peaks subside while the C-O-C peak emerges. At the power of 1 W, a strong absorption of the C-O-C groups indicates a good retention of the PEO character within the films.

Analogous results were obtained for the similar experiments performed with duty cycle fixed at 0.2. The details of these depositions are also given in Table 3.7. The XPS and FTIR spectra shown in Figure 3.42 demonstrate the same trends as observed for D=0.4. Thus, both experiments reveal an improvement of retention of the PEO character with reducing discharge power and this correlates well with similar findings obtained for low pressure plasma polymerization [72-87, 89-91, 150, 151, 152, 153] and by atmospheric pressure PECVD [92, 93]. In the latter case, note that higher values of discharge power (30-80 W) [92] and (8-13 W) [93] were used in contrast to 1-6 W depositions reported here.

In order to study the effect of power modulation, the following two sets of the experiments were performed. First, the modulation frequency and high voltage were fixed at 1000 Hz and at 2.2 kV, respectively, and the number of cycles per T_{ON} was changed sequentially from 4 to 1. As a consequence, T_{ON} was shortened from 0.8 to 0.2 msec, T_{OFF} was extended from 0.2 to 0.8 msec and duty cycle correspondingly decreased from 0.8 to 0.2 (Table 3.8).

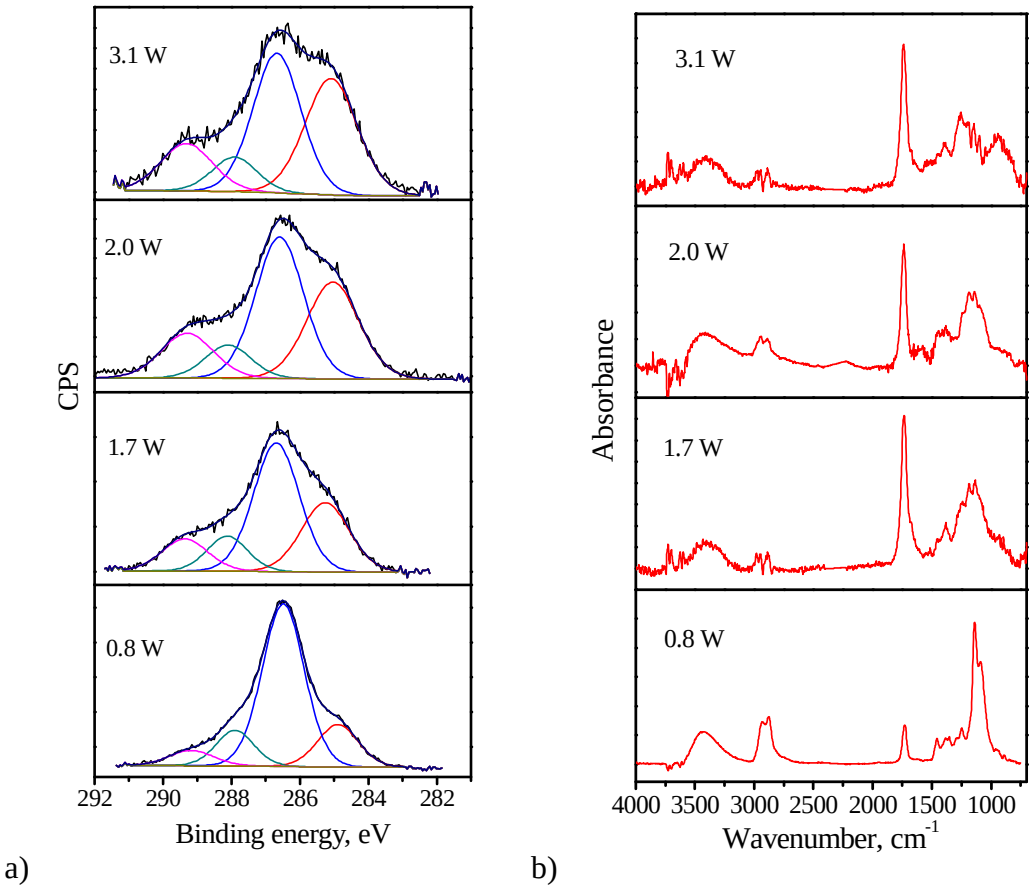

Figure 3.42. The C1s XP a) and FTIR b) spectra of the PEO-like plasma polymers deposited by atmospheric pressure SDBD at different average powers an duty cycle fixed at 0.2 (Ar flow rate Φ = 1.0 slm, electrode-substrate distance 3 mm, f_{AC} = 5 kHz, f_M = 1 kHz).

Figure 3.43 and Figure 3.44 show significant changes in chemical composition of the films produced this way. The C 1s XPS spectra reveal that at the highest duty cycle the relative importance of the C-O-C groups is comparable with the C-C/C-H groups whereas with decreasing duty cycle ethers start dominating the spectra. The overall increase in retention of the C-O-C groups is improved from 47 % at D=0.8 to 65 % at D=0.2. It is also apparent that the contribution from carbon doubly and triply bound to oxygen is reduced with decreasing duty cycle. This trend is even more evident in the FTIR spectra showing a substantial enhancement of absorption of the C-O-C groups (~1100 cm^{-1}) relative to the C=O groups (1730 cm^{-1}) as duty cycle decreases. Similar to the spectra given above, the C=C groups are not observable here, probably except for D=0.8 where a small peak at ~1600 cm^{-1} may be indicative of their presence. In this case, however, availability of the C=C groups

is not given by better retention of the precursor's structure but rather by enhanced fragmentation of the monomer and recombination of created radicals with formation of unsaturated functionalities.

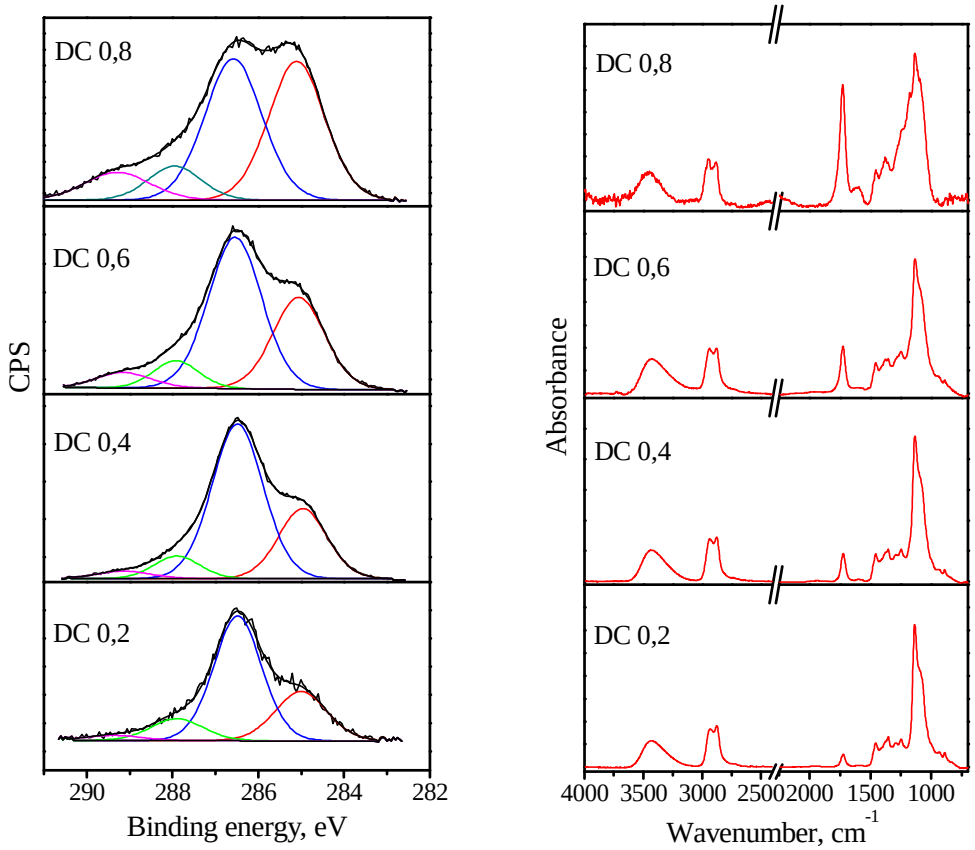

a) b)

Figure 3.43. The C1s XP spectra a) and FTIR spectra b) of the PEO-like plasma polymers deposited by atmospheric pressure SDBD at different duty cycles (T_{ON} and T_{OFF} variable, the experimental details are given in Table 3.8).

Parameters	**Data**			
f_M (Hz)	1000			
Cycles per T_{ON}	1	2	3	4
T_{ON} (msec)	0.2	0.4	0.6	0.8
T_{OFF} (msec)	0.8	0.6	0.4	0.2
D	0.2	0.4	0.6	0.8
u_{AC} (kV)	2.2			
Average power (W)	0.5	1.0	1.5	2.0
C–O–C (%)	65	62	58	47

Table 3.8. The data experimental parameters of the SDBD depositions with variable duty cycles.

The second type of the experiments with pulsing was performed with T_{ON} fixed and with different modulation frequencies (Figure 3.44). For example, the modulation frequency of 1000, 500 and 200 Hz was applied with T_{ON} fixed at 0.4 msec. Such change of modulation frequency was equivalent to increase of T_{OFF} from 0.6 to 4.6 msec and, correspondingly, to a decrease of duty cycle from 0.4 to 0.08. The XPS (Figure 3.44a) showed only a slight increase in retention of the C-O-C groups from 53 to 61 %, whereas both XPS and FTIR (Figure 3.44b) revealed a decrease of the carbonyl-based species with decreasing duty cycle. These experiments confirmed the trend observed in the first set where T_{ON} and T_{OFF} varied simultaneously, however the changes in chemical composition of the plasma polymers were not so large regardless of the extended range of duty cycles.

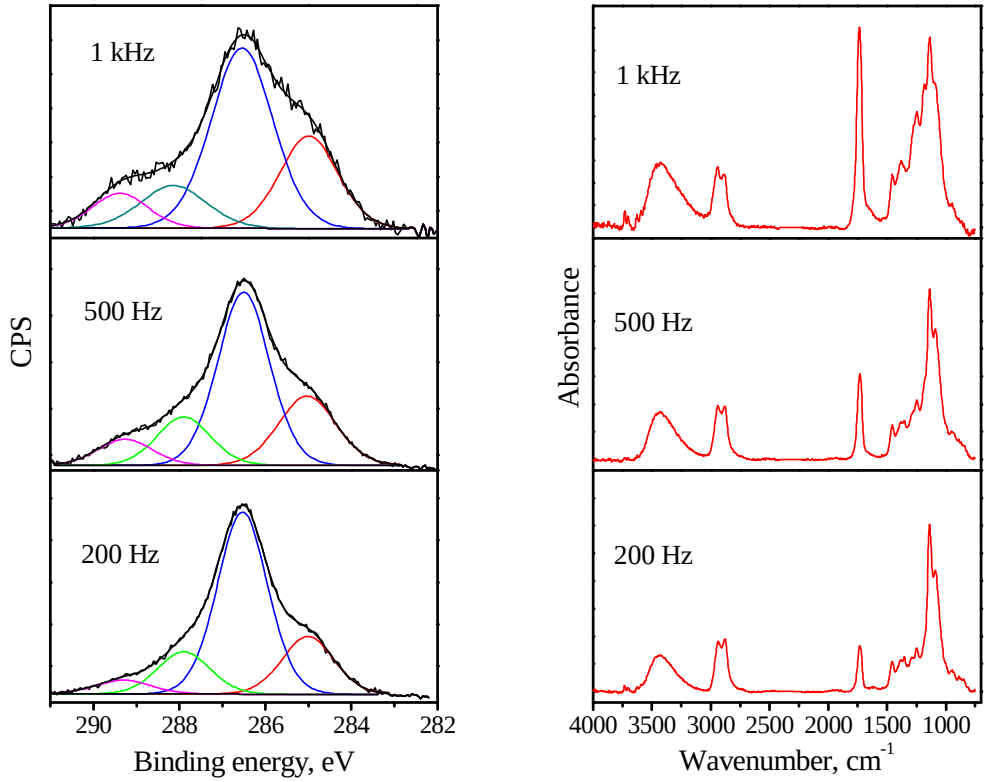

a) b)

Figure 3.44. The C1s XP spectra a) and the FTIR-RAS spectra b) of the PEO-like plasma polymers at different duty cycles (Ar flow rate 1 slm, distance 3 mm, u_{AC} = 3.9 kV_{p-p}).

Parameters	Data						
f_M (Hz)	1000	500	200	2000	1000	500	200
Cycles per T_{ON}	2			1			
T_{ON} (msec)	0.4	0.4	0.4	0.2	0.2	0.2	0.2
T_{OFF} (msec)	0.6	1.6	4.6	0.3	0.8	1.8	4.8
D	0.4	0.2	0.08	0.4	0.2	0.1	0.04
u_{AC} (kV)	3.9						
Average power (W)	2.5	1.2	0.5	2.7	1.4	0.7	0.3
C–O–C (%)	53	53	61	57	64	69	69

Table 3.9. The experimental parameters of the SDBD depositions at different duty cycles.

The better retention of precursor's structure with increasing T_{OFF} (decreasing duty cycle) was very well documented in low pressure PECVD. The effect was attributed a) to reduced ion bombardment of growing film and b) to free-radical attack on the vinyl bond which promoted polymerization. When plasma is on, significant fragmentation of the monomer molecules occurs resulting in substantial loss of the C-O-C structure. After switching off the plasma, negative substrate potential decays fast, thus minimizing ablation and bond cleavage processes by highly energetic ions. Therefore, during plasma off times, polymerization via opening of the double bond induced by free radicals proceeds in the absence of ion bombardment and the overall chemistry is more selective in terms of retention of the C-O-C structure. In many cases, however, it was not explicitly stressed that reducing duty cycle with other parameters held constant (including the peak power, P_{peak}) leads to reduction of effective power, i. e. power averaged over a period of pulsing, $P_{av} = P_{peak} \cdot D$, and a similar degree of retention can be achieved simply by performing plasma polymerization in CW mode but at lower power equivalent to P_{av}. Nevertheless, pulsed discharges prove very useful under very low average wattage where CW plasmas are unstable or cannot be maintained at all.

In our study, the data on retention of the C-O-C groups from all the depositions were summarized into a single plot in dependence on average power (Figure 3.45). In particular, the following experiments presented earlier in Table 3.7, Table 3.8 and Table 3.9 were included: variation of high voltage, u_{AC} , at fixed T_{ON},

T_{OFF} and D; variation of T_{OFF} (and therefore D) at fixed T_{ON} and u_{AC}; simultaneous variation of both T_{ON} and T_{OFF} (and therefore D) at fixed u_{AC}. Apparently, all the data points obey a single dependence on average power regardless of the way how the latter was achieved. The average power is, therefore, a crucial parameter determining the properties of PEO-like plasma polymers.

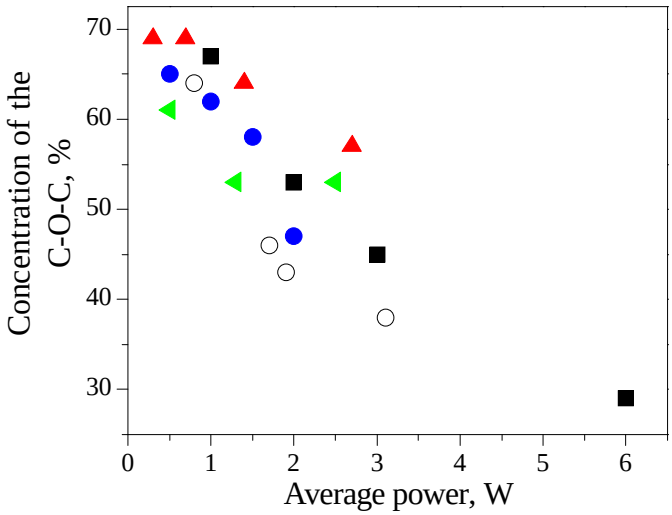

Figure 3.45. Retention of the C–O–C groups in dependence on average power for different regimes of the SDBD deposition.

■ - T_{ON} = 0.4 msec, T_{OFF} = 0.6 msec, D = 0.4, u_{AC} variable;
○- T_{ON} = 0.2 msec, T_{OFF} = 0.8 msec, D = 0.2, u_{AC} variable;
▲ - T_{ON} = 0.2 msec, u_{AC} = 3.9 kV, T_{OFF} and D variable;
◀ - T_{ON} = 0.4 msec, u_{AC} = 3.9 kV, T_{OFF} and D variable;
● – u_{AC} = 2.2 kV, T_{ON}, T_{OFF} and D variable.

3.3.4. Protein adsorption

Since PEO-like films are intended to be used in biomedical applications, their stability in water was also tested. The samples were soaked in distilled water for 24 hours and the FTIR spectra of the films before and after soaking were compared. Figure 3.46 shows that the chemical composition of the films does not change upon contact with water and that PEO-like character of the deposits remains unperturbed. The lower overall intensity of IR absorption after immersion in water indicates partial solubility of the films which may be given by low cross-linking density of the polymeric network and by low average molar mass of the soluble fraction. The effect of decreasing molar mass can be attributed to termination of chain propagation by

oxygen which results in the formation of peroxy- and hydroperoxy-radicals followed by their decay to the carbonyl-based species.

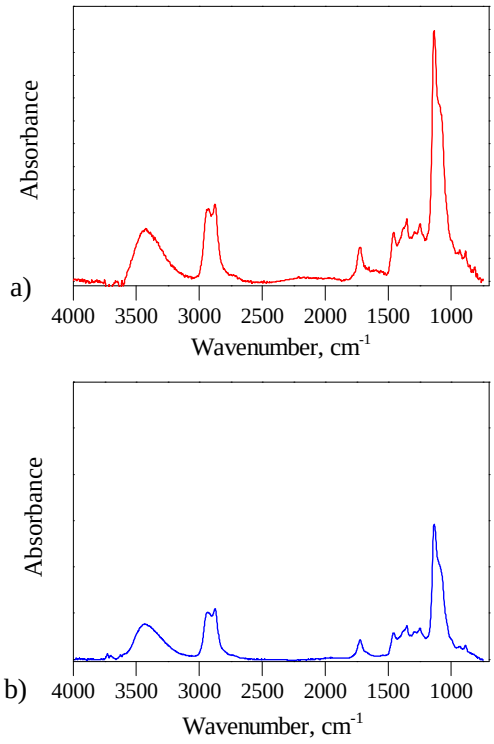

Figure 3.46. The FTIR-RAS spectra of the PEO-like plasma polymers a) before and b) after immersion in water (u_{AC} = 4.9 $kV_{p\text{-}p}$, f_{AC} = 5 kHz, f_M = 1 kHz, D = 0.4).

Several films were deposited on crystals for QCM analysis at different average powers. Figure 3.47 shows the kinetic curves of fibrinogen adsorption on such films in terms of QCM frequency shift. In the case of 1.0 W and 1.5 W powers, the frequency does not change substantially with time. A slight decrease of the curves is attributed mainly to temporal drifts in the measuring electrical circuit and its value (3 Hz/30 min) is normal for QCM measurements in liquids. This proves that fibrinogen hardly adsorbs on the surface of the PEO-like plasma polymers deposited at low average powers, i. e. with good retention of the ether structure. On the contrary, the film deposited at an average power of 3.0 W, which has only 46 % of the C-O-C groups, does not exhibit the non-fouling properties: fast adhesion of fibrinogen occurs within first 5 minutes after introducing the protein into the solution. Therefore, ~60 % retention of the C-O-C groups appears to be sufficient for

the films to behave as non-fouling, which correlates well with the value of 65-70 % reported in several works for low pressure PEO-like plasma polymers [80, 153].

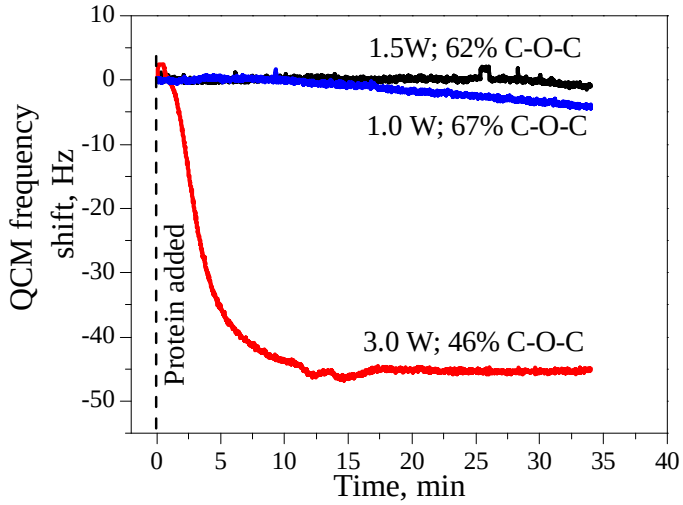

Figure 3.47. The ability of the PEO-like plasma polymers to resist fibrinogen adsorption (Ar flow rate 1.0 slm, electrode-substrate distance 3 mm, f_{AC} = 5 kHz, f_M = 1 kHz, D = 0.4).

Summary

The properties of PEO-like plasma polymers prepared by amplitude-modulated AC surface dielectric barrier discharge at atmospheric pressure were investigated. The use of SDBD leads, under appropriate operational conditions, to fabrication of thin films resembling conventional PEO's. The thickness of the deposits was smaller at increased power of discharge and it was suggested that the decrease of deposition rate is caused by enhanced photolytical processes, probably under contribution of metastable argon atoms.

Average power delivered to the discharge was found to be the key parameter influencing the chemical composition of resultant plasma polymers. The content of the ether groups changed between 67 to 29 % when changing average power of discharge between 1 W to 6 W. Similar chemical changes are obtained when varying u_{AC}, other pulsing parameters (T_{ON}, T_{OFF}, D) being held constant or vice versa, provided that average power is equivalent. Reduced retention of the C-O-C structure leads to the loss of the non-fouling properties of deposited films. The plasma polymers deposited at 1.0 and 1.5 W average power, i. e. those with more than 60 %

of the ethers, withstood the accumulation of fibrinogen whereas the film with lower amount of the ethers failed.

Conclusion

The following objectives have been achieved:

- Two methods (low pressure plasma-assisted thermal vapour deposition and atmospheric pressure amplitude modulated AC surface dielectric barrier discharge) were developed for fabrication of PEO-like plasma polymers. Both may compete in deposition of the films with non-fouling properties.
- Specific power of discharge is a key parameter governing the chemical composition and structure of resultant films.
- The plasma polymers with high concentration of the ether groups were fabricated. The maximal retention was up to 80 % for the low pressure and 67 % for the atmospheric pressure methods.
- The plasma polymers have complex structure where mixtures of low molar mass chains are entangled within a polymeric network, cross-link density thereof controlled by specific power. The networks with adjustable number of monomer units between cross-links were developed.
- The films exhibit a complex behavior when in contact with aqueous solutions with swelling/dissolution phenomena strongly dependent in cross-link density.
- The concentration of the ether groups was found to be the main factor influencing the non-fouling properties. The concentration of about 65 % was found to suffice for the films to resist adsorption of proteins, adhesion of cells and development of fibrin networks.

Bibliography

1 H. Biederman, *Plasma polymer films*, Imperial College Press, London, 2004.

2 D. K. Lam, R. F. Baddour, A. F. Stancell, *Plasma Chemistry of Polymers*, Marcel Dekker, New York, 1976.

3 H. Yasuda, *Plasma Polymerization*, Academic press, New York, 1985.

4 H. Biederman, Y. Osada, Eds., *Plasma polymerization processes*, Vol. 3, Elsevier Science Publishers, Amsterdam, Netherlands, 1992.

5 R. Harrop, P. J. Harrop, *Thin Solid Films*, 3, 1969, 109.

6 D. J. Morrison, T. Robertson, *Thin Solid Films*, 15, 1973, 87.

7 I. H. Pratt, T. C. Lausmann, *Thin Solid Films*, 10, 1972, 151.

8 J. M. Tibbitt, M. Sten, T. Bell, *Thin Solid Films*, 39, 1975, L43.

9 H. Biederman, S. M. Ojha, L. Holland, *Thin Solid Films*, 41, 1977, 329.

10 H. Biederman, P. Bílková, J. Jezek, P. Hlídek, D. Slavínská, *J. Non-Cristalline Solid*, 218, 1997, 44.

11 I. Kholodkov, H. Biederman, D. Slavinska, A. Choukourov, M. Trchova, *Vacuum*, 70, 4, 2003, 505.

12 V. Stelmashuk, H. Biederman, D. Slavinska, M. Trchova, P. Hlidek, *Vacuum*, 75, 2004, 207-215.

13 M. Mišina, H. Koshelyev, H. Biederman, A. Choukourov, D. Slavinska, E. Fuoco, L. Hanley, *Proceedings of SVC*, Dallas, May, 2004.

14 J. Kousal, J. Hanuš, A. Choukourov, P. Hlidek, H. Biederman, D. Slavinska, J. Zemek, *Surf. Coat. Technol.*, 200, 2005, 472-475.

15 Y. Yamada, K. Tanaka, K. Saito, *Surf. Coat. Technol.*, 43/44, 1990, 618.

16 A. Choukourov, A. Grinevich, J. Hanuš, J. Kousal, D. Slavinska, H. Biederman, A. Bowers, L. Hanley, *Thin Solid Films*, 502, 2006, 40-43.

17 J. Kousal, J. Hanuš, A. Choukourov, O. Polonskyi, H. Biederman, D. Slavínská, *Plasma Process. Polym.*, 6, 2009, S803-S807.

18 O. Kylián, J. Hanuš, A. Choukourov, J. Kousal, D. Slavinská, H. Biederman, *J. Phys. D: Appl. Phys.*, 42, 2009, 142001.

19 H. Biederman, V. Stelmashuk, I. Kholodkov, A. Choukourov, D. Slavinská, *Surf. Coat. Technol.*, 174-175, 2003, p. 27-32.

20 A. Choukourov, J. Hanuš, J. Kousal, A. Grinevich, Y. Pihosh, D. Slavínská, H. Biederman, *Vacuum*, 81, 2006, 517-526.

21 O. Kylián, J. Kousal, A. Artemenko, M. Petr, O. Polonskyi, D. Slavínská, H. Biederman, *Surf. Coat. Technol.*, 205, 2011, S558-S561.

22 S. L. Madorsky, S. Strauss, D. Thompson, L. Williamson, *J. Polymer Sci.*, 4, 1949, p. 639.

23 S. L. Madorsky, *J. Polymer Sci*., 9, 1952, p. 133.

24 P. P. Luff, M. White, *Thin Solid Films*, 6, 1970, p. 175.

25 A. V. Amelin, O. F. Pozdnyakov, V. R. Regel, T. R. Sanfirana, *Soviet Phys. – Solid State*, 12, 1970, p. 2034.

26 J. A. Lane, *Brighton College of Tech.*, Project Report No.156, 1967.

27 M. White, *Vacuum*, 15, 1965, p. 449.

28 N. Grassie, H. W. Melville, *Proc. Roy. Soc*., A199, 1949, 14.

29 J. F. Kinstle, *J. Polymer Sci.*, 15, 1977, p. 467.

30 H. Usui, H. Koshikawa, K. Tanaka, *J. Vac. Sci. Technol. A*, 13(5), 1995.

31 H. Usui, H. Kikuchi, K. Tanaka, S. Miyata, T. Watanabe, *J. Vac. Sci. Technol. A*, 16(1), 1998.

32 J. Hanuš, L. Hanyková, A. Choukourov, J. Kousal, O. Polonskyi, D. Slavínská, H. Biederman, Plasma Process. Polym., 6, 2009, S362-S365.

33 A. Choukourov, J. Hanus, J. Kousal, A. Grinevich, Y. Pihosh, D. Slavinska, H. Biederman, *Vacuum*, 80, 2006, p. 923.

34 S. Masuda, K. Akutsu, M. Kuroda, Y. Awatsu, Y. Shibuya, *IEEE Trans. Ind. Appl*, 24, 1988, p. 223.

35 V. I. Gibalov, G. J. Pietsch, *J. Phys. D, Appl. Phys.*, 33, 2000, p. 2618.

36 J. M. Williamson, D. D. Trump, P. Bletzinger, B. N. Ganguly, *J. Phys. D, Appl. Phys.*, 39, 2006, p. 4400.

37 M. Šimek, S. Pekárek, V. Prukner, *Plasma Chem. Plasma Process*, 30, 2010, p. 607.

38 H. Biederman, *Plasma Polymer Films*, Chapter 8, M. Kogoma: *Application of Atmospheric Pressure Discharge for Plasma Polymer Processes*, Imperial College Press, London, p. 279-288, 2004.

39 O. Goossens, E. Dekempeneer, D. Vangeneugden, R. Van de Leest, C. Leys, *Surface and Coatings Tech.*, 142–144, 2001, p. 474.

40 R. Prat, Y. J. Koh, Y. Babukutty, M. Kogoma, S. Okazaki, M. Kodama, *Polymer* 41, 2000, p. 7355.

41 N. De Geyter, R. Morent, S. Van Vlierberghe, P. Dubruel, C. Leys, L. Gengembre, E. Schacht, E. Payen, *Progress in Organic Coatings*, 64, 2009, p. 230.

42 I. Topala, N. Dumitrascu, G. Popa, *Nuclear Instr. And Meth., in Phys. Research B*, 267, 2009, p. 442.

43 S. Paulussen, R. Rego, O. Goossens, D. Vangeneugden, K. Rose, *Surface and Coatings Tech.,* 200, 2005, p. 672.

44 D. F. Williams, *Definitions in Biomedicals. Proceedings of a Cosensus Conference of the European Societz for Biomaterials,* March 3-5, Vol. 4, Elsevier, Chester, England, 1986.

45 D. F. Williams, *Definitions in Biomedicals. Proceedings of a Cosensus Conference of the European Societz for Biomaterials,* Vol. 4, Elsevier, Chester, England, 1987.

46 B. D. Ratner, A. S. Hoffman, F. J. Schoen, J. E. Lemons, Eds., *Biomaterials Science, An Introduction to Materials in Medicine*, Academic Press, 1996, p. 484.

47 T. van Os Menno, *Surface modification by plasma polymerization: film deposition, tailoring of surface properties and biocompatibility,* Anthony Roach Press, Netherlands, Enschede, 2000.

48 M. M. Amiji, *Biomaterials*, 16, 1995, p. 593.

49 L. Tang, Y. Wu, R. B. Timmons, *J. Biomed. Mater.Res.,* 42, 1998, p. 156.

50 A. Dekker, K. Reitsma, T. Beugeling, A. Bantjes, J. Feijen, W. G. van Aken, *Biomaterials*, 12, 1991, p. 130.

51 V. Panchalingam, B. Poon, H. -H. Huo, C. R. Savage, R. B. Timmons, R. C. Eberhart, *J. Biomater. Sci. Polym. Ed.*, 5, 1993, p. 131.

52 K. N. Ekdahl, B. Nilsson, C. G. Golander, H. Elwing, B. Lasen, U. R. Nilsson, *J. Colloid Interface Sci.*, 158, 1993, p. 121.

53 E. Ostuni, L. Yan, G. M. Whitesides, *Colloids Surf. B: Biointerfaces*, 15, 1999, p. 3.

54 J. D. Andrade, V. Hlady, *Adv. Polym. Sci.*,79, 1986, p. 1.

55 J. L. Ortega-Vnuesa, P. Tengvall, I. Lundstrom, *Thin Solid Films*, 324, 1998, p. 257.

56 H. T. Spijker, R. Bos, W. van Oeveren, J. de Vries, H. J. Busscher, *Colloids and Surfaces B: Biointerfaces*, 15, 1999, p. 89.

57 M. Malmsten, J. -A. Johansson, N. L. Burns, H. K.Yasuda, *Colloid and Surfaces B: Biointerfaces*, 6,1996, p. 191.

58 N. L. Burns, K. Holmberg, *Progr. Colloid Polym. Sci.*, 100, 1996, p. 271.

59 C. Werner, U. Konig, A. Augsburg, C. Arnhold, H. Korber, R. Zimmermann, H. -J. Jacobasch, *Colloidals and Surfaces A: Physicochem. Eng. Aspects*, 159, 1999, p. 519.

60 N. L. Burns, K. Holmberg, C. Brink, *J. Colloid Interface Sci.*, 178, 1996, p. 116.

61 R. I. Mahato, *Biomaterials for delivery and targeting of proteins and nucleic acids*, CRC Press, USA, 2005.

62 K. J. Kitching, V. Pan, B. D. Ratner, *Biomedical Applications of Plasma-Deposited Thin Films*, In: *Plasma Polymer Films*, Ed., H. Biederman, Imperial College Press, London, p. 392.

63 L. Li, S. Chen, J. Zheng, B. D. Ratner, S. Jiang, *J. Phys. Chem. B*, 109, 2005, p. 2934.

64 K. D. Hinds, "*Protein Conjugation, Cross-Linking, and PEGylation*", in: *Biomaterials for Delivery and Targeting of Proteins and Nucleic Acids*, R. I. Mahato, Ed., CRC Press, London, 2004, p. 712.

65 J. H. Lee, H. B. Lee, J. D. Andrade, *Prog. Polym. Sci.*, 20, 2004, p. 1043.

66 J. D. Andrade, S. Nagaoka, S. Cooper, T. Okano, S. W. Kim, *ASAIO J.*, 10, 1987, 75.

67 Y. Ikada, *Polymers in Medicine*, K. Dusek, Ed., Springer-Verlag, Berlin, 1984, p. 103.

68 M. Amiji, K. Park, *J. Biomater. Sci. Polym.*, Ed., 4, 1993, 217.

69 Ch. Weiss, *Human Physiology*, R. F. Schmidt, G. Thews, Eds., Ch. 16, Springer-Verlag, Berlin, 1983.

70 L. Vroman, *Blood*, Natural History Press, New York, 1967.

71 R. F. A. Zwaal, H. C. Hemker, Eds., *Blood Coagulation*, Elsevier, Amsterdam, 1986.

72 G. P. Lopez, B. D. Ratner C. D. Tidwell, C. L. Haycox, R. J. Rapoza, T. A. Horbertt, *J. Biomed. Res.*, 26, 1992, p. 415.

73 Y. V. Pan, T. C. McDevitt, T. K. Kim, D. Leach-Scampavia, P. S. Stayton, D. D. Denton, B. D. Ratner, *Plasmas Polym.*, 7, 2002, p. 171.

74 E. Sardella, P. Favia, R. Gristina, M. Nardulli, R. d'Agostino, *Plasma Processes Polym.*, 3, 2006, p. 456.

75 E. E. Johnston, J. D. Bryers, B. D. Ratner, *Langmuir*, 21, 2005, p. 870.

76 F. Palumbo, P. Favia, M. Vulpio, R. d'Agostino, *Plasmas Polym.*, 6, 2001, p. 163.

77 M. Shen, M. S. Wagner, D. G. Castner, B. D. Ratner, T. A. Horbett, *Langmuir*, 19, 2003, p. 1692.

78 A. R. Denes, E. B. Somers, A. C. L. Wong, F. Denes, *J. Appl. Polym. Sci.*, 81, 2001, p. 3425.

79 E. Sardella, R. Gristina, G. S. Senesi, R. d'Agostino, P. Favia, *Plasma Process. Polym.*, 1, 2004, p. 63.

80 E. Sardella, R. Gristina, G. Ceccone, D. Gilliland, A. Papadopoulou-Bouraoui, F. Rossi, G. S. Senesi, L. Detomaso, P. Favia, R. d'Agostino, *Surf. Coat. Technol.*, 200, 2005, p. 51.

81 P. Favia, E. Sardella, R. Gristina, R. d'Agostino, *Surf. Coat. Technol*., 169-170, 2003, p. 707.

82 F. Bretangol, O. Kylian, M. Hasiwa, L. Ceriotti, H. Rauscher, G. Ceccone, D. Gilliland, P. Colpo, F. Rossi, *Sensors and Actuators B*, 123, 2007, p. 283.

83 Q. Cheng, K. Komvopoulos, *J. Phys. Chem. C*, 113, 2009, p. 213.

84 B. W. Muir, A. Tarasova, T. R. Gengenbach, T. J. Menzies, L. Meagher, F. Rovere, A. Fairbrother, K. M. McLean, P. G. Hartley, *Langmuir*, 24, 2008, p. 3828.

85 Z. Zhang, B. Menges, R. B. Timmons, W. Knoll, R. Foerch, *Langmuir*, 19, 2003, p. 4765.

86 Y. J. Wu, R. B. Timmons, J. S. Jen, F. E. Molock, *Colloids Surf. B.*, 18, 2000, p. 235.

87 L. -Q. Chu, W. Knoll, R. Foersch, *Chem. Mater.*, 18, 2006, p. 4840.

88 K. E. Bremmell, P. Kingshott, Z. Ademovic, B. Winther-Jensen, H. J. Griesser, *Langmuir*, 22, 2006, p. 313.

89 D. Beyer, W. Knoll, H. Ringsdorf, J. -H. Wang, R. B. Timmons, P. Sluka, *J. Biomed. Mater. Res.*, 36, 1997, p. 181.

90 Z. Ademovic, J. Wei, B. Winther-Jensen, X. Hou, P. Kingshott, *Plasma Processs Polym.*, 2, 2005, p. 53.

91 Z. Ademovic, B. Holst, R. A. Kahn, I. Jorring, T. Brevig, J. Wie, X. Hou, B. Winter-Jensen, P. Kingshott, *J. Mater. Sci.: Mater. Med.*, 17, 2006, p. 203.

92 B. Nisol, C. Poleunis, P. Bertrand, F. Reniers, *Plasma Process. Polym*., 7, 2010, p. 715.

93 G. Da Ponte, E. Sardella, F. Fanelli, A. Van Hoeck, R. d'Agostino, S. Paulussen, P. Favia, *Surface and Coatings Tech.*, 205, 2011, p. 5525.

94 I. Gordeev, M. Šimek, V. Prukner, A. Choukourov, H. Biederman, *Plasma Process. Polym*. 2012, 9, p. 83.

95 M. Salerno, I. Bykov, *Microscopy& Analysis*, 20, 2006, S5.

96 J. E. Sader, J. W. M. Chon, P. Mulvaney, *Rev. Sci. Instrum.*, 70, 1999, p. 3967.

97 H. Hertz, "*On the Contact of Elastic Bodies*", In: *Miscellaneous Papers*, P. Lenard, Ed., Macmillan & Co, London, 1896, p. 146.

98 H. Hertz, "*On the Contact of Rigid Elastic Solids and on Hardness*", In: *Miscellaneous Papers*, P. Lenard, Ed., Macmillan & Co, London, 1896, p. 163.

99 I. N. Sneddon, *Int. J. Engng. Sci.*, 3**,** 1965, p. 47.

100 H. -J. Butt, B. Capella, M. Kappl, *Surf. Sci. Rep.*, 59, 2005, p. 1.

101 A. Chilkoti, B. D. Ratner, *Chemical derivatization methods for enchancing the analytical capabilities of x-ray photoelectron spectroscopy and static secondary*

ion mass spectrometry. In: Surface Characterization of Advanced Polymers, L. Sabatini, P. G. Zambonin (Eds.), VSH, Weinheim, 1993.

102 C. L. Rinsch, X. Chen, V. Panchangam, R. C. Eberhart, J. –H. Wang, R. B. Timmons, *Langmuir*, Vol. 12, No. 12, 1996, p. 2995.

103 M. W. Mosseson, J. P. DiOrio, I. Hernandez, J. F. Hainfeld, J. S. Wall, G. Grieninger, *Biophys. Chem.*, 112, 2004, p. 209.

104 C. Rodriguez-Emmenegger, E. Hasan, O. Pop-Georgievski, M. Houska, E. Brynda, A. B. Alles, *Macromol. Biosci.*, 2011, DOI: 10.1002/mabi.201100425.

105 C. Rodriguez-Emmenegger, E. Brynda, T. Riedel, Z. Sedlakova, M. Houska, A. B. Alles, *Langmuir*, 25, 2009, p. 6328.

106 D. R. Lide, *Handbook of Chemistry and Physics*, 76th Ed., CRC Press, New York, 1995.

107 M. White, *Thin Solid Films*, 18, 1973, 157-172.

108 N. Boonthanom, M. White, *Thin Solid Films*, 24, 1974, 295-306.

109 R. W. B. Pearse, A. G. Gaydon, *The identification of molecular spectra*, Wiley, New York, 1976.

110 M. M. Fares, J. Hacaloglu, S. Suzer, *Eur. Polym. J.*, 30(7), 1994, p. 845-850.

111 K. Ettre, P. F. Varadi, *Anal. Chem.*, 34(7), 1962, p. 752-757.

112 L. V. Smirnov, N. P. Kulikova, N. V. Platonova, *Polym Sci. U.S.S.R.*, 9(11), 1967, p. 2849-2856.

113 Z. Peng, L. –X. Kong, *Polym. Degrad. Stab.*, 92, 2007, p. 1061-1071.

114 T. Yoshihara, H. Tadokoro, S. Murahashi, *J. Chem. Phys.*, 41, 1964, p. 2902.

115 M. A. K. L. Dissanayake, R. Frech, *Macromolecules*, 28, 1995, p. 5312.

116 P. Harder, M. Grunze, R. Dahint, G. M. Whitesides, P. E. Laibinis, *J. Phys. Chem. B*, 102, 1998, p. 426.

117 O. Wolff, E. Seydel, D. Johannsmann, *Faraday Disscuss*. 91, 1997, p. 107.

118 G. Montaudo, M. S. Montaudo, *Polymer Characterization Methods, in: Mass Spectrometry of Polymers*, G. Montaudo, R. P. Lattimer, Eds., CRC Press, London, 2001, p. 600.

119 L. Hanyková, J. Spěváček, M. Ilavský, *Polymer*, 42, 2001, p. 8607.

120 P. J. Flory, J. Rehner, *J. Chem. Phys.*, 11, 1943, p. 521.

121 H. Lin, T. Kai, B. D. Freeman, S. Kalakkunnath, D. S. Kalika, *Macromolecules*, 38, 2005, p. 8381.

122 P. G. De Gennes, *Scaling Concepts in Polymer Physics*, Cornell University Press, Ithaca, 1979, p. 325.

123 Y. Huang, I. Szleifer, N. A. Peppaps, *Macromolecules*, 35, 2002, p. 1373.

124 D. Bar-Howell, N. A. Peppas, *Polym. Bull.*, 13, 1985, p. 91.

125 R. A. Scott, N. A. Peppas, *Macromolecules*, 32, 1999, p. 6139.

126 V. P. Privalko, A. P. Lobodina, *Eur. Polym. J.*, 10, 1974, p. 1033.

127 S. Kalakkunnath, D. S. Kalika, H. Lin, B. D. Freeman, *Macromolecules*, 38, 2005, p. 9679.

128 M. Iza, G. Stoianovici, L. Viora, J. L. Grossiord, G. Couarraze, *J. Control. Release*, 52, 1998, 41.

129 L. H. Sperling, *Introduction to Physical Polymer Science*, 4th edition, Wiley-Interscience, Hoboken, NJ, 2006, p. 845.

130 A. E. Tonelli, E. Helfand, *Macromolecules*, 7, 1974, p. 59.

131 S. Kalakkunnath, D. S. Kalika, H. Lin, B. D. Freeman, *J. Polym. Sci. Part B: Polym. Phys*, 44, 2006, p. 2058.

132 L. Detomaso, R. Gristina, G. S. Senesi, R. D`Agostino, P. Favia, Biomaterials, 26, 2005, 3831-41.

133 F. Brétagnol, H. Rauscher, M. Hasiwa, O Kylián, G. Ceccone, L. Hazell, A. J. Paul, O. Lefranc, F. Rossi, *Acta Biomaterialia*, 4, 2008, 1745-51.

134 S. Han, C. Kim, D. Kwon, *Polymer*, 38, 1997, p. 317-323.

135 A. Choukourov, A. Grinevich, N. Saito, O. Takai, *Surf. Sci.*, 601, 2007, p. 3948.

136 K. L. Prime, G. M. Whitesides, *J. Am. Chem. Soc*., 115, 1993, p. 10714.

137 M. J. Bridgett, M. C. Davies, S. P. Denyer, Biomaterials, 13, 1992, p. 411.

138 R. Llanos, M. V. Sefton, *J. Biomater. Sci., Polymer Edn.*,4, 1993, p. 381.

139 J. M. Anderson, A. G. Gristina, S. R. Hanson, L. A. Harker, R. J. Johnson, K. Merritt, P. T. Naylor, F. J. Schoen, *"Host Reactions to Biomaterials and Their Evaluation", in: Biomaterials Science, An Introdaction to Materials in Medicine,* B. D. Ratner, A. S. Hoffman, F. J. Schoen, J. E. Lemons, Eds., Academic Press, New York, 1996, p. 165.

140 R. B. Timmons, A. J. Griggs, "*Pulsed Plasma Polymerization*", In: *Plasma Polymerization Processes*, H. Biederman, Ed., Imperial College Press, London, 2004.

141 B. Dong, J. M. Bauchire, J. M. Pouvesle, P. Magnier, D. Hong, *J. Phys. D: Appl. Phys*, 41, 2008, p. 155201.

142 N. de Geyter, R. Morent, C, Leys, L. Gengembre, E. Payen, Surf. Coat. Technol., 201, 2007, p.7066.

143 E. A. Sosnin, T. Oppenlander, V. F. Tarasenko, *J. Photochem. Photobiol. C: Photochem. Rev.*, 7, 2006, p. 145.

144 N. Merbahi, N. Sewraj, F. Marchal, Y. Salamero, P. Millet, *J. Phys. D: Appl. Phys*, 37, 2004, p. 1664.

145 S. Lordanova, I. Koleva, *Spectrochim. Acta B*, 62, 2007, p. 344.

146 A. Bogaerts, *Spectrochim. Acta B*, 64, 2009, p. 1266.

147 Y. Morita, T. Higashiguchi, S. Kubodera, *Appl. Phys. B*, 82, 2006, p. 31.

148 F.T. Zhen, J. Nan, W. Long, *Chin. Phys. Soc.*, 14, 2005, p. 2256.

149 *Interpreting Infrared, Roman, and Nuclear Magnetic Resonance Spectra*, R. Nyquist, Ed., Academic Press, Amsterdam, Netherlands, 2001.

150 A. Choukourov, O. Polonskyi, J. Hanus, J. Kousal, A. Grinevich, D. Slavinska, H. Biederman, *Plasma Process. Polym.*, 6, 2009, p. 521.

151 A. Choukourov, A. Grinevich, O. Polonskyi, J. Hanus, J. Kousal, D. Slavinska, H. Biederman, *J. Phys. Chem. B*, 113, 2009, p. 2984.

152 A. Choukourov, I. Gordeev, O. Polonskyi, A. Artemenko, L. Hanykova, I. Krakovsky, O. Kylian, D. Slavinska, H. Biederman, *Plasma Process. Polym.*, 7, 2010, p. 445.

153 A. Choukourov, I. Gordeev, D. Arzhakov, A. Artemenko, J. Kousal, O. Kylian, D. Slavinska, H. Biederman, *Plasma Process. Polym.*, 9, 2012, 48.

List of Tables

List of Abbreviations

PEO	poly(ethylene oxide)
PTFE	poly(tetrafluoroethylene)
PVC	poly(vinyl chloride)
PMMA	poly(methyl methacrylate)
DVE	di(ethylene) glycol vinyl ether
DGE	diethylene glycol
TGE	triethylene glycol
DSS	2,2-dimethyl-2-silapentane-5-sulfonate
THF	tetrahydrofuran
TFAA	trifluoroacetic anhydride
PS	polystyrene
SAM	self-assembled monolayers
IgG	immunoglobulin
BSA	bovine serum albumin
R.f.	radio frequency
DC	direct current
MW	microwave
UV	ultraviolet
VUV	vacuum ultraviolet
PECVD	plasma-enhanced chemical vapor deposition
APPLD	atmospheric pressure plasma liquid deposition
DBD	dielectric barrier discharge
SDBD	surface dielectric barrier discharge
PIE	plasma induced emission
QCM	quartz crystal microbalance
OES	optical emission spectroscopy
MS	mass spectroscopy
NMR	nuclear magnetic resonance
MAS	magic angle spinning
GPC	gel permeation chromatography
AFM	atomic force microscopy

XPS	x-ray photoelectron spectroscopy
FTIR-RAS	fourier transform infra-red reflection adsorption spectroscopy
SPR	surface plasmon resonance
SIMS	secondary ion mass spectroscopy

Author’s contribution

The author participated in development and installing of the experimental setups for plasma-assisted thermal vapour deposition and SDBD treatment. The author performed all the depositions and mastered the in-situ diagnostics of OES, mass spectroscopy and QCM. The following post-deposition analyses were also performed solely by the author: water contact angle measurements, FTIR, XPS, AFM, protein adsorption measurements. The author is indebted to Doc. Ivan Krakovský for the GPC measurements, to Doc. Lenka Hanyková for the NMR measurements, to Dr. Jaroslav Kousal for ellipsometric measurements, to Ing. Cesar Rodriguez for the blood tests, to Dr. Marta Vandrovcová and Dr. Jessica Ponti for cell adhesion tests. The author participated in processing and evaluation of the data obtained in the mentioned measurements.

List of publications

Journal articles refereed:

1. A. Choukourov, I. Gordeev, O. Polonskyi, A. Artemenko, L. Hanykova, I. Krakovsky, O. Kylian, D. Slavinska, H. Biederman. *Ply(ethylene oxide)-like plasma polymers produced by plasma-assisted vacuum evaporation.* Plasma Process. Polym. 2010, 7, p. 445.
2. Martin Drábik, Ondřej Kylián, Oleksandr Polonskyi, Juraj Čechvala, Anna Artemenko, Ivan Gordeev, Andrei Choukourov, Danka Slavınska, Ira Matolínová, Hynek Biederman. *Super-Hydrophobic Coatings Prepared by RF Magnetron Sputtering of PTFE.* Plasma Processes and Polymers, 2010, 7, p. 544.
3. Andrei Choukourov, Ivan Gordeev, Dmitry Arzhakov, Anna Artemenko, Ondřej Kylián, Jaroslav Kousal, Oleksandr Polonskyi, Josef Pešička, Danka Slavínská, Hynek Biederman. *Nanocomposite gold/poly(ethylene oxide)-like plasma polymers prepared by plasma-assisted vacuum evaporation and magnetron sputtering.* Surface & Coatings Technology, 2011, 25, p. 2830.
4. Ondřej Kylián, Martin Drábik, Oleksandr Polonskyi, Juraj Čechvala, Anna Artemenko, Ivan Gordeev, Andrei Choukourov, Iva Matolínová, Danka Slavínská, Hynek Biederman. *Deposition of nanostructured fluorocarbon plasma polymer films by RF magnetron sputtering of polytetrafluoroethylene.* Thin Solid Films, 2011, 519, 19, p. 6426.
5. Andrei Choukourov, Ivan Gordeev, Dmitry Arzhakov, Anna Artemenko, Jaroslav Kousal, Ondřej Kylián, Danka Slavınska, Hynek Biederman. *Does Cross-Link Density of PEO-Like Plasma Polymers Influence Their Resistance to Adsorption of Fibrinogen?* Plasma Process. Polym., 2012, 9, p. 48.
6. I. Gordeev, M. Šimek, V. Prukner, A. Choukourov, H. Biederman. *Surface DBD for deposition of PEO-like plasma polymers.* Plasma Process. Polym., 2012, 9, p. 83.
7. I. Gordeev, A. Choukourov, M. Šimek, V. Prukner, H. Biederman. *PEO-like plasma polymers prepared by atmospheric pressure surface dielectric barrier discharge.* Plasma Process. Polym., 2012, DOI:10.1002/ppap.201100213.

Proceedings and other:

1. I. Gordeev, A. Choukourov, O. Polonskyi, D. Slavinska, H. Biederman. *Deposition of thin films by plasma polymerization for biomedical application.* WDS'09 Proceedings of Contributed Papers, Part III, ISBN 978-80-7378-103-3 p. 182-188, 2009.
2. D. Arzhakov, A. Artemenko, I. Gordeev, A. Choukourov, D. Slavinska, H. Biederman. *Nanocomposite metal/poly(ethylene oxide)-like plasma polymer films and their properties*. WDS'10 Proceedings of Contributed Papers, Part III, ISBN 978-80-7378-141-5, p. 19-24, 2010.
3. Anna Artemenko, Ondřej Kylián, Jaroslav Kousal, Andrei Choukourov, Juraj Čechvala, Ivan Gordeev, Oleksandr Polonskyi, Danka Slavınska, Hynek Biederman. *Aging of amino-rich plasma polymers deposited by RF magnetron sputtering of nylon.* 24th Symposium on Plasma Physics and Technology, 14th – 17th June, Prague, Czech Republic, ISBN 978-80-01-04548-0, p. 39, 2010.
4. Ivan Gordeev, Milan Šimek, Václav Prukner, Andrei Choukourov, Hynek Biederman. *Surface DBD for deposition of PEO-like plasma polymers.* 24th Symposium on Plasma Physics and Technology, 14th – 17th June, Prague, Czech Republic, ISBN 978-80-01-04548-0, p. 44, 2010.

5. Martin Drábik, Ondřej Kylián, Oleksandr Polonskyi, Juraj Čechvala, Anna Artemenko, Ivan Gordeev, Andrei Choukourov, Danka Slavınska, Ira Matolínová, Hynek Biederman. *Deposition of nanostructured fluorocarbon plasma polymer films by RF magnetron sputtering of PTFE.* 24th Symposium on Plasma Physics and Technology, 14th – 17th June, Prague, Czech Republic, ISBN 978-80-01-04548-0, p. 94, 2010.
6. A. Artemenko, A. Choukourov, I. Gordeev, J. Kousal, O. Kylian, O. Polonskyi, D. Slavinska, H. Biederman. *Investigation of properties of plasma polymers deposited by RF magnetron sputtering of Nylon.* Plenary conference "Eco-sustainable Food Packaging based on Polymer Nanomaterials" COST FA0904, Meeting in Jassy, June 28-29, Romania, Book of abstract, 2010.
7. Andrei Choukourov, Ivan Gordeev, Anna Artemenko, Ondřej Kylián, Jaroslav Kousal, Oleksandr Polonskyi, Josef Pešička, Danka Slavınska, Hynek Biederman. *Nanocomposite gold/PEO-like plasma polymers.* Twelfth International Conference on Plasma Surface Engineering, 13th–17th September, Garmisch-Partenkirchen, Germany, Abstracts, p. 76, 2010.
8. Anna Artemenko, Ondřej Kylián, Jaroslav Kousal, Andrei Choukourov, Juraj Čechvala, Ivan Gordeev, Oleksandr Polonskyi, Danka Slavınska, Hynek Biederman. *Deposition of amino-rich coatings by RF magnetron sputtering of Nylon: investigation of their properties related to biomedical applications.* Twelfth International Conference on Plasma Surface Engineering, 13th–17th September, Garmisch-Partenkirchen, Germany, Abstracts, p. 107, 2010.
9. Ivan Gordeev, Anna Artemenko, Andrei Choukourov, Václav Prukner, Milan Šimek, Hynek Biederman. *Surface DBD for deposition of PEO-like plasma polymers.* Twelfth International Conference on Plasma Surface Engineering, 13th–17th September, Garmisch-Partenkirchen, Germany, Abstracts, p. 359, 2010.
10. Ivan Gordeev, Václav Prukner, Milan Šimek, Andrei Choukourov, Hynek Biederman. *Surface DBD discharge for preparation of non-fouling plasma polymer films.* 3rd International Conference on Plasma Medicine, Book of abstracts, Liebniz Institute for Plasma Science and Technology (INP Greifswald), 19th–24th September, Greifswald, Germany, p. 120, 2010.
11. Andrei Choukourov, Ivan Gordeev, Dmitry Arzhakov, Danka Slavínská, Hynek Biederman. *Mass-spectroscopical study of plasma-assisted thermal degradation of poly(ethylene oxide).* 63rd Annual Gaseous Electronics Conference and 7th International Conference on Reactive Plasmas, October 4–8, Paris, France, Bulletin of the American Physical Society, p. 108, 2010.
12. Ivan Gordeev, Vaclav Prukner, Milan Simek, Andrei Choukourov, Hynek Biederman. *Influence of SDBD discharge parameters on deposition and properties of PEO-like plasma polymers*. IX Workshop on Frontiers in Low Temperature Plasma Diagnostics, 9th–12th May, Greifswald/Zinnowitz, Germany, Book of abstract, p. 87, 2011.
13. Andrei Choukourov, Ivan Gordeev, Dmitry Arzhakov, Anna Artemenko, Jaroslav Kousal, Ondřej Kylián, Danka Slavínská, Hynek Biederman. *Elastic Properties of PEO-like Plasma Polymers.* 18th International Colloquium on Plasma Processes, July 4-8, Nantes, France, Abstract booklet, p. 205, 2011.
14. Anna Artemenko, Marta Vandrovcova, Ondřej Kylian, Jaroslav Kousal, Andrei Choukourov, Ivan Gordeev, Oleksandr Polonskyi, Danka Slavinska, Lucie Bačakova, Hynek Biederman. *Influence of the sterilization processes on the properties of RF magnetron sputtered amino-rich thin films*. International Symposium on Plasma Chemistry, July 24-29, Philadelphia, USA, Book of abstract, 2011.
15. Dmitry Arzhakov, Ivan Gordeev, Andrei Choukourov, Anna Artemenko, Ondřej Kylián, Jaroslav Kousal, Oleksandr Polonskyi, Josef Pešička, Danka Slavínská, Hynek Biederman. *Nanocomposite silver/poly(ethylene oxide)-like plasma polymers prepared by plasma-assisted vacuum evaporation and magnetron sputtering.*

International Symposium on Plasma Chemistry, July 24-29, Philadelphia, USA, Book of abstract, 2011.

16. Andrei Choukourov, Ivan Gordeev, Dmitry Arzhakov, Anton Serov, Pavel Solař, Martin Drabik, Oleksandr Polonskyi, Anna Artemenko, Jaroslav Kousal, Ondřej Kylián, Danka Slavínská, Hynek Biederman. *Nanostructured plasma polymers and their nanocomposites.* VI International Symposium on Theoretical and Applied Plasma Chemistry, September 5-9, Ivanovo, Russian Federation, p. 7, 2011.
17. Andrei Choukourov, Dmitry Arzhakov, Ivan Gordeev, Danka Slavínská and Hynek Biederman. *Formation of nano-patterns during initial stages of plasma polymer growth.* Nanoworkshop 2011, 5th International workshop on polymer/metal nanocomposites, September 20-22, Bari, Italy, Book of abstracts, p. 46, 2011.
18. I. Gordeev, D. Arzhakov, P. Solar, A. Serov, A. Artemenko, O. Polonskyi, J. Ponti, J. Kousal, O. Kylian, A. Choukourov, D. Slavinska and H. Biederman. *Nano-structured amphiphilic plasma polymers for tuning the adhesion of cells.* 55th Annual Society of Vacuum Coaters Technical Conference & Exhibition, April 28– May 3, Santa Clara, California, USA, Book of abstracts, 2012.
19. Ivan Gordeev, Milan Šimek, Václav Prukner, Andrei Choukourov, Hynek Biederman. *Comparison of various deposition strategies to prepare non-fouling plasma polymer films by atmospheric-pressure surface DBD.* 4th International Conference on Plasma Medicine, June 17-21 Orléans, France, Book of abstract, p. 118, 2012.
20. Ivan Gordeev, Milan Šimek, Václav Prukner, Anna Artemenko, Andrei Choukourov, Hynek Biederman. *Aging of PEO-like plasma polymer films prepared by atmospheric and low pressure discharges.* 4th International Conference on Plasma Medicine, June 17-21 Orléans, France, Book of abstract, p. 122, 2012
21. Andrei Choukourov, Ivan Gordeev, Anna Artemenko, Martin Petr, Oleksandr Polonskyi, Marta Vandrovcova, Ondřej Kylian, Lucie Bačakova, Danka Slavinska, Hynek Biederman. *Resistance of plasma polymers to sterilization techniques used in biomedical applications.* 4th International Conference on Plasma Medicine, June 17-21 Orléans, France, Book of abstract, p. 49, 2012